

**Analysis of embryonic development
in *Tribolium castaneum* using a
versatile live fluorescent
labelling technique**

by

Matthew Alan Benton

Darwin College

University of Cambridge

This dissertation is submitted for the degree of Doctor of Philosophy

SUMMARY

Studies on new arthropod models are shifting our knowledge of embryonic patterning and morphogenesis beyond the *Drosophila* paradigm. In contrast to *Drosophila*, most insect embryos exhibit the short or intermediate-germ type and become enveloped by extensive extraembryonic membranes. The genetic basis of these processes has been the focus of active research in several insects, especially *Tribolium castaneum*. The processes in question are very dynamic, however, and to study them in depth we require advanced tools for fluorescent labelling of live embryos. In my work, I have used a transient method for strong, homogeneous and persistent expression of fluorescent markers in *Tribolium* embryos, labelling the chromatin, membrane, cytoskeleton or combinations thereof. I have used several of these new live imaging tools to study the process of cellularisation in *Tribolium*, and I found that it is strikingly different to what is seen in *Drosophila*. I was also able to define the stage when cellularisation is complete, a key piece of information that has been unknown until now. Lastly, I carried out extensive live imaging of embryo condensation and extraembryonic tissue formation in both wildtype embryos, and embryos in which *caudal* gene function was disrupted by RNA interference. Using this approach, I was able to describe and compare cell and tissue dynamics in *Tribolium* embryos with wild-type and altered fate maps. As well as uncovering several of the cellular mechanisms underlying condensation, I have proposed testable hypotheses for other aspects of embryo formation.

The work presented in this thesis will serve as a foundation for future studies on cellularisation and tissue morphogenesis in *Tribolium*. Furthermore, the live imaging method, the fluorescent labelling constructs, and the analysis I carried out should be easily adaptable to other non-model arthropod species.

DECLARATION

This dissertation is the result of my own work. Except where explicitly stated in the text, it includes nothing that is the outcome of work done in collaboration.

It does not exceed 60,000 words.

None of the work presented here has been, or will be, submitted for any other degree or qualification.

Results presented here have also been published in the following article:

Benton, M.A., Akam, M. and Pavlopoulos, A. (2013). Cell and tissue dynamics during *Tribolium* embryogenesis revealed by versatile fluorescence labelling approaches. *Development* 140, 3210–3220.

Other results presented here are being prepared for publication in the following article:

van der Zee, M., Benton, M.A. and Rabouille, C. (Manuscript in preparation). The gap junction protein Innexin7a is essential for basal cell closure during cellularization of the *Tribolium castaneum* blastoderm.

ACKNOWLEDGEMENTS

I would like to thank my supervisor, Michael Akam, for giving me the freedom and support to pursue my own projects. I would also like to thank my unofficial supervisor, Tassos Pavlopoulos, for helping me achieve many of the goals of my main project. I thank Carlo Brena for introducing me to that horrible animal, *Strigamia maritima*, and Barbora Konopova for teaching me how to look after the other horrible animal, *Gryllus bimaculatus*, and for introducing me to the fantastic flour beetle. I also thank Ken Siggins for keeping the lab running and providing help with too many things to list here, and for the laughter. Lastly, I want to thank my PhD siblings, especially Jack Green and Vera Hunnekühl, the last few years may not have been possible without our daily coffee and “science-talks”, and best of luck to Erik Clark!

As always, I thank my family on both sides of the world, especially my Mother, for everything over the years. I thank all of my English/Welsh family for welcoming me to this country and helping me settle in when I was “fresh off the boat”, especially my Gran and my Uncle Alan, who is very much missed. And I thank Bianca Schmitt for making everyday a better day, for supporting me through some tough times, and for encouraging me to get out of my comfort zone and explore the world.

I thank Maurijn van der Zee for a great collaboration, and I look forward to working together again in the future. I also thank Kristen Panfilio for stimulating conversations about extraembryonic patterning, and Andrew Peel for relaxed conversations about embryo condensation (on a beach in Crete).

I thank my friend and former flatmate Dan Brinkman for the times staying in gaming and the times going out partying (and the times staying in gaming and partying). I also thank the rest of the Frank Young crew, especially Nicole Wong and Amélie Deblauwe for the support, the laughter, and the weekly coffee. More generally, I thank all those crazy people in Darwin who have made that place my home away from home, and thanks to all members of Barcomm (past and present) for making Darwin Bar the great social hub that it is.

I thank Liz Duncan and Peter Dearden for encouraging me to come to Cambridge for my Ph.D in the first place.

I thank all of the people mentioned in the text who provided me with beetle lines, fly lines, plasmids and other reagents, and I thank Matt Wayland in the imaging facility for looking after the microscopes and for upgrading the inverted system.

During my PhD, I was funded by the Cambridge Commonwealth Trusts, the John Stanley Gardiner Studentship (Department of Zoology), the CT Taylor studentship, the Cambridge Philosophical Society, the Gilchrist Foundation and Darwin College.

Last of all, I thank you for reading this thesis, I hope you enjoy it and find it useful.

TABLE OF CONTENTS

SUMMARY	II
DECLARATION.....	III
ACKNOWLEDGEMENTS	IV
TABLE OF CONTENTS	VI
1. GENERAL INTRODUCTION	1
1.1 The evolution of development	1
1.2 Phylogeny of the arthropods	2
1.3 Phylogeny of the insects	2
1.4 Arthropods as a group to study	4
1.5 Currently available molecular tools in arthropods	5
2. MATERIALS AND METHODS.....	7
2.1 <i>Tribolium</i> husbandry	7
2.2 <i>Tribolium</i> egg dechoriation for microinjection and/or live imaging.....	7
2.3 <i>Tribolium</i> egg dechoriation for fixation.....	8
2.4 <i>Tribolium</i> egg fixation	8
2.5 RNA extraction and cDNA synthesis	9
2.6 Genomic DNA extraction	9
2.7 <i>Tribolium</i> gene cloning	9
2.8 Double-stranded RNA synthesis	10
2.9 Cloning of mRNA templates and transgenesis constructs	10
2.10 Capped, single stranded RNA synthesis	11
2.11 Microinjection of <i>Tribolium</i> embryos.....	12
2.12 <i>Tribolium</i> embryo live imaging	13
2.13 RNA <i>in situ</i> hybridization probe synthesis	13
2.14 RNA <i>in situ</i> hybridisation protocol.....	13
2.15 <i>Drosophila</i> husbandry and microinjection.....	14
3. THE USE OF TRANSIENT EXPRESSION AS A METHOD FOR LIVE IMAGING	15
3.1 Introduction.....	15
3.1.1 The advent of fluorescent live imaging	15

3.1.2	Fluorescent live imaging in arthropods	15
3.1.3	Transient fluorescent labelling	16
3.1.3	Transient fluorescent labelling in arthropods	16
3.2	Results	17
3.2.1	Transient expression of fluorescent nuclear, membrane and actin markers in <i>Tribolium</i>	17
3.2.2	Persistence of expression of fluorescent reporters	22
3.2.3	Transient expression of a photo-convertible marker in <i>Tribolium</i>	23
3.2.4	Transient expression in <i>Drosophila</i>	25
3.2.5	Transient expression via DNA injection	25
3.3	Discussion	27
3.3.1	Transient expression in <i>Tribolium</i>	27
3.3.2	Problems with the fusion constructs	27
3.3.3	Application of transient expression to other arthropods	28
3.3.4	Transient expression via DNA injection	29
3.3.5	Other applications of transient expression	29
4.	CELLULARISATION IN <i>TRIBOLIUM</i> – A MORE WIDELY CONSERVED MODE THAN <i>DROSOPHILA</i>?	31
4.1	Introduction	31
4.1.1	Holoblastic cleavage	31
4.1.2	Meroblastic cleavage	32
4.1.3	Involvement of the yolk across all forms of cleavage	33
4.1.4	Cellularisation in hemimetabolous insects	34
4.1.5	Cellularisation in holometabolous insects	35
4.1.6	Cellularisation in <i>Drosophila</i>	35
4.1.7	Can information about <i>Drosophila</i> cellularisation be applied to other arthropods?	36
4.2	Results	37
4.2.1	Membrane ingression	37
4.2.2	Basal cell closure	39
4.2.3	<i>Innexin-7a</i> has a novel role in cellularisation in <i>Tribolium</i>	40

4.2.4	Yolk cleavage in <i>Tribolium</i>	42
4.2.5	Effect of yolk cleavage on the germband	44
4.3	Discussion	46
4.3.1	Membrane invagination prior to uniform blastoderm formation	46
4.3.2	Evolution of a columnar blastoderm – a case for heterochrony?	48
4.3.3	Cell closure without contractile actin rings and the role of <i>inx7a</i>	49
4.3.4	Formation of the yolk spheres – delayed cellularisation?	49
5.	A LIVE IMAGING STUDY OF GERMBAND CONDENSATION	51
5.1	Introduction	51
5.1.1	<i>Drosophila</i> as a model system for the study of morphogenesis	51
5.1.2.	Morphogenetic consequences of short/intermediate germ development	52
5.1.3	Condensation and morphogenesis in <i>Tribolium</i>	53
5.2	Results	54
5.2.1	Dynamics of <i>Tribolium</i> germband condensation and elongation, and extraembryonic development	54
5.2.2	Altered fate map, tissue and cell dynamics in <i>Tc-cad</i> knock-down embryos	61
5.2.3.	Formation of the differentiated blastoderm	65
5.2.4	Cell shape changes during condensation	66
5.2.5	Cell intercalation and cell contraction	70
5.2.6	Gastrulation of the mesoderm	71
5.2.7	A possible role for the yolk system in <i>Tribolium</i> morphogenesis	76
5.2.8	Serosa window closure	80
5.3	Discussion	81
5.3.1	Formation of the differentiated blastoderm	81
5.3.2	The contribution of cell shape change to condensation.....	83
5.3.3	The role of convergent extension in condensation and axis elongation	84
5.3.4	The role of the yolk in condensation	85
5.3.5	The amnion/serosa boundary during condensation	86

5.3.6 Genetic evidence supporting my proposed model.....	87
5.3.7 Future work on condensation	88
6. APPENDIX - EXPRESSION PATTERN OF <i>TRIBOLIUM SERPENT</i>	90
6.1 Introduction.....	90
6.2 Results and Discussion.....	91
7. CONCLUDING REMARKS	98
7.1 Combining the study of gene regulatory networks with cell biology	98
7.2 Future directions	99
8. MOVIE LEGENDS	100
9. BIBLIOGRAPHY.....	103

1. GENERAL INTRODUCTION

During my PhD, I have developed new tools for the fluorescent live imaging of embryogenesis in the beetle *Tribolium castaneum*, and I have used these tools to study cellularisation and condensation of the germband. My aim when developing these tools was to allow myself and others to study the cell behaviours underlying embryogenesis, not just in *Tribolium*, but in a range of non-model arthropod species.

The overall layout of my thesis is as follows. In this section I present a broad introduction to the field of evolution and development, and the animals I am most interested in. Due to the diversity of my different projects, I have chosen to divide my work into three main results chapters, each with its own introduction and discussion. First of all, I present transient expression as a method for fluorescent live imaging in insects, and the tools I have developed using this method. Secondly, I present my work on cellularisation in *Tribolium*, which has not been studied before in detail, and turns out to be remarkably different to *Drosophila*. Lastly, I present my work on the morphogenesis of germband condensation and extraembryonic development in *Tribolium*. I also present data from an unfinished project in an appendix section. As each chapter contains extensive discussion, I felt it unnecessary to have an overall final discussion, and instead present a short section of concluding remarks at the end. Movies and high-quality versions of each figure are provided on the CD.

1.1 The evolution of development

In classical developmental biology, researchers are interested in studying how specific developmental events occur in an organism. Thanks to the incredible advances in biochemistry, genetics and cell biology that have occurred in the past century, it is now possible to understand developmental processes from the overall tissue level, right down to the DNA, RNA and protein level. Due to the time investment required to develop advanced techniques in any given animal, developmental biology research is largely focussed on several key “model systems”, such as the mouse, *Mus musculus*, the frog, *Xenopus laevis*, the zebrafish, *Danio rerio*, the nematode, *C. elegans*, and the fruit fly, *Drosophila melanogaster*. A tremendous amount of information is now available about developmental processes in each of these animals, and there is still more that we do not understand than we do. However, if we

are to understand how any developmental process came to be, how it evolved in the first place, we need to be able to look at that process in different animals and compare the similarities and differences.

People have been comparing development in multiple animals for hundreds of years, even before the theory of natural selection was presented in 1858 (Darwin, 1859; Darwin and Wallace, 1958). It is only in the current molecular era, however, that we are able to study the actual molecules of inheritance, and therefore, study how these molecules change when developmental processes change. The modern name for this old field is evolution and development, or evo-devo for short. In recent years, there has been a huge push towards studying the evolution of development in many diverse animals. Thanks to this push, it is now possible to study and compare developmental processes at a molecular level within and between each of the bilaterian superphyla; deuterostomes, ecdysozoans and lophotrochozoans, as well as non-bilaterian lineages (for a broad summary of this work see Carroll, 2005)

1.2 Phylogeny of the arthropods

The phylum Arthropoda (located within the superphylum Ecdysozoa) is the most species-rich phylum on the planet. Proposed phylogenies of the arthropods have changed frequently over the years, and while certain aspects are still unresolved, the broad lineages seem to be supported (Fig. 1.1). Extant arthropods are broadly divided into the Chelicerata (e.g. spiders, scorpions, horseshoe crabs), Myriapoda (e.g. millipedes and centipedes), the paraphyletic Crustacea (e.g. brine shrimp, lobsters, barnacles) and the Hexapoda, which probably branch within the Crustacea and together constitute the monophyletic “Pancrustacea” (Regier et al., 2010). The hexapods are further divided into the entognaths (wingless hexapods such as springtails), and the insects. In the pre-molecular era, extensive comparative embryology studies were carried out within and between each of these subphyla, although the most attention was paid to the insects (Anderson, 1973; Waddington and Counce, 1972a; Waddington and Counce, 1972b).

1.3 Phylogeny of the insects

The insects are broadly divided into the Hemimetabola and the Holometabola, and the phylogenetic relationships are more well resolved for the latter than the former (Fig. 1.1).

Holometabolous insects hatch from the egg in a larval state that is drastically different from the adult. After one or more moults, the larvae undergo an extensive metamorphosis into the adult form. Similar to segmentation, this form of development allows greater evolvability of a species, as the morphology and behaviour of the larvae can evolve semi-independently to that of the adult. An example of this is when the larvae of an insect live in a completely different environment to the adult form, such as the aquatic environment of mosquito larvae versus the terrestrial/aerial environment of the adult. This evolutionary flexibility may be one reason why holometabolous insects comprise approximately 85% of all insect species (Grimaldi and Engel, 2005).

Hemimetabolous insects (paleopterans, polyneopterans and paraneopterans) do not undergo a true metamorphosis after hatching. Instead, hatched larvae/nymphs are morphologically similar to the adult form, except that they generally lack wings. They then undergo one or more moults before attaining the adult form. While the larvae and adult forms of hemimetabolous insects do not have the flexibility of holometabolous insects, they benefit from not having an extended metamorphosis period, during which the insect would be vulnerable to predators.

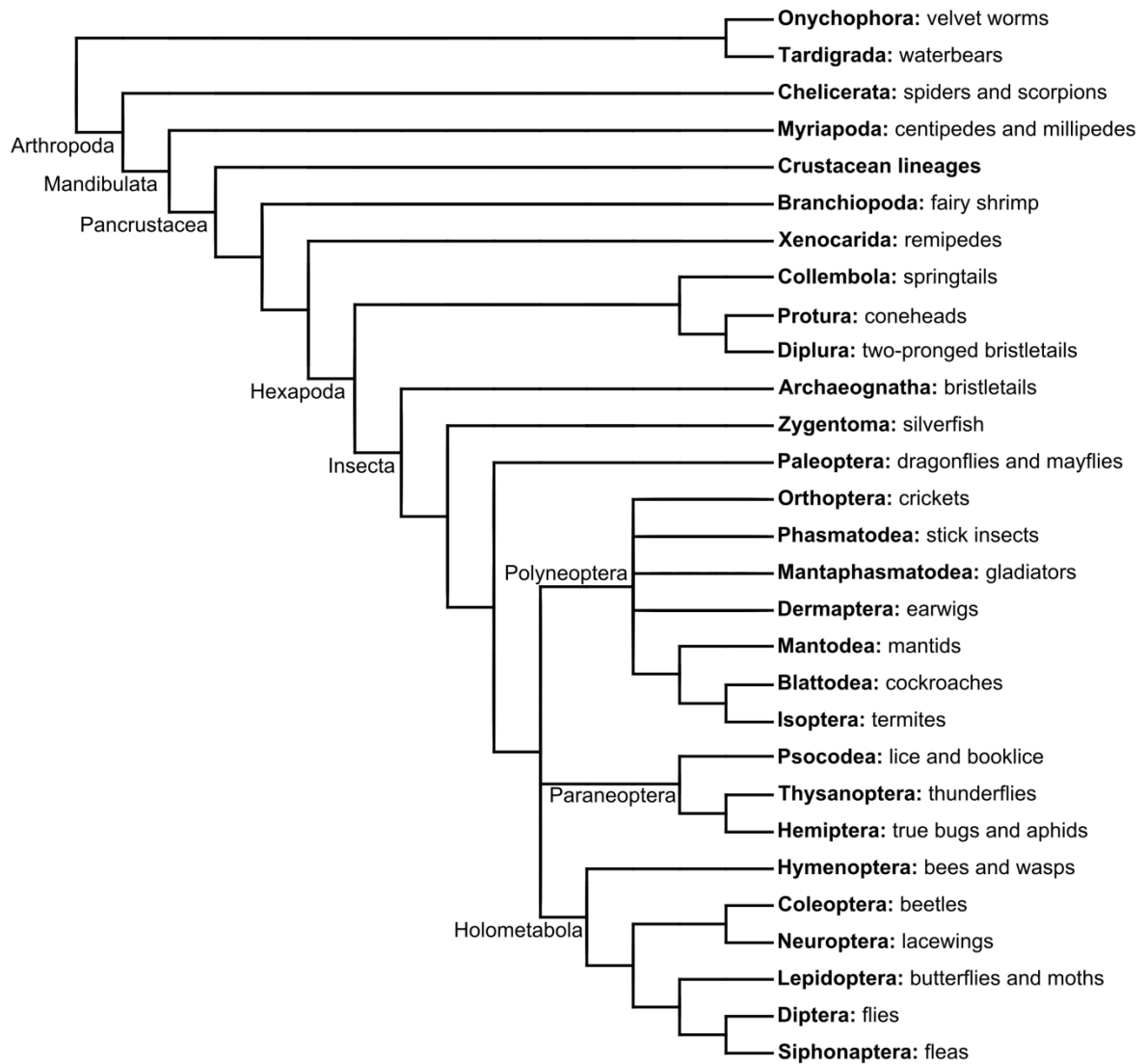


Fig. 1.1. Phylogeny of the euarthropods. Fig. drawn from Oakley et al. (2013), Regier et al., (2010) and Trautwein et al. (2012). As discussed in these references, not all phylogenetic relationships shown are strongly supported.

1.4 Arthropods as a group to study

Despite the amazing success and diversity of this phylum, the only major arthropod model system for studying developmental biology is the fruit fly, *Drosophila melanogaster*. This insect may well be the most intensely studied animal in the world, but when compared with what we know about other arthropods from classical studies, it is a bit odd in many ways. The best studied example relates to the manner in which the *Drosophila* embryo makes its segments.

The process of segmentation is the division of the embryo into repeated metameric units along the anterior-posterior axis. One benefit of segmentation may be that it increases the evolvability of an animal by allowing specific parts of the body to become specialised without affecting other parts of the body. Whatever the reason, segmentation is found in each of the most successful animal lineages; vertebrate chordates, annelid worms, and arthropods (Peel et al., 2005). Across these lineages, the vast majority of animals undergo segmentation by the repeated addition of segments at the posterior part of the embryo/larvae/adult.

One of the exceptions to this mode of segmentation is observed in all of the higher flies (e.g. *Drosophila*), which exhibit no posterior growth, and instead make all of their segments simultaneously. This mode of segmentation is found in several other insect lineages, but the rest of the arthropods undergo sequential addition of segments, and it is almost certainly the ancestral state for arthropods. Unfortunately, because of the focus on the developmental biology of *Drosophila* as a model system for the arthropods, we have very little information on the molecular mechanisms underlying sequential segmentation. Furthermore, several other major changes accompanied this transition from sequential segmentation to simultaneous segmentation (see “5. A live imaging study of germband condensation”), and we have very little understanding of how these processes occur.

1.5 Currently available molecular tools in arthropods

With the increased interest in the evolution of development, modern molecular techniques have been developed for several non-insect arthropods, such as the spider *Parasteatoda* (formerly *Achaearanea*) *tepidariorum*, the centipede *Strigamia maritima*, and the malacostracan crustacean *Parhyale hawaiiensis* (Brena and Akam, 2012; Hilbrant et al., 2012; Pavlopoulos and Averof, 2005). The same can be said for many more insect species, such as the cockroach *Periplaneta americana* (order Blattodea), the cricket *Gryllus bimaculatus* (order Orthoptera), the true bug *Oncopeltus fasciatus* (order Hemiptera), the aphid *Acyrtosiphon pisum* (order Hemiptera), the wasp *Nasonia vitripennis* (order Hymenoptera), the honeybee *Apis mellifera* (order Hymenoptera), and the beetle *Tribolium castaneum* (order Coleoptera) (Angelini and Kaufman, 2005; Chesebro et al., 2012; Duncan et al., 2013; Kainz et al., 2011; Lynch et al., 2012; Nunes Da Fonseca et al., 2008; Wilson and Dearden, 2011). Molecular and genetic techniques have also been applied to *Drosophila* species other than *melanogaster* and to other dipterans (Kalinka et al., 2010; Rafiqi et al., 2008).

Amongst these species, the largest focus has been on the beetle *T. castaneum*, and it is now the best insect system for studying developmental biology apart from *Drosophila melanogaster*. Techniques available for studying embryogenesis in *Tribolium* include protein immunohistochemistry, RNA *in situ* hybridisation, gene knockdown via RNA interference (RNAi), transgenesis, and limited fluorescent live imaging. This popularity is due to a number of factors. First of all, *Tribolium* is a pest species, and has been cultured in labs for decades for genetic and ecological studies (Sokoloff and Shrode, 1962). It is easy to culture at a range of temperatures, and goes through the entire life cycle in approximately one month (at 32°C) on wheat-meal flour and yeast with no additional water required. Secondly, the size and structure of the egg are similar to *Drosophila*, and several techniques from *Drosophila* eggs can be directly applied to *Tribolium* eggs, without changing the protocol. Lastly, and most importantly, *Tribolium* exhibits many developmental traits that are more ancestral for insects than those seen in *Drosophila*. For example, *Tribolium* undergoes segmentation by sequentially adding segments from the posterior of the embryo.

Fluorescent live imaging techniques have proven to be incredibly useful for studying embryogenesis in many animals. Unfortunately, such techniques are very limited in the arthropods other than *Drosophila*. During my PhD, I have developed new tools for fluorescent live imaging of embryogenesis in *Tribolium* and other arthropods (“3. The use of transient expression as a method for live imaging”). I have used these tools to study two developmental processes that occur in *Tribolium* that are more representative of insects than what is seen in *Drosophila*; formation of a cuboidal blastoderm epithelium following cellularisation (“4. Cellularisation in *Tribolium* – a more widely conserved mode than *Drosophila*?”), and the condensation of a multilayered embryo with extensive extraembryonic epithelium (“5. A live imaging study of germband condensation”).

2. MATERIALS AND METHODS

2.1 *Tribolium* husbandry

Beetles were reared at 32°C in plastic boxes that had a mesh-covered window in the lid to allow air-flow. For stock keeping, beetles were reared on a coarse flour that was made by mixing 1 kg of whole wheat flour (purchased from an organic food store) with 50 g dry yeast powder (purchased from Sainsbury's supermarket) and 1 g Fumagilin-B (Medivet). All components were sieved with a 800 µm steel sieve (Retsch test sieve 200mm x 50mm). When collecting eggs, beetles were reared on white flour (purchased from an organic food store) that had been sieved with a 300 µm sieve (Retsch test sieve 200mm x 50mm) to remove particulates. Strains used were vermilion-white (kindly provided by Gregor Bucher), and nGFP (kindly provided by Michalis Averof). For more information on *Tribolium* husbandry, refer to The Beetle Book (Bucher, 2009).

2.2 *Tribolium* egg dechoriation for microinjection and/or live imaging

Eggs were transferred to a small egg basket (made by melting 225 µm aperture mesh onto one end of a section cut from a 15 mL falcon tube). The basket was then placed in a 50 mm petri-dish that was filled with ddH₂O and embryos were rinsed for 15 seconds. "Rinsed" means the liquid was sucked up from outside the basket then squirted into the basket. The basket was then transferred to a petri-dish containing bleach (SIGMA #239305) diluted with ddH₂O to a final concentration of 0.5% hypochlorite, and embryos were rinsed for 30 seconds. The basket was then transferred to a petri-dish containing ddH₂O and embryos were rinsed for 15 seconds. The basket was then transferred back to the petri-dish containing bleach, and embryos were rinsed for a further 30 seconds. The basket was then transferred to a petri-dish containing ddH₂O and embryos were rinsed for 15 seconds, and this rinse was repeated in clean ddH₂O 4 times. The basket was then inverted over a glass slide or a glass bottom petri-dish (MatTek corporation, Part Number P35G-0-20-C), and ddH₂O was used to rinse the embryos out of the basket and onto the slide/petri-dish.

2.3 *Tribolium* egg dechoriation for fixation

Eggs were transferred to a small egg basket (as above). The basket was then placed in a 50 mm petri-dish that was filled with ddH₂O and embryos were rinsed for 15 seconds. “Rinsed” means the liquid was sucked up from outside the basket then squirted into the basket. The basket was then transferred to a petri-dish containing bleach (SIGMA #239305) diluted with ddH₂O to a final concentration of 2% hypochlorite, and embryos were rinsed for 1 minute. The basket was then transferred to a petri-dish containing ddH₂O and embryos were rinsed for 15 seconds. The basket was then transferred back to the petri-dish containing bleach, and embryos were rinsed for 1 minute. The basket was then transferred to a petri-dish containing ddH₂O and embryos were rinsed for 15 seconds, and this was repeated 4 times. The basket was then inverted over a 1.5mL eppendorf tube, and ddH₂O was used to rinse the embryos out of the basket and into the tube.

2.4 *Tribolium* egg fixation

Starting with dechorionated embryos in an eppendorf tube, all ddH₂O was replaced with 500 μ L fixation buffer (8% formaldehyde and 67 mM EDTA in 1x PBS [137 mM NaCl, 2.7 mM KCl, 10mM Na₂HPO₄, 1.8 mM KH₂PO₄]) and 500 μ L heptane. The tube was placed on a rocker for 20 minutes at room temperature. The aqueous layer (bottom layer) was then replaced with 500 μ L ice cold 100% methanol and the tube was shaken vigorously for 1 minute. After the embryos had settled, the top layer and the embryos at the interphase (that still retain their chorion) were transferred to a different tube and an equal volume of methanol was added. These latter embryos were then repeatedly sucked up and expelled through a 0.8- μ m steel needle (Terumo #NM-2138R). After several rounds of this, any embryos that had sunk to the bottom of the tube were recombined with the other dechorionated embryos. A further 500 μ L of 100% methanol was then added to the tube of dechorionated embryos, and it was inverted several times. The liquid in the tube was then replaced with 1 mL 100% methanol, before the tube was inverted. This was repeated three times. Embryos were then stored in 100% methanol at -20°C. When fixing a large number of embryos (>50 μ L volume), the fixation was carried out in 15 mL falcon tubes rather than 1.5 mL eppendorf tubes and the volumes of all liquids were increased 10 fold.

2.5 RNA extraction and cDNA synthesis

Total RNA was extracted from 0-72 hour old embryos using the TRIzol reagent (Invitrogen, #15596-026) according to the manufacturer's instructions, with the following changes. At the start of the protocol, 5 µg of LPA (SIGMA #56575) was added per 300 µL TRIzol to increase the quantity of RNA recovered. Following RNA precipitation, but prior to the 75% ethanol wash, a butanol wash was carried out to further clean the RNA.

cDNA synthesis was carried out using the "Superscript III First-strand Synthesis System for RT-PCR" kit (Invitrogen #18080-051), according to the manufacturer's instructions. The template was total RNA extracted from 0-72 hour old *Tribolium* embryos, and oligo(dT) primers were used.

2.6 Genomic DNA extraction

Drosophila genomic DNA (gDNA) was extracted by homogenizing a single adult in 50 µL squish buffer (10mM TrisCl pH8.2, 1mM EDTA, 25mM NaCl, 200 µg/mL Proteinase K). The mixture was incubated for 30 minutes at 30°C, then incubated for 2 minutes at 85°C to inactivate the Proteinase K. 2 µL of this was used for PCR.

2.7 *Tribolium* gene cloning

About 1 kb of *Tribolium caudal* isoform A (Schulz et al., 1998) coding sequence, also containing 400 bp in common with isoform B, was amplified from embryonic cDNA (0-72 hour old embryos) with primers Tcas_Cad_F (ACTACAACCTCGACCAACA) and Tcas_Cad_R (GAAGAAGCAACAAGAAGGCA).

About 0.85 kb of the *Tribolium* ortholog of *Glial cells missing* was identified by BLAST, and was PCR amplified from cDNA (0-72 hour old embryos) with primers Tcas_GCM_F (CGTGCACATCCTGAAGAAGA) and Tcas_GCM_R (CTGTTGTTGCTGTCGTCGTT).

About 1 kb of the *Tribolium* ortholog of *Serpent* (Gillis et al., 2008) was PCR amplified from cDNA (0-72 hour old embryos) with primers Tcas_Srp_F (TCCCGCTGCTTTGATCTAGT) and Tcas_Srp_R (TGCGATGACTGTGACGTGTA).

PCR was carried out using Taq DNA polymerase (Roche #11647687001). PCR products were ligated into plasmid pGEM-T Easy (Promega #A1360) according to manufacturer's instructions, then transformed into bacteria DH5α

(Invitrogen #18258-012) according to manufacturer's instructions. Plasmid was extracted from liquid culture using the "QIAprep Spin Miniprep" kit (QIAGEN #27106) according to manufacturer's instructions. Primers were designed using "Primer3 – PCR primer design tool" (Untergasser et al., 2012). Cloned fragments were sequenced to confirm identity.

2.8 Double-stranded RNA synthesis

Double-stranded RNA was prepared as described in "The Beetle Book" (Bucher, 2009), except that a phenol:chloroform extraction and isopropanol precipitation was carried out instead of the lithium chloride precipitation.

2.9 Cloning of mRNA templates and transgenesis constructs

The mRNA templates pT7-H2B-RFP and pT7-myr-RFP were created by Anastasios Pavlopoulos, for more information refer to Benton et al. (2013). The GAP43-YFP construct was created by Rembold et al. (2006) and kindly provided by Mette Handberg-Thorsager in the pCS2+ expression vector.

The myr-tandem-Tomato construct (Pfeiffer et al., 2010) was amplified from *Drosophila* genomic DNA via nested PCR (Strain kindly provided by Matthias Landgraf). The outer primers were Dm_myrtTom_Out_F (GAGCGCCGGAGTATAAATAGAG) and Dm_myrtTom_Out_R (CCATTCATCAGTTCCATAGG). The inner primers had synthetic ends to introduce a PsiI restriction site at the 5' Dm_myrtTom_F_PsiI (GCGCACATGTGCAACAAATGCTGCAG) and a NotI site at the 3' Dm_myrtTom_R_NotI (ATATGCGGCCGCTTACTTGTAAGCTCGTCCATACC). After digestion with PsiI and NotI restriction enzymes, the construct was ligated into NcoI/NotI-digested vector pT7-H2B-RFP, replacing H2B-RFP with myr-tdTom, to generate pT7-myr-tdTom.

The LifeAct motif (Riedl et al., 2008) was excised from plasmid pDlifeAct-YFP (provided by JianYing Yang) using the NcoI and BamHI restriction enzymes. EGFP was amplified from plasmid pCS2lynGFP (Kindly provided by Mette Handberg-Thorsager) by PCR using primers EGFP_F_BamHI (GTCAGGATCCTCGCCACCAGATCCATGGTGAGCAAGGGCGA) and EGFP_R_NotI

(ATATGCGGCCGCTTACTTGTACAGCTCGTCC). The NcoI/BamHI-digested LifeAct and BamHI/NotI-digested EGFP coding sequences were cloned in a triple-fragment ligation into NcoI/NotI-digested vector pT7-H2B-RFP, replacing H2B-RFP with LifeAct-EGFP, to generate pT7-LA-GFP.

The Actin binding protein-tandem Eos Fluorescent protein construct (Izeddin et al., 2011) was kindly provided by Christian Specht as plasmid pDendra2-N-ABPtdEosFP. The ABPtdEosFP coding sequence was excised as NcoI/NotI fragment from pDendra2-N-ABPtdEosFP and cloned into NcoI/NotI-digested vector pT7-H2B-RFP, replacing H2B-RFP with ABPtdEosFP, to generate pT7-ABPtdEosFP.

To create the Sqh-GFP construct, the *Tribolium* ortholog of *Spaghetti squash* (*Tc-Sqh*, identified by BLAST) was amplified from cDNA (0-24 hour old embryos) via nested PCR. The outer primers were Tc_Sqh_Out_F (CCCTTATTCCTTGACTCT) and Tc_Sqh_Out_R (CCTTGAATAACCCTCACT). The inner primers had synthetic ends to introduce a PciI restriction site at the 5' Tc_Sqh_F_PciI (ATATGGATCCTTGCTCATCCTTATCCT) and a BamHI site at the 3' Tc_Sqh_R_BamHI (ATATGGATCCTTGCTCATCCTTATCCT). EGFP was amplified from plasmid pCS2lynGFP by PCR using primers EGFP_F_BamHI (GTCAGGATCCTCGCCACCAGATCCATGGTGAGCAAGGGCGA) and EGFP_R_NotI (ATATGCGGCCGCTTACTTGTACAGCTCGTCC). The PciI/BamHI-digested Sqh and BamHI/NotI-digested EGFP coding sequences were cloned in a triple-fragment ligation into NcoI/NotI-digested vector pT7-H2B-RFP, replacing H2B-RFP with Sqh-EGFP, to generate pT7-Sqh-GFP.

The GAP43YFP coding sequence was excised as BamHI/NotI fragment from pCS2+GAP43YFP and cloned into BamHI/NotI-digested vector pSLEFA-dsRed-SV40pA (kindly provided by Michalis Averof), replacing dsRed with GAP43YFP, to generate pSLEFA-GAP43YFP-SV40pA.

All PCR reactions were carried out using the Phusion High-Fidelity system (New England Biolabs, catalog number E0553L).

2.10 Capped, single stranded RNA synthesis

Plasmids were linearised as follows: pCS2+-GAP43-YFP was digested with NsiI, pT7-H2B-Ruby was digested with EcoRI, pT7-ABPtdEosFP was digested with EcoRI, pT7-LA-GFP was digested with EcoRI, pT7-myr-RFP was linearized with EcoRI, pT7-myr-tdTom was linearized with EcoRI, pT7-sqh-GFP was linearized with PstI. Linearized DNA was purified

by a phenol:chloroform and a chloroform extraction, then precipitated and resuspended in nuclease-free water to give a concentration of approximately 500 ng/μl. Capped mRNA was prepared from linearized plasmid DNA using either the T7 (for pT7) or SP6 (for pCS2+) mMESSAGE mMACHINE (Ambion #AM1344 and #AM1340) kit, according to the manufacturer's instructions. After digestion with TURBO-DNase, RNA was purified by a phenol:chloroform and a chloroform extraction and an equal volume of isopropanol was added. RNA was precipitated by centrifugation, and resuspended in 5 μl nuclease-free water and quantified on a Nanodrop spectrophotometer.

2.11 Microinjection of *Tribolium* embryos

After dechoriation, eggs were either mounted on a microscope slide or on a glass bottom petri-dish (MatTek corporation, Part Number P35G-0-20-C) that had a window cut in the side of the dish to allow injection, depending on the subsequent requirements. Eggs were lined up in a small amount of water using a single-strand paintbrush. Gaps were left between neighbouring eggs to prevent asphyxiation. After completely drying the water, the eggs were covered with Voltalef 10S Halocarbon oil. The needle was inserted into the egg at the anterior pole and the tip of the needle was moved into approximately the centre of the egg before injecting any solution. Needles were prepared on a needle puller (Sutter Instrument Co. Model P-87) using borosilicate capillaries with an outer diameter of 1 mm and an inner diameter of 0.58 mm and an internal filament (Warner instruments, model number G100F-4). Before use, the tips were bevelled using a microgrinder (Narishige, EG-4) to give an angled opening. Pressure for microinjection was supplied by nitrogen gas and regulated with a Pico-injector system (Medical Systems Corporation, model number PLI-100). Following injection, eggs were kept at 32°C.

Capped mRNAs were injected at concentrations between 0.5-3 μg/μl diluted in injection buffer (5mM KCl, 10mM NaH₂PO₄). For co-injection of different constructs or dsRNA for RNAi, RNA was combined before injection. When combining RNA, the total concentration was kept below 3 μg/μl to prevent blockage of the needle. Immediately before injection, RNA was centrifuged for 2 minutes at 13,000 RPM.

2.12 *Tribolium* embryo live imaging

Live imaging was carried out on Leica SP1 upright, SP5 upright and SP5 inverted (with temperature regulated enclosure) confocal microscopes at the Department of Zoology Imaging Facility (University of Cambridge) and at the Advanced Light Microscopy Facility (EMBL, Heidelberg). Image stacks of 10-40 focal planes (z-step of 0.5-3 μm) were taken with a 20x/0.7 multi-immersion objective or a 40x/1.3NA oil-immersion objective at 2-5 min intervals. Using these conditions, embryos developed normally for at least 15 hours tested during these experiments. Processing of confocal data was carried out using FIJI (Schindelin et al., 2012) and cell tracking with the MTrackJ plugin (Meijering et al., 2012).

2.13 RNA *in situ* hybridization probe synthesis

Starting with the gene of interest in plasmid pGem, PCR amplification was carried out using primers M13F (GTAAAACGACGGCCAGT) and M13R (AACAGCTATGACCATG). PCR products were cleaned up using QIAquick PCR purification kit (QIAGEN #28104) and quantified on a Nanodrop spectrophotometer. Approximately 1 μg of DNA was combined with 2 μL digoxigenin (DIG) RNA labelling mix (Roche #11277073910), 2 μL 10x Transcription buffer (Roche, included with RNA polymerase), 2 μL T7 (Roche #10881767001) or SP6 (Roche, Roche #10810274001) RNA polymerase (depending on orientation of gene) plus DEPC H₂O up to a total volume of 20 μL . The reaction mix was incubated for 2 hours at 37°C, then 1 μL TURBO DNase (from Ambion Megascript kit #AM1344) was added and the mixture was incubated for a further 15 minutes at 32°C. A lithium chloride precipitation was then carried out, and the RNA was resuspended in 30 μL DEPC H₂O. RNA was then quantified on a Nanodrop spectrophotometer and stored at -20°C.

2.14 RNA *in situ* hybridisation protocol

The protocol used was initially as described by Schinko et al. (2009). As I progressed with my experiments, however, I was able to simplify the protocol without negatively affecting the results. The changes are as follows.

On day 1, instead of carrying out steps 11-17, the embryos were rehydrated from 100% methanol through a methanol:PBT (0.1% Tween 20 diluted in PBS) series (75:25, 50:50, 25:75), 5 minutes each. The solution was then replaced with PBT and the tube was inverted, this was then repeated three times.

At step 20, the probe was diluted in 100 μL of Hyb A (instead of 30 μL) at a concentration of 2 ng/ μL . After adding the diluted probe, the embryos were allowed to settle to the bottom of the tube, then the solution was pipetted up and down to ensure thorough distribution of probe.

At step 29, BM Purple (Roche #11442074001) was used instead of NBT/BCIP solution. Alternately, for FastRed staining 1 FastRed tablet (Roche #11496549001) was dissolved in 2 mL 0.1M Tris-HCl pH 8.2, then centrifuged for 2 minutes at 13,000RPM. Embryos were washed 3 times (five minutes each) in 0.1M Tris-HCl pH8.2. The Tris solution was then replaced with 200 μL FastRed solution. When transferring embryos in FastRed solution to a staining block, a glass Pasteur pipette with the tip broken off was used to prevent the embryos sticking to the pipette tip.

2.15 *Drosophila* husbandry and microinjection

Drosophila were reared and injected essentially as described in Roberts (1986).

3. THE USE OF TRANSIENT EXPRESSION AS A METHOD FOR LIVE IMAGING

3.1 Introduction

3.1.1 The advent of fluorescent live imaging

For many decades, live imaging has been used to study embryonic development in different arthropods. For most of this time, researchers relied on brightfield microscopy and have been limited to studying broad processes in eggs of animals that have appropriate optical properties. Some examples of this are yolk streaming and yolk contractions in insects (Counce, 1961), cell lineage analysis in crustaceans (Extavour, 2005; Hejnol et al., 2006), embryo formation in spiders (Akiyama-oda and Oda, 2003) and timing of segment formation in a myriapod (Brena and Akam, 2012).

More recently, fluorescent live imaging has been developed and used in many metazoans, and has proven to be superior to brightfield microscopy in many ways (for a review see Mavrakakis et al., 2010). Using fluorescent methods it is possible to label individual cellular components, such as the nucleus, cell membranes, and the cytoskeleton. Fluorescent live imaging can be used to study a wide range of developmental processes, from a broad tissue level to a sub-cellular level. Furthermore, when combined with confocal microscopy it is possible to make optical sections to visualise what is occurring in deep tissues without damaging the embryo. The vast majority of live imaging tools rely on the creation of transgenic lines and there are many such lines for the nematode worm, *Caenorhabditis elegans*, the zebrafish, *Danio rerio*, the mouse, *Mus musculus* and the fruit fly, *Drosophila melanogaster*. In order to study the evolution of development, however, it is necessary to examine the development of a range of more closely related animals.

3.1.2 Fluorescent live imaging in arthropods

Within the last few years, transgenic lines for live imaging have been developed for the beetle, *Tribolium castaneum* (Sarrazin et al., 2012), the cricket *Gryllus bimaculatus* (Nakamura et al., 2010) and the amphipod crustacean *Parhyale hawaiiensis* (Kontarakis et al., 2011). The tools available are still limited, however, especially in the beetle and the cricket.

This is due to a number of factors. First of all, it took many years to develop transgenesis for each of these animals, and the creation of a transgenic line takes many months in each animal. Secondly, even after successfully introducing a construct for live imaging into the genome of an animal, there is a good chance that the construct will not work as it does in other animals.

At the current rate, it would take many more years to develop fluorescent live imaging tools in the other emerging model arthropod species. Furthermore, in some species it is not possible to establish lab cultures, and therefore, the creation of transgenic lines is not feasible. It is my belief, therefore, that a different method is required to allow fluorescent live imaging in non-model arthropod species.

3.1.3 Transient fluorescent labelling

A non-transgenic method for live imaging has been applied in several animals, including the zebrafish, *Danio rerio* (for a full list of animals see Benton et al., 2013). This method is known as transient expression and involves the microinjection of *in vitro* transcribed mRNA encoding fluorescent protein constructs into embryos (Hatta et al., 2006). Using this transient expression, it is possible to obtain strong ubiquitous expression, which appears within a few hours of injection and lasts for several days (Hatta et al., 2006). Microinjection of plasmid DNA encoding a fluorescent construct downstream of a promoter can also be carried out, however, this results in mosaic labelling of cells (Hatta et al., 2006).

3.1.3 Transient fluorescent labelling in arthropods

Transient expression for fluorescent labelling of cells has been successfully applied in the spider *Parasteatoda* (formerly *Achaearanea*) *tepidariorum* (Kanayama et al., 2010). This method can only be used to label small clones of cells, however, as it is currently not possible to inject prior to cellularisation (Kanayama et al., 2010). Given that most insects go through a syncytial stage, I wanted to see whether it was possible to use transient expression for ubiquitous, uniform expression of fluorescent markers in insect embryos. More specifically, I was interested in developing new tools for live imaging in *Tribolium castaneum*. There is currently only a single transgenic line for live imaging of the entire *Tribolium* embryo, which ubiquitously expresses the Green Fluorescent Protein tagged with a nuclear localization signal (nGFP, Sarrazin et al., 2012).

To label a specific cellular component, a DNA construct is created whereby the coding sequence of a fluorescent protein of your choice is fused to that of a protein, or a fragment of a protein. When transcribed and translated, the resulting fusion protein will be transported to the cellular component, or compartment, that is specified by the non-fluorescent half of the fusion. To this end, I set out to find or develop fluorescent markers for different components of the cell, such as histones, cell membranes and F-actin. I also wanted a photoconvertible fluorescent marker in order to label specific clones of cells for cell lineage analysis.

3.2 Results

3.2.1 Transient expression of fluorescent nuclear, membrane and actin markers in *Tribolium*

To begin with, I wanted to test whether microinjection of mRNAs encoding fluorescent fusion proteins would result in strong fluorescent signal in *Tribolium* embryos. To do this, I synthesized capped mRNA from a template encoding a fusion protein that had the coding sequence of *Drosophila* histone *H2B* fused to that of the *Ruby* monomeric *Red Fluorescent Protein* (H2B-RFP) (created by Anastasios Pavlopoulos), and microinjected it at 3 $\mu\text{m}/\mu\text{L}$ into *Tribolium* eggs. In the eggs of many arthropod species (including *Tribolium*), the optical properties of the yolk make it difficult to detect fluorescent labelling of structures deep within the yolk. Therefore, in order to visualize fluorescent signal in nuclei and the blastoderm as soon as it became visible, eggs were injected with mRNA 4-6 hours after egg lay (when nuclei are at the surface of the egg, and blastoderm formation is underway).

One hour post injection, detectable fluorescence was visible in half the injected eggs in nuclei near the middle of the egg, but not at the termini (Fig. 3.1 (D) and Table 3.1). The strength of the fluorescent signal, and the number of eggs exhibiting fluorescence increased over the following hours (Fig. 3.1 (D-F) and Table 3.1). Three hours post injection, strong, uniform and ubiquitous expression was visible in 61% of eggs (Fig. 3.1 (F), Fig. 3.2 (A) and Table 3.1). I also injected H2B-RFP mRNA at 1 $\mu\text{g}/\mu\text{l}$, and found that the fluorescent signal was weaker than at the higher concentration (Fig. 3.1 (A-C)). The use of a histone marker that labels chromatin throughout the cell cycle made it possible to follow mitotic divisions unambiguously (Fig. 3.2 (B-B''')), unlike the nGFP transgenic line that only labels nuclei during interphase (Sarrazin et al., 2012). I injected a total of 200 eggs on two different days to

account for biological and environmental variability, and comparable results were found on both days (Table 3.1).

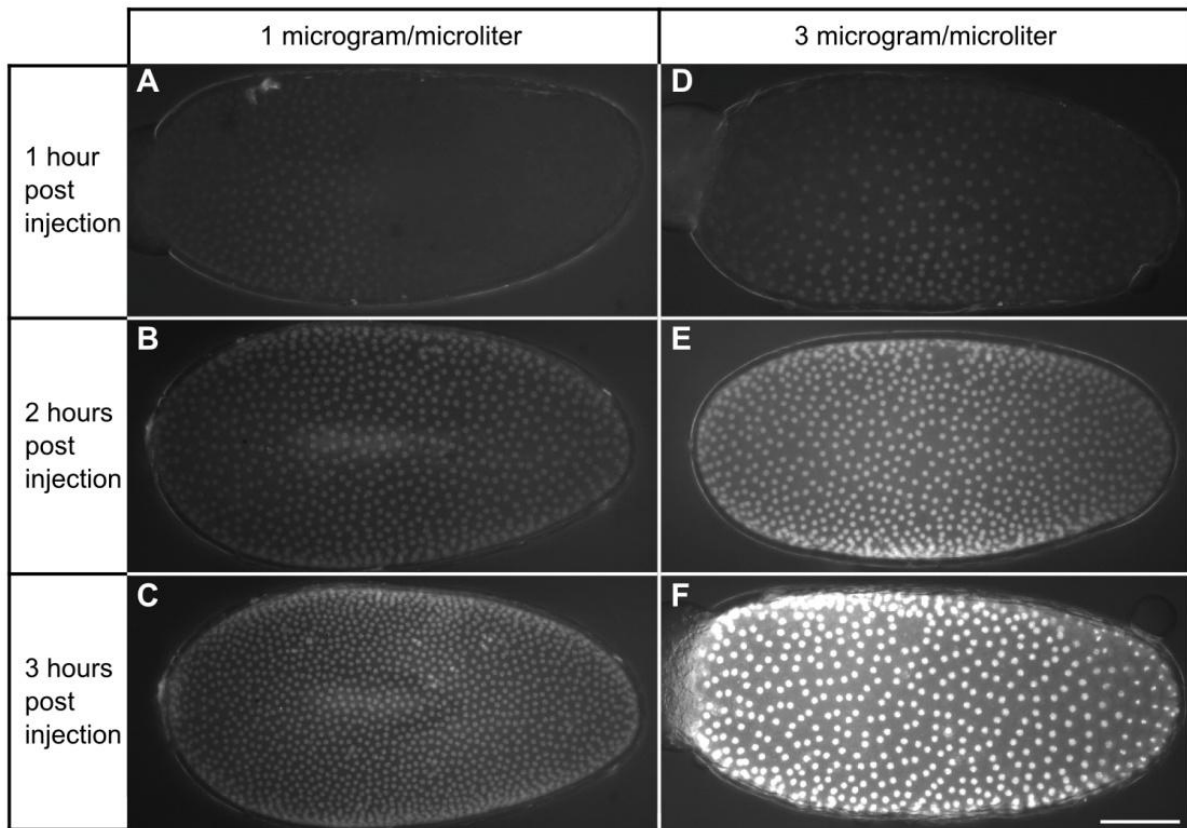


Fig. 3.1. Fluorescent protein expression in transiently labelled *Tribolium* embryos. (A-F) Embryos injected with mRNA encoding H2B-RFP (A-C) at a concentration of 1 $\mu\text{g}/\mu\text{l}$, or (D-F) at a concentration of 3 $\mu\text{g}/\mu\text{l}$, shown at different times after injection. Representative embryos for each condition and time-point were imaged on an epifluorescence microscope using identical settings. Injection of the high mRNA concentration consistently produces a stronger fluorescent signal than the low concentration. (A, D) One hour post injection, weak fluorescence is detected in a fraction of preblastoderm nuclei. (B, E) A more homogeneous and stronger fluorescence is detected two hours post injection. (C, F) Three hours post injection, ubiquitous, uniform and strong fluorescence is detected in all nuclei across the entire embryo. Note dividing nuclei at posterior in (F). All images were captured at multiple focal planes that were combined into a single focused image using the Helicon Focus software. Anterior is to the left. Scale bar is 100 μm .

To image cell outlines, I first tested two fusion constructs that had been used successfully to mark cell outlines in *Drosophila*, one of which was supplied by Anastasios

Pavlopoulos, the other I cloned from *Drosophila* genomic DNA (see “2. Materials and methods”). Each construct (myr-RFP and myr-tdTom) combines a fluorescent protein with a myristoylation signal, which should cause the fusion protein to be localized to the membrane. Surprisingly, following microinjection of mRNA for either construct (as described for H2B-RFP), the fluorescent signal that was visible in either the blastoderm or the germband was diffuse and non-localised (not shown).

Next, I tested a fusion construct called GAP43-YFP that was originally created in zebrafish (Rembold et al., 2006), but has also been shown to work in *Drosophila* (Mavrakis et al., 2009) and the polychaete worm *Platynereis dumerilii* (D. Arendt and M. Handberg-Thorsager, personal communication). This fusion protein gets anchored to lipids of the inner surface of plasma membranes via the GAP43 palmitoylation signal (Mavrakis et al., 2009).

When *Tribolium* eggs were injected with capped mRNA encoding GAP43-YFP (as described above for H2B-RFP), the expressed fusion protein cleanly labelled cell outlines, marking both the apical and basolateral domains of forming cells in blastoderm stage embryos (Fig. 3.2 (C-C’’)). The expression kinetics and survival rates were comparable to those observed following injection of H2B-RFP (Table 3.1). By injecting a mixture of the mRNAs encoding the H2B-RFP and GAP43-YFP fusion proteins, I was able to label both the nuclei and the cell borders of the same embryo and carry out two-channel live imaging of *Tribolium* embryogenesis (Fig. 3.2 (D-D’’)). Using 3 $\mu\text{g}/\mu\text{L}$ total mRNA (see “2. Materials and methods), the expression kinetics and survival rates were comparable to individual injections of either H2B-RFP or GAP43-YFP at the equivalent concentrations.

To image filamentous actin (F-actin) cytoskeleton, I fused the LifeAct motif (Riedl et al., 2008) to the coding sequence of EGFP (construct hereafter called LA-GFP). The LifeAct motif has been shown to encode a peptide that reversibly binds to F-actin in several animals, without affecting normal F-actin dynamics (Riedl et al., 2008). Prior to blastoderm formation, *Tribolium* exhibits an extensive cortical actin network (personal observation), and therefore, I injected capped mRNA for LA-GFP 2-3 hours after egg lay at 3 $\mu\text{g}/\mu\text{l}$. Weak diffuse fluorescence was visible 3 hours after injection, and 6 hours after injection uniform cortical expression was detected in 70% of eggs (Table 3.1 and Fig. 3.2 (E-E’’)). Survival rates were comparable to those observed for all other constructs (Table 3.1).

Lastly, contractions of non-muscle myosin II have been shown to be a major driving force of morphogenesis in *Drosophila* (Martin et al., 2009), and therefore, I was interested to develop a marker for myosin in *Tribolium*. In *Drosophila*, myosin dynamics are visualised through the use of a transgenic line that has a fluorescent protein fused to the *spaghetti-*

squash gene (the myosin regulatory light chain) (Royou et al., 2002; Royou et al., 2004). I made a similar fusion protein by fusing the coding sequence of the *Tribolium Spaghetti-squash* ortholog with GFP to generate Sqh-GFP. Unfortunately, following microinjection of capped mRNA, the only visible fluorescent signal was diffuse and non-localised.

Table 1. Overview of *Tribolium* embryo injection and transient fluorescence labelling

Treatment	No. embryos injected	No. embryos survived 24 hpi ¹	No. fluorescent embryos			No. embryos with uniform fluorescence	
			1 hpi ¹	2 hpi ¹	3 hpi ¹	3 hpi ¹	6 hpi ¹
Non-injected	200	156	0	0	0	0	0
Buffer-injected	200	159	0	0	0	0	0
H2B-RFP	200	153	103	186	196	121	N/A
GAP43-YFP	200	122	192	196	197	92	N/A
H2B-RFP/ GAP43-YFP	200	148	N/A	N/A	N/A	N/A	N/A
LA-GFP	200	126	N/A	N/A	140	N/A	140
ABP-tdEosFP ²	200	119	N/A	N/A	128	N/A	0 ²

¹ hpi, hours post injection.

² ABP-tdEosFP produced heterogeneous fluorescent patterns, probably due to the binding properties of the protein in *Tribolium*. A bright spot of fluorescence was always visible near the injection site (either in the yolk or cortical layer) that diminished over time.

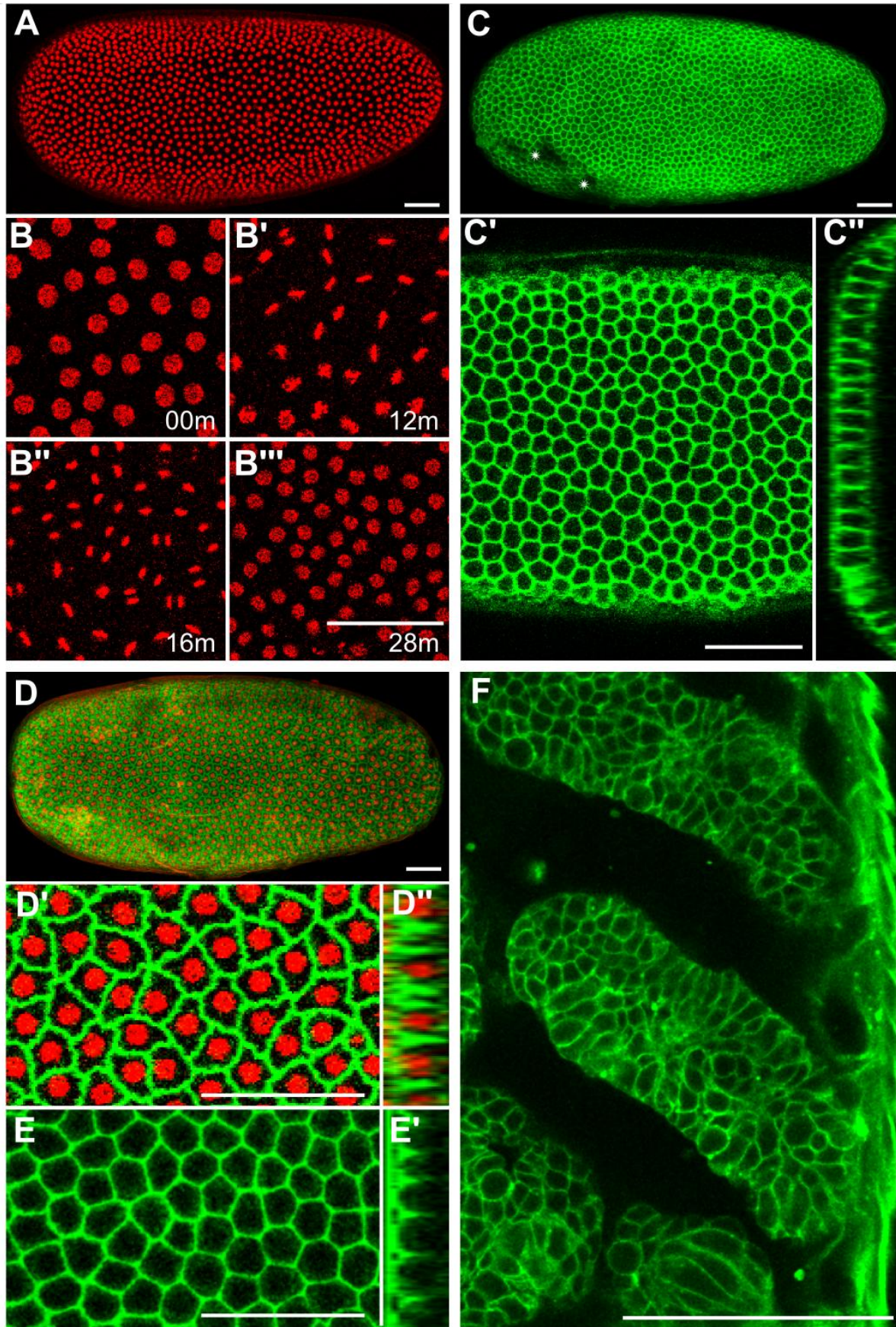


Fig. 3.2. Fluorescence labelling of *Tribolium* embryos with nuclear, membrane and actin markers. (A) Average intensity projection of a blastoderm labelled with H2B-RFP. (B-B'') Time series of H2B-RFP-labeled chromatin (B) before, (B'-B'') during and (B'') after the synchronous 12th mitotic division. Single optical slices are shown timed against (B). (C-C'') Uniform blastoderm labelled with GAP43-YFP: (C) Average intensity projection of the entire embryo, (C') single optical slice and (C'') transverse section that shows labelling of the entire membrane surface. Asterisks in C denote blemishes on the vitelline membrane locally impairing fluorescent signal. (D-D'') Embryo at the uniform blastoderm stage with H2B-RFP-labeled nuclei and GAP43-YFP-labeled membranes: (D) Average intensity projection, (D') optical slice and (D'') transverse section. (E-E') Uniform blastoderm labelled with the actin marker LA-GFP: (E) Single optical slice and (E') transverse section showing cortical actin fluorescence around the apical surface. (F) Single optical slice through two developing thoracic limbs and the pleuropod of an embryo 48 hours after injection with GAP43-YFP mRNA. Anterior is to the left in most panels, except in cross-sections (C''), (D'') and (E') where apical is to the left, and in (F) where the ventral midline is to the left and anterior is to the top. Scale bars are 50 μ m.

3.2.2 Persistence of expression of fluorescent reporters

I examined the persistence of the transiently expressed fluorescent reporters by injecting pre-blastoderm eggs with capped mRNA for GAP43-YFP at 3 μ g/ μ L, and incubating the eggs at 32°C in a dark and moist environment. I periodically checked expression levels on an epifluorescence microscope. Similar to previous experiments, most eggs exhibited uniform expression at the blastoderm stage. 24 hours after injection, however, considerable variability in expression levels was detected between embryos. Secondly, the levels of fluorescence sometimes varied within the same embryo with some germbands exhibiting stronger expression in the anterior of the germband. Rarely, I observed unilateral expression in a germband.

The levels of fluorescence began to diminish in all embryos about 48 hours after injection, yet cell outlines were still clearly visible on a confocal microscope (Fig. 3.2 (F)). Despite the observed variability, many eggs exhibited bright, uniform, and persistent fluorescence, suggesting that transient labelling methods can be applied for *Tribolium* live imaging until at least 48 hours post injection.

3.2.3 Transient expression of a photo-convertible marker in *Tribolium*

One of the downsides of this transient expression approach is that it is not possible to specifically label individual cells. Having this ability would greatly facilitate cell tracking during the major cell movements and tissue rearrangements observed during *Tribolium* embryogenesis. With this goal in mind, I tested whether it is possible to mark specific cells by using photo-convertible fluorescent proteins. I employed a construct that combines an actin-binding peptide (ABP) with a tandem Eos fluorescent protein (tdEosFP; Izeddin et al., 2011). ABP-tdEosFP is designed to bind reversibly to F-actin cytoskeleton and can be converted from the “green form” to the “red form” upon illumination with a 405nm laser.

As described for the other constructs above, I synthesized and injected capped mRNA encoding ABP-tdEosFP into *Tribolium* eggs 4-6 hours after egg lay at 3 $\mu\text{g}/\mu\text{L}$ and 1 $\mu\text{g}/\mu\text{L}$. One hour after injection, specific labelling of the cortical actin layer became visible in the region near the injection site. A bright spot of fluorescence (normally in the yolk) was also visible near the injection site. Over the following hours, the fluorescent signal near the injection site became brighter, while the spot of fluorescence in the yolk became weaker. After 3-5 hours, however, no eggs exhibited uniform expression.

To attempt to overcome the problem of non-uniform expression, I injected mRNA earlier during embryogenesis, 2-3 hours after egg lay. This approach gave similar results to those already described. Six hours after injection, however, expression was visible in all blastoderm cells (Table 3.1), allowing any part of the blastoderm to be imaged. Furthermore, I was able to generate patches of cells differentially labelled to their neighbours by photo-converting ABP-tdEosFP from the green to the red fluorescent form in the blastoderm (Fig. 3.3 (A-A’’)). Survival rates were comparable to those following injection of other constructs (Table 3.1).

I also wanted to test the lifetime of the photo-converted form of ABP-tdEosFP. To do this, I illuminated a single limb bud of a developing embryo with the 405nm laser 26 hours after injection and photo-converted almost all of the fluorescent protein (Fig. 3.3 (B-B’’)). 48 hours after injection, the red photo-converted form of ABP-tdEosFP was at high enough levels to see labelling of the growing limb (Fig. 3.3 (C’-C’’)). The same limb was also labelled with green unconverted ABP-tdEosFP that must have been newly synthesized in the meantime since photo-conversion (Fig. 3.3 (C)). This result shows that the injected mRNA is present at sufficient levels for strong expression for more than 24 hours.

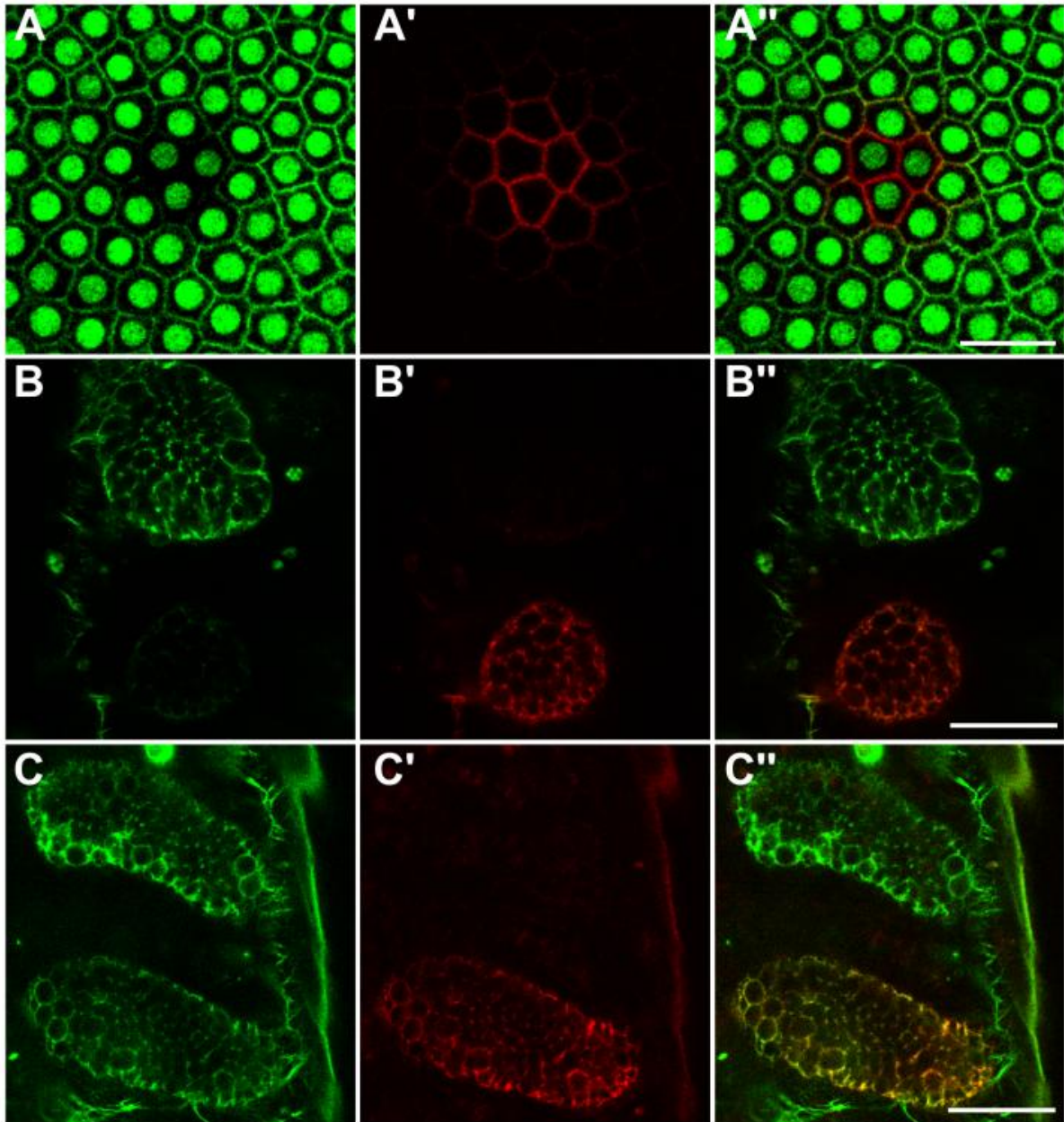


Fig. 3.3. Fluorescence labelling of *Tribolium* embryos with photoconvertible ABP-tdEosFP. (A-A'') Optical sections through the blastoderm of a transgenic embryo ubiquitously expressing nuclear GFP (Sarrazin et al., 2012), which was injected with ABP-tdEosFP mRNA and photoconverted in the central region. (A) nGFP and unconverted ABP-tdEosFP fluorescence detected at similar levels in the green channel, (A') photoconverted ABP-tdEosFP fluorescence detected in the red channel, and (A'') overlay of the two channels. (B-B'') Optical sections through developing limb-buds of an embryo 26 hours after injection with ABP-tdEosFP mRNA. Most of the protein in the bottom limb-bud has been photoconverted: (B) Green channel showing unconverted ABP-tdEosFP, (B') red channel showing converted ABP-tdEosFP, and (B'') overlay of the two channels. (C-C'') Optical

sections through the same limbs shown in B-B'' 22 hours later. Both green unconverted and red converted ABP-tdEosFP are detected in the photoconverted limb. Anterior is to the top in all panels, and ventral midline is to the left in B-C''. Scale bars are 25 μ m.

3.2.4 Transient expression in *Drosophila*

After finding that this method works in *Tribolium*, I decided to test the method in *D. melanogaster*, which develops much faster than *T. castaneum*. Although several transgenic lines are available for live imaging in *D. melanogaster* itself, a transient labelling method would still be useful for other *Drosophila* species with limited live imaging resources. I injected mRNA encoding H2B-RFP into 1-3 hour old *D. melanogaster* embryos. Expression of the construct was visible within 2 hours, and became stronger and more uniform over the following hours (Fig. 3.4). However, the strength of the fluorescent signal was weaker than what I observed in *Tribolium*. Furthermore, I did not observe uniform expression in any embryos.

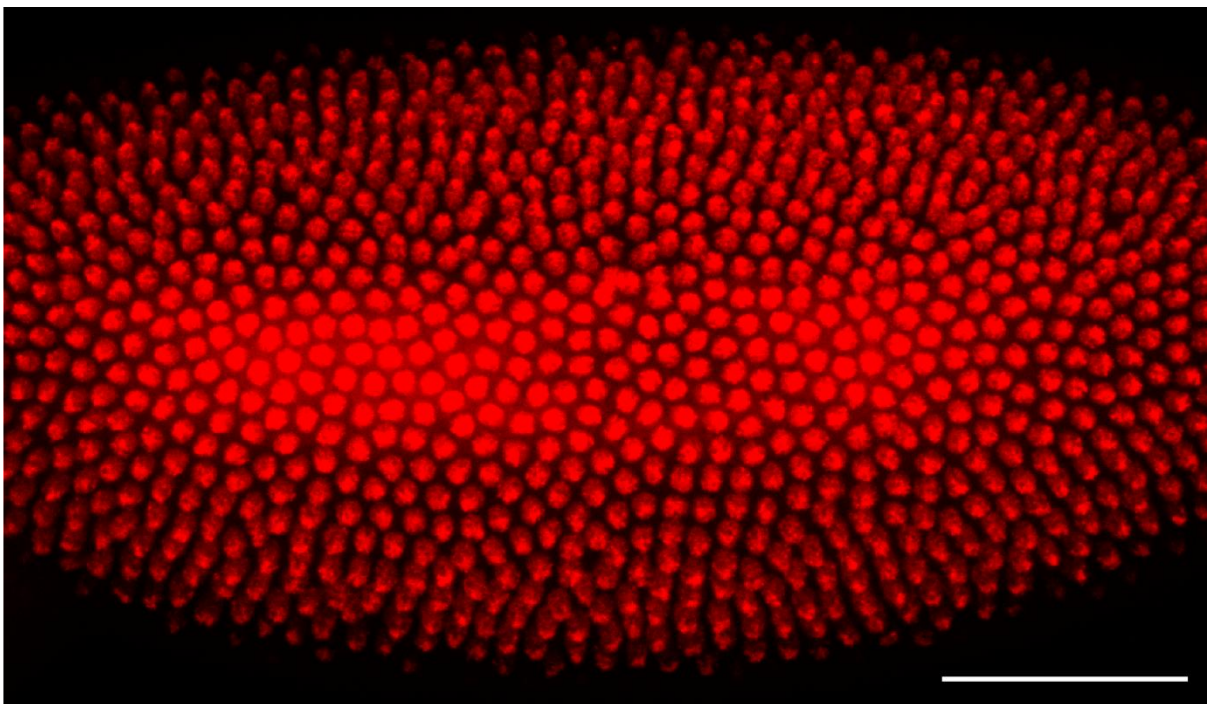


Fig. 3.4. Transient expression of H2B-RFP in *D. melanogaster* blastoderm, 3 hours post injection. Image is average projection of a z-stack. Anterior is to the left. Scale bar is 50 microns.

3.2.5 Transient expression via DNA injection

I was also interested to see whether the microinjection of plasmid DNA (encoding a fusion protein downstream of a promoter) into *Tribolium* embryos would result in mosaic

expression, as observed in zebrafish (Hatta et al., 2006). To test this, I combined the GAP43-YFP fusion construct with the ubiquitous *Tribolium* EFA promoter (Sarrazin et al., 2012). I then co-injected this plasmid DNA into 2-3 hour old eggs at 50ng/ μ L (as is used in zebrafish), with capped mRNA for H2B-RFP at 3 μ g/ μ L (to allow visualization of the embryonic/extraembryonic nuclei).

Approximately 6 hours after injection, broad uniform expression of the marker could be seen in the blastoderm of less than half the eggs (Fig. 3.5 (A)). The strength of the fluorescence varied between eggs, but was never as strong as after injection of capped mRNA. During later stages of development, expression was strong and ubiquitous in the yolk and the serosa (Fig. 3.5 (B-C)). In the germband, however, expression was only strong in a handful of scattered cells and was weak or absent in most cells (Fig. 3.5 (B-C)).

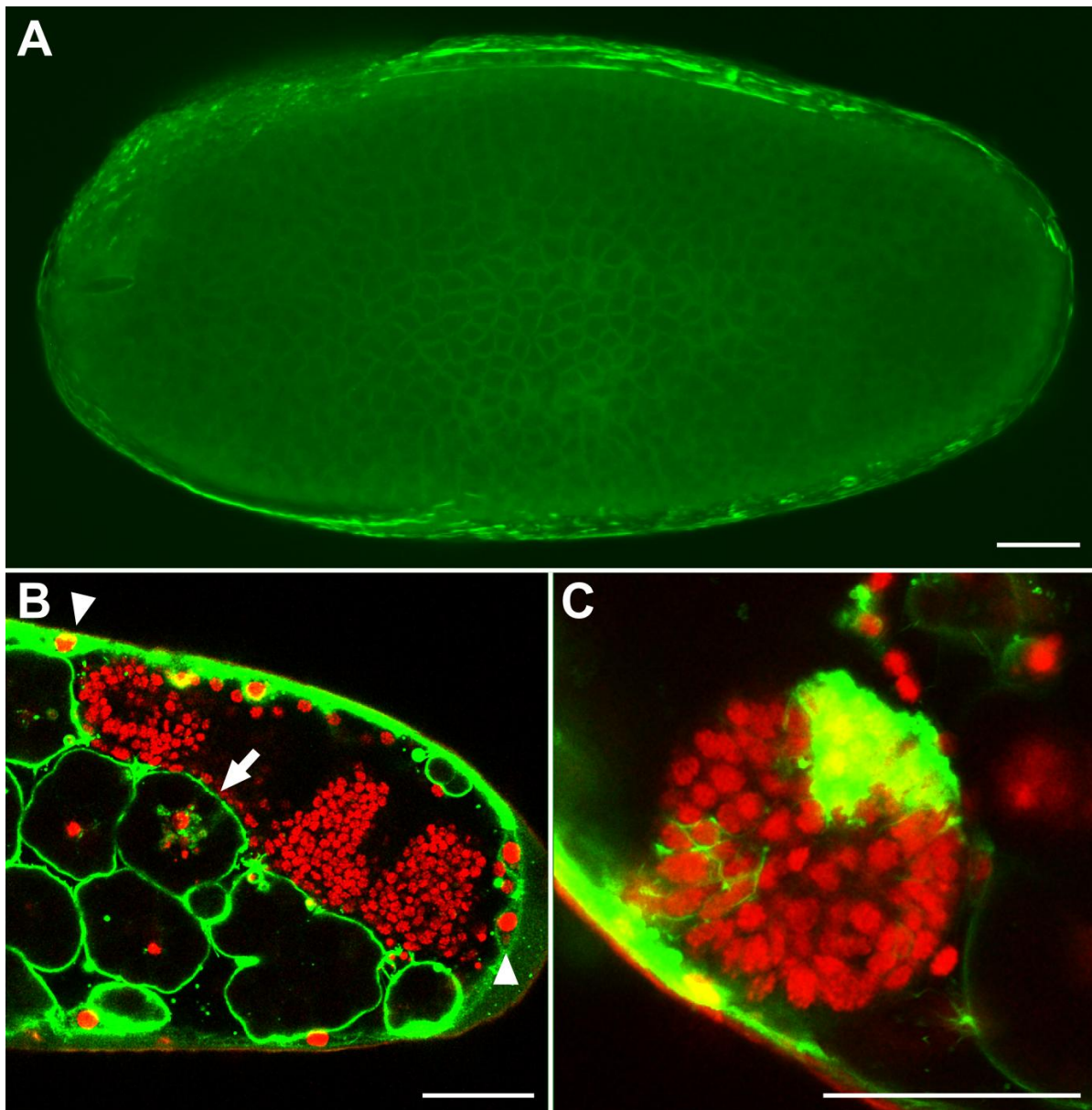


Fig. 3.5. Transient expression of EFA-GAP43-YFP DNA and H2B-RFP mRNA. (A) Embryo showing weak expression of GAP43-YFP 5.5 hours after injection. Image is a maximum focus projection of a stack taken on a compound microscope. (B) Optical section through posterior region of egg 31 hours post injection. Green shows uniform GAP43-YFP labelling of the membrane surrounding the yolk spheres (arrow) and ubiquitous but not uniform labelling of the serosa cells (compare expression levels of two serosa cells marked with arrowheads). Red shows uniform H2B-RFP labelling of germ band, serosa and yolk nuclei. (C) optical section of an anterior appendage of same embryo as shown in (B). Green shows mosaic GAP43-YFP labelling of cells in the appendage. Red shows uniform H2B-RFP labelling of nuclei. Scale bars are 50 μ m.

3.3 Discussion

3.3.1 Transient expression in *Tribolium*

I have here shown that transient expression of injected mRNA can be used in *Tribolium* for strong, ubiquitous and uniform labelling of different cellular components. The same approach also works in *Drosophila*, although the resulting fluorescence is weaker than in *Tribolium* and is non-uniform at the blastoderm stage. In *Tribolium*, I was able to observe strong fluorescent signal of fusion proteins less than an hour after injection, even in pre-blastoderm stage embryos. This means that the embryonic energids have the potential to translate mRNA into protein several hours before the mid-blastula transition, which likely occurs after nuclei reach the surface of the egg.

3.3.2 Problems with the fusion constructs

Out of the tested constructs, three resulted in non-specific, diffuse fluorescent signal. For two of these constructs (myr-RFP and myr-tdTOM), the protein fragment that was supposed to drive localisation comes from *Drosophila*, and it may be the case that this fragment does not work in *Tribolium* cells. For the third construct (Sqh-GFP), the protein that was supposed to drive localisation comes from *Tribolium*, and it is therefore surprising that this construct did not work. As the native Sqh protein is part of a multi-protein complex, it may be that a Sqh-GFP fusion protein needs to be provided maternally. A fourth construct (ABP-tdEosFP) labelled F-actin as expected, but did not label the blastoderm uniformly as was observed for the other F-actin marker (LA-GFP). This is very surprising, as the ABP peptide is almost

identical to the LifeAct peptide. I had assumed that it was the uniform diffusion of mRNA in the egg that resulted in uniform expression across the blastoderm. This result might suggest, however, that protein diffusion also plays a role, and for some reason the ABPtdEosFP fusion protein does not diffuse as freely as the other proteins.

3.3.3 Application of transient expression to other arthropods

Both transient expression for live imaging, and the fusion protein constructs I have used have been shown to work in multiple animals by myself and by other groups (Izeddin et al., 2011; Riedl et al., 2008; D. Arendt, personal communication; A. Pavlopoulos, personal communication). The approach for live imaging presented here should, therefore, be readily applicable to the embryos of other arthropods. If this proves to be true, it will greatly decrease the time required to characterise different aspects of embryogenesis in non-model animals. Furthermore, it will facilitate the study of comparative morphogenesis in diverse animals, or in groups of closely related species.

One example where this may be useful is with different *Drosophila* species. Although genomic and molecular biology techniques exist for several different *Drosophila* species, there is a significant lack of live imaging tools in species other than *D. melanogaster*. Using the constructs and the approach presented here, it should be possible to carry out live imaging quickly and easily in a range of different species. This would make it possible to study micro-evolutionary changes in embryonic morphogenesis in a way that has not been possible before.

There are two major obstacles to applying transient expression for live imaging to non-model species. The first of these is the ability to microinject embryos at an early stage without causing morphological defects. If it is not possible to inject prior to cellularization (as is currently the case in the spider *P. tepidariorum*), it may not be possible to achieve ubiquitous expression of a fluorescent marker. One way around this would be to utilise liposomal transfection reagents, such as DOTAP (Yasuda et al., 2005), which has been shown to allow transfection of RNA into insect cells in culture (Meyer et al., 1994). This obstacle also needs to be overcome for transgenic approaches, and therefore, needs to be established for either fluorescent live imaging approach.

The second obstacle is delivering sufficient levels of mRNA into embryos to achieve strong expression of the construct. This proved not to be a problem for *Tribolium* eggs, which are comparable in size to those of *Drosophila*. Other arthropods with much larger eggs may

pose more of a problem, however, and it may be necessary to perform multiple injections into the same egg.

3.3.4 Transient expression via DNA injection

I found that injection of plasmid DNA encoding a fluorescent marker downstream of a promoter resulted in early broad expression, followed by mosaic expression in the germband. The early ubiquitous expression suggests that the plasmid DNA is initially active everywhere (although diffusion of protein and mRNA is likely to also be occurring). If true, this means microinjection of plasmid DNA could be useful for identifying promoter elements that are active at the blastoderm stage.

At later stages, expression became mosaic in germbands, which suggests the plasmid is being silenced in or lost from the majority of cells. Despite this mosaicism, microinjection of plasmid DNA may still be useful as a first step in identifying germband stage promoters. For example, it would be easy to inject several hundred eggs and screen for fluorescence in the region of interest. If any cells show fluorescent expression, the putative promoter could then be used to generate transgenic animals for further analysis.

In the serosa cells and the yolk spheres, fluorescence remained ubiquitous, although the fluorescence was stronger in some serosa cells than others. The ubiquitous fluorescence in the serosa cells is likely left over from the blastoderm stage. Serosa cells do not seem to divide at all from when they are specified at the blastoderm stage (see “5. A live imaging study of germband condensation”), and therefore, the initial fluorescence would not be diluted. The cells with stronger fluorescence are likely those in which the plasmid had not been silenced. The expression in the yolk spheres can be explained by the fact that for much of the time from the blastoderm stage onwards, each yolk sphere is a single large multinucleated cell. Expression in a few energids would therefore be shared across the whole cell. At the stage shown in Fig. 3.5 (B), the yolk has become cleaved into yolk spheres, however, these may still be connected in the centre of the egg (Also see “4. Cellularisation in *Tribolium* – a more widely conserved mode than *Drosophila*?”).

3.3.5 Other applications of transient expression

Traditionally, transient expression in *Drosophila* has been used for the over-expression of native genes (Chasan and Anderson, 1989). I have not yet tried this in *Tribolium*, but I predict that it should work just as easily as transient expression of fluorescent protein constructs. If

this proves to be true, it opens up a wide avenue of new possibilities for genetic manipulation of non-model species. First of all, it would be possible to co-inject capped mRNA for a native gene and for a fluorescent construct to allow simultaneous over-expression of genes and live imaging. This would be a complementary approach to the concurrent RNAi and transient expression of fluorescent markers that I have found to work in *Tribolium* (see “4. Cellularisation in *Tribolium* – a more widely conserved mode than *Drosophila*?” and “5. A live imaging study of germband condensation”). Secondly, it may be possible to carry out simultaneous RNAi knock-down of a gene, and overexpression of a different gene, or even a mutated form of the same gene (if the dsRNA was designed to match the transcribed but non-translated regions of the gene to be knocked-down). These more advanced manipulations would allow fine scale analysis of genetic networks.

A key limitation of the transient expression approach is the inability to modulate the function of the injected mRNA in a temporal and spatial manner. I have overcome this problem for the live imaging by testing a photo-convertible marker. One way to overcome this for overexpression or RNAi knock-down of native genes would be to chemically cage the RNA molecules prior to injection, then specifically un-cage the RNA in the region of interest using laser irradiation (Ellis-davies, 2007). To allow visualisation of the embryonic tissue and confirm the specificity of the un-caging, the caged RNA could be co-injected with non-caged mRNA for a photo-convertible marker such as that used here, ABPtdEosFP.

4. CELLULARISATION IN *TRIBOLIUM* – A MORE WIDELY CONSERVED MODE THAN *DROSOPHILA*?

4.1 Introduction

In arthropod embryos, there is huge diversity in the mechanism and timing of cell formation and cell division. Despite this diversity, we only have molecular data on cellularisation in a handful of species, and almost everything we know about the process comes from the studies in *Drosophila*. As discussed in a later section, several aspects of *Drosophila* cellularisation are not representative of insects in general. I was therefore interested to study how cellularisation occurs in *Tribolium* and to compare my findings with what is known from *Drosophila*.

The different modes of cellularisation can be broadly separated into two classes. The first class is called holoblastic cleavage, whereby nuclear division is accompanied by complete cytokinesis. The other class is called meroblastic cleavage, and it refers to situations where nuclear division is not accompanied by cytokinesis, resulting in a multi-nucleated egg cell. While holoblastic cleavage is normally considered the ancestral state for arthropods, both classes seem to be present in basal arthropods and panarthropods (Anderson, 1973). Therefore, it is not possible to determine which represents the ancestral state for the phylum.

4.1.1 Holoblastic cleavage

In this work I am using the term holoblastic cleavage in the strictest sense, such that only eggs which undergo complete cytokinesis from the first nuclear division onwards are included. Under this definition, holoblastic cleavage is observed in many animal lineages, and the specific pattern of cleavage has long been used as a defining phylogenetic character (for a recent review see Hejnol, 2010). The patterns of cleavage in arthropods have been used to try and discover whether the sister lineage to the Panarthropoda is the Cycloneuralia (“Ecdysozoa hypothesis”) or Annelida (“Articulata hypothesis”, Alwes and Scholtz, 2004). Modern molecular approaches have now shown that the sister lineage to Panarthropoda is the Cycloneuralia (Telford et al., 2008), a situation that is supported by the lack of true spiralian cleavage in arthropods.

Some members of all non-insect arthropod lineages exhibit holoblastic cleavage, including the non-insect hexapods (Anderson, 1973). Examples of holoblastic cleavage are most common for the crustaceans, where the process is best studied (Anderson, 1973; Browne et al., 2005). Amongst the myriapods, several lineages have been described to undergo holoblastic cleavage, for example the diplopods, symphylans and pauropods (Anderson, 1973). In some of these yolk rich eggs, cleavage occurs in a modified way such that not all blastomeres contain nuclei (e.g. *Hansaniella agilis*, Anderson, 1973). In the most basal arthropod lineage, the chelicerates, holoblastic cleavage is found in several groups, including mites (e.g. *Caloglyphus*, Anderson, 1973) and the viviparous scorpions (e.g. *Heterometrus scaber*, Anderson, 1973).

4.1.2 Meroblastic cleavage

In the strict usage of meroblastic cleavage, the class includes all eggs that do not exhibit complete cytokinesis from the first nuclear divisions. Using this definition, meroblastic cleavage can be observed in all arthropod lineages in a variety of forms (Anderson, 1973). Another way of describing meroblastic cleavage is to say that it is the growth of membranes in between more than two nuclei. This growth of membranes is the process that we term cellularisation.

The most common starting point for animals exhibiting meroblastic cleavage is for the energids to be located within the yolk, where they undergo synchronous divisions without being separated by a plasma membrane (intralecithal divisions). At this point, the embryo can be thought of as a large multinucleated cell. From this stage, development can proceed in a number of ways. At one end of the spectrum, the energids remain within the yolk and membrane ingresses from the surface to compartmentalise the yolk and energids. This compartmentalisation can result in pyramid like structures, as seen in the spider *Parasteatoda* (formerly *Achaearanea*) *tepidariorum*, which cellularises sometime around the 8-16 nuclei stage (Kanayama et al., 2010; Mittmann and Wolff, 2012) and the centipede, *Strigamia maritima* (Brena and Akam, 2012). In the centipede, however, it is unclear whether the compartments also contain nuclei.

At the opposite end of the spectrum, energids migrate to the surface of the egg, where membrane ingresses and separates the energids from each other and from the underlying yolk, thereby forming a cellularised blastoderm overlying a large yolk cell. This is what occurs in the vast majority of insects (described in later sections).

A large number of variations exist between these two extremes. The most comprehensive review of arthropod cleavage patterns is Anderson (1973). Unfortunately, very little work has been carried out on cleavage/cellularisation in non-insect arthropods using molecular tools.

4.1.3 Involvement of the yolk across all forms of cleavage

Although it is not the focus of this study, some attention needs to be paid to the role that yolk plays in cleavage/cellularisation. Most arthropod eggs are characterised as containing a high amount of yolk when they are laid. This yolk allows the embryo to develop without any external nutrients. Furthermore, yolk often persists in larvae, allowing them to survive for a long time after hatching without needing to feed. For example, centipede larvae can develop for 2 months and pass through three moults with only their internal yolk store (C. Brena and M. Akam, unpublished). However, densely packed yolk may inhibit cytokinesis, and therefore, high levels of yolk has been suggested as the reason why many arthropods undergo meroblastic cleavage (Anderson, 1973). Whether this is true or not, the yolk of embryos can behave quite independently to the energids.

At some point, the embryos of most arthropods reach a blastoderm stage, defined as a cellular epithelium overlying a yolk mass, and this can be seen as a landmark stage. How this stage is reached, however, varies greatly. In embryos that have undergone holoblastic cleavage, the yolk is usually distributed amongst the blastomeres, a situation which is typified by the amphipod crustacean, *Parhyale hawaiiensis* (Browne et al., 2005). This animal exhibits total cleavage in the early stages, and yolk is found in all blastomeres (Browne et al., 2005). From the 8-cell stage onwards, however, divisions become asynchronous, and yolk becomes segregated to the centre of the egg while nucleated cells become smaller and situated at the surface of the egg (Browne et al., 2005). Following this segregation, very few nuclei are visible in the centre of the egg, and surface cells are largely devoid of yolk (Browne et al., 2005). In *Parhyale*, it has not been shown whether the yolk mass is made up of multiple blastomeres, or whether they become fused into one yolk cell, as has been described for other crustaceans (e.g. *Palinurus japonicas*, Anderson, 1973). In other crustaceans, yolk is segregated into a specific blastomere from the first division onwards (e.g. *Tetraclita rosea*, Anderson, 1973)

In embryos that have undergone meroblastic cleavage, it is also possible for yolk to be distributed amongst the blastomeres, for example as seen in *P. tepidariorum* (Mittmann and

Wolff, 2012). When cellularisation occurs in this animal, each nucleus and its surrounding cytoplasm is located in a large mass of yolk, and there is also a central mass of membrane bound yolk that does not seem to contain nuclei or cytoplasm (Kanayama et al., 2010). As development proceeds and cells divide, the nuclei and their cytoplasm migrate to the surface of the egg, and yolk is somehow segregated to the centre, perhaps in a similar way to what is seen in *Parhyale*.

In the typical insect mode of cellularisation, the yolk is segregated to the centre of the egg prior to cellularisation (see next section). However, some energids remain in the yolk as vitellophages, where they are thought to digest the yolk. During later stages of embryogenesis in many insects, the yolk becomes cleaved into compartments called “yolk spheres” (Anderson, 1972a; Anderson, 1972b). This cleavage is reminiscent of cell cleavage that is seen in other arthropods. Yolk spheres are usually transient structures, and their purpose is unknown. It is important to note that these yolk spheres are not the same thing as what has been referred to as “yolk spheres” in *Drosophila* (for example in Reed et al., 2004) After dorsal closure, remaining yolk is engulfed by the gut and digested therein.

4.1.4 Cellularisation in hemimetabolous insects

Except for some parasitic hymenoptera, all insects that have been looked at cellularise by membrane ingression after nuclei and their surrounding cytoplasm have migrated to the surface of the egg (Counce, 1961). However, the process of cellularisation in the hemimetabolous insects is more diverse than in the holometabolous insects. For example, in some hemimetabolous insects, such as the damselfly *Platycnemis pennipes*, energids emerge at the surface in a uniform distribution across the egg (Anderson, 1972a). In other hemimetabolous insects, such as the locust *Schistocerca gregaria*, energids emerge at the surface of the egg in a polarised fashion, with a higher concentration of energids at the posterior of the egg (Ho et al., 1997). This pattern is further modified in some hemimetabolous insects, such as the termite *Kaloterme flavicollis*, in which energids emerge at a higher density at the position of the future germ rudiment and cellularise immediately, thereby forming a differentiated blastoderm (Anderson, 1972a).

Another difference found in some hemimetabolous insects relates to whether energids are in contact with each other prior to cellularisation. In some hemimetabolous insects, such as *Rhodnius prolixus*, when nuclei emerge at the surface of the egg they form a continuous layer of cytoplasm, known as a syncytial blastoderm (Anderson, 1972a). Membrane then

ingresses between nuclei, and closes basally to form a cellularised blastoderm (Anderson, 1972a). In other hemimetabolous insects, again exemplified by *Schistocerca gregaria*, energids are scattered across the egg surface when they cellularise, and therefore, no syncytial blastoderm stage exists (Ho et al., 1997).

4.1.5 Cellularisation in holometabolous insects

In holometabolous insects, energids usually emerge at the surface of the egg in a uniform distribution. In some species, energids do emerge in a polarised pattern, however, a uniform distribution is always formed prior to any further divisions (Anderson, 1972b). When nuclei first emerge they may be located some distance from each other, but they do share a common cytoplasm, and therefore, exist in a syncytial environment. This syncytial blastoderm is a key characteristic of holometabolous insects (Anderson, 1972b). As development proceeds, several rounds of more or less synchronous nuclear divisions take place at the surface of the egg. At some point during, or after, these divisions, membrane begins to ingress between the nuclei. After the last synchronous division, the membrane closes basally, thereby completing cellularisation.

In most holometabolous insects (and hemimetabolous insects that have a uniform blastoderm), the uniform cellularised blastoderm is made up of cuboidal cells. Irrespective of germband type, the cells that are fated to become the embryo proper undergo a cuboidal to columnar shift during germband formation (for more information on this process see “5. A live imaging study of germband condensation”). In dipterans, however, all cells of the blastoderm are already columnar when cellularisation is complete, reflecting the greater proportion of cytoplasm as opposed to yolk in the egg (Anderson, 1973). This situation is exemplified in the fruit fly, *Drosophila melanogaster*, which is also the arthropod species in which cellularisation has been most thoroughly studied in (see next section).

4.1.6 Cellularisation in *Drosophila*

In *Drosophila* embryos, nuclei reach the surface of the egg after 10 rounds of division (Mazumdar and Mazumdar, 2002). Upon reaching the surface, nuclei undergo several more rounds of division and cellularisation is completed at nuclear cycle 14 (Mazumdar and Mazumdar, 2002). Membrane begins invaginating during the first mitosis after nuclei reach the surface, however, ingressed membrane almost completely retracts to the surface during the following interphase (Daniels et al., 2012). This process repeats with each division until

nuclear cycle 14 (Daniels et al., 2012). These transient furrows are called metaphase furrows, and they are required for the proper separation of chromosomes during mitosis (Kotadia et al., 2010). Metaphase furrows are not normally considered part of the cellularisation process.

At the beginning of nuclear cycle 14, very shallow membrane furrows are visible at the surface of the egg (Daniels et al., 2012). From this starting point, membrane invaginates between nuclei then closes off basally to form a cellularised blastoderm. This process of cellularisation has been separated into four phases (reviewed in Harris et al., 2009; Lecuit, 2004; Mazumdar and Mazumdar, 2002), although these four phases are sometimes referred to simply as the slow phase (phases 1-3) and the fast phase (phase 4). During phase 1, adherens junctions form near the top of the invaginated membranes and nuclei begin elongating in the apical-basal axis as membrane ingresses. From this stage, the base of the invaginating membrane is referred to as the furrow canal. During phase 2, membrane continues to ingress, and nuclei complete their elongation. During phase 3, membrane continues to ingress at a slow rate (0.3 $\mu\text{m}/\text{minute}$) until it reaches the basal ends of the nuclei. During phase 4, the rate of membrane ingression more than doubles (0.8 $\mu\text{m}/\text{minute}$), and continues until it reaches a depth of around 35 μm . At this point, membrane ingression stops, and furrow canals split tangentially to seal off the bases of cells, thereby completing cellularisation.

The process of cellularisation involves a number of cytoskeletal components. Before membrane invagination even begins, an extensive microtubule network exists around each nucleus, setting up the basic cell architecture. The main driving force for membrane invagination now seems to be the specific trafficking of membrane vesicles from the golgi apparatus. Lastly, basal closure of membrane is driven by the contraction of F-actin rings, which are connected to the furrow canals.

4.1.7 Can information about *Drosophila* cellularisation be applied to other arthropods?

Although we now have a vast amount of information about cellularisation in *Drosophila*, we do not know how applicable it may be to other insects, let alone other arthropods. First of all, it is known that making a columnar blastoderm during cellularisation (as *Drosophila* does) is a derived trait of dipterans (Anderson, 1973), and we have no way of knowing how this transition has affected cellularisation and basal cell closure. Secondly, we do not have enough detailed information about the dynamics of membrane ingression in other insects to determine if metaphase furrows are conserved elsewhere. Lastly, very little research has been

done on the yolk system in *Drosophila*, and the cleavage of yolk into spheres after blastoderm formation has not been reported. For each of these reasons, it would be informative to be able to study cellularisation in an insect that retains more ancestral characters, including a cuboidal blastoderm, and yolk cleavage.

With this goal in mind, I set out to study cellularisation in *Tribolium castaneum*, which is known to have a blastoderm made up of cuboidal cells (Handel et al., 2000). To achieve this, I used several of the transient labelling tools described in chapter one for live imaging of membrane and actin dynamics. I was also interested to see if the yolk of *Tribolium* is cleaved into yolk spheres, which would make this animal a good system for studying this process. The study of blastoderm cellularisation was carried out in collaboration with Maurijn van der Zee as part of a larger project (van der Zee *et al.*, manuscript in prep.). In this chapter I will present work that I was directly involved in, as well as some necessary background information that M.v.d. Zee gathered.

4.2 Results

4.2.1 Membrane ingression

To visualise the timing of membrane ingression in relation to when nuclei reach the surface of the egg, I performed live imaging on nGFP embryos that had been injected 2-3 hours after egg lay with mRNA encoding GAP43-YFP. Instead of using the nGFP line, I could have co-injected H2B-RFP with GAP43-YFP to label the nuclei. Confocal imaging using two channels takes longer, however, and increases the rate of bleaching, and for this situation I did not need histone labelling.

When the nuclei were still located within the yolk, the membrane at the surface of the egg showed no sign of ingression (Fig. 4.1(A')), and exhibited the appearance of a "lawn of grass" (Fig. 4.1 (A)). When nuclei reached the surface of the egg, membrane began to ingress around them (Fig. 4.1 (B') and Mov. 1.1). Numerous membrane vesicles were also visible around each nucleus (Fig. 4.1 (B)). Following a round of division, membrane continued to ingress between nuclei (Fig. 4.1 (C)), until it reached a final depth of approximately 13 μm (Fig. 4.1 (D)). After one more round of division, the uniform blastoderm was formed and membrane closed off basally (see next section). Nuclei remained spherical when membrane ingressed between them, rather than becoming elongated as is seen in *Drosophila* (Fig. 4.1 (D')). I found it easier to visualise the dynamics of ingressed membrane during division

without labelled nuclei, and therefore, I carried out timelapse microscopy on wildtype embryos that were transiently expressing GAP43-YFP. During a division, ingressed membrane stayed at the same depth (Fig. 4.1 (E-J)), and new membrane grew in between the divided nuclei to separate them (Fig. 4.1 (E-J) and Mov. 4.2).

The dynamics of F-actin during cellularisation (as shown by embryos transiently expressing LA-GFP) were the same as those seen for membrane (not shown).

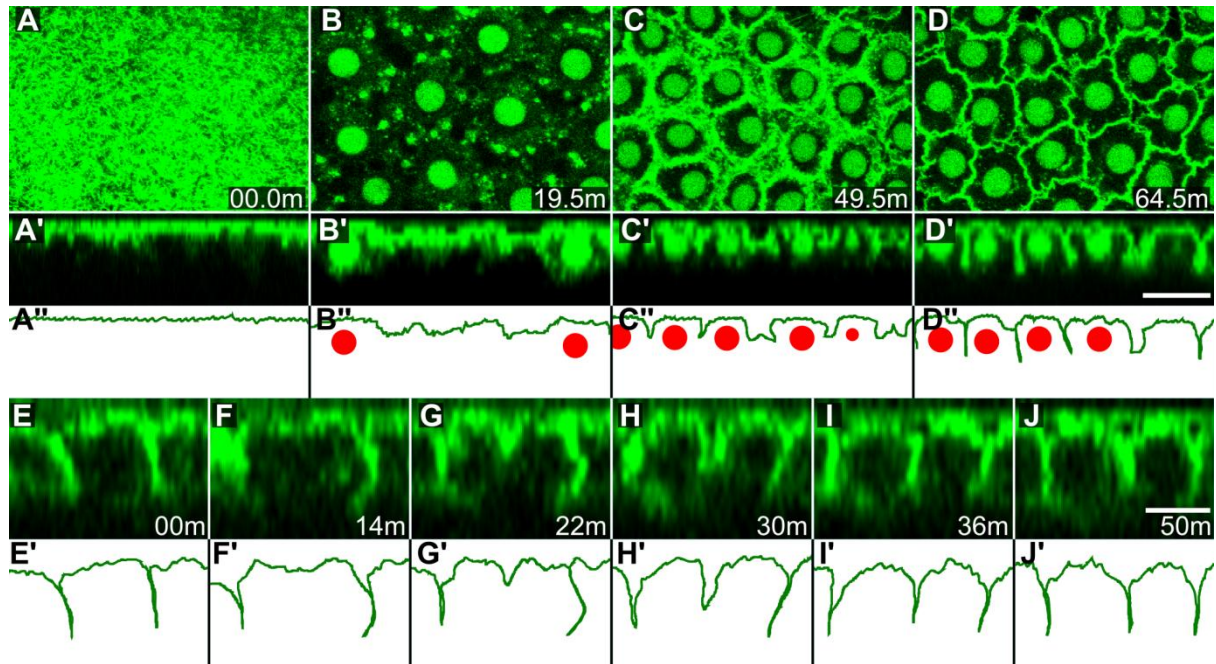


Figure 4.1. Membrane ingression during cellularisation. (A-D'') time series of membrane ingression during cellularisation in an nGFP transgenic embryo also labelled with GAP43-YFP, timed from just before nuclei reach the surface of the egg as shown in (A). (A-D) optical sections either at the level of the membrane in (A), or at the level of the nuclei in (B-D). (A'-D') orthogonal views from same time points. (A''-D'') schematics of orthogonal views, showing membrane in green and nuclei in red. When nuclei are not visible in the orthogonal views it is because the cross section did not bisect them. (E-J) time series of orthogonal views of membrane ingression during final uniform blastoderm division in a GAP43-YFP labelled embryo, timed from just before division begins as shown in (D). (E'-J') schematics of orthogonal views, showing membrane in green. (E, E') prior to division a single proto-cell is visible. (F, F') when the nucleus divides (not visible) the membrane moves further apart. (G, G') following separation of the chromosomes (not visible), membrane begins to invaginate between the new nuclei. (H, H' and I, I') membrane continues to invaginate between new

nuclei. (*J, J'*) two new proto-cells are visible. Scale bar in (*A-D*) is 20 μM , scale in (*E-J*) is 10 μM .

4.2.2 Basal cell closure

At the beginning of the uniform blastoderm stage the surface of the egg was covered by a layer of nuclei, which were separated by membranes laterally but still open to the yolk/underlying periplasm basally (Fig. 4.2 (*A-A''*) and Mov. 4.3 (*A-C*)). Secondly, the subapical membranes appeared ruffled (Fig. 4.2 (*A'*) and Mov. 4.3 (*A*)), which is a sign of low membrane tension (Rauzi and Lenne, 2011). At this point, the previously frequent nuclear divisions stopped, and the interphase of nuclear cycle 13 lasted for approximately two hours. Approximately one hour into this interphase, the membrane had not ingressed any further, and ring-like membrane structures became visible at the basal parts of the proto-cells (Fig. 4.2 (*B'-B''*) and Mov. 4.3 (*B*)). These rings constricted (Fig. 4.2 (*C'-C''*)), and by the end of the interphase they had closed completely, thereby completing basal cell closure (Fig. 4.2 (*D'-D''*)). Also by the end of this period, subapical membranes were no longer ruffled (Fig. 4.2 (*A-D*) and Mov. 4.3 (*A*)), a change that likely reflects tightening of membranes and formation of cell-cell junctions. Shortly after cellularisation is complete, germ rudiment condensation occurred and the embryonic cells elongated to become a columnar epithelium (See “5. A live imaging study of germband condensation”).

Basal closure of membrane in *Tribolium* looks identical to what is seen in *Drosophila*, therefore, it seemed likely that basal cell closure in *Tribolium* is also driven by constriction of F-actin rings. When I carried out live imaging of cellularisation in *Tribolium* eggs expressing LA-GFP, however, I could not see any ring structures at the base of the proto-cells. To check whether this absence is an artefact of the LA-GFP fusion protein, M.v.d. Zee and I looked at actin in fixed embryos with either phalloidin or an anti-actin antibody. With either stain, actin rings were not visible, confirming the results of the LA-GFP live imaging.

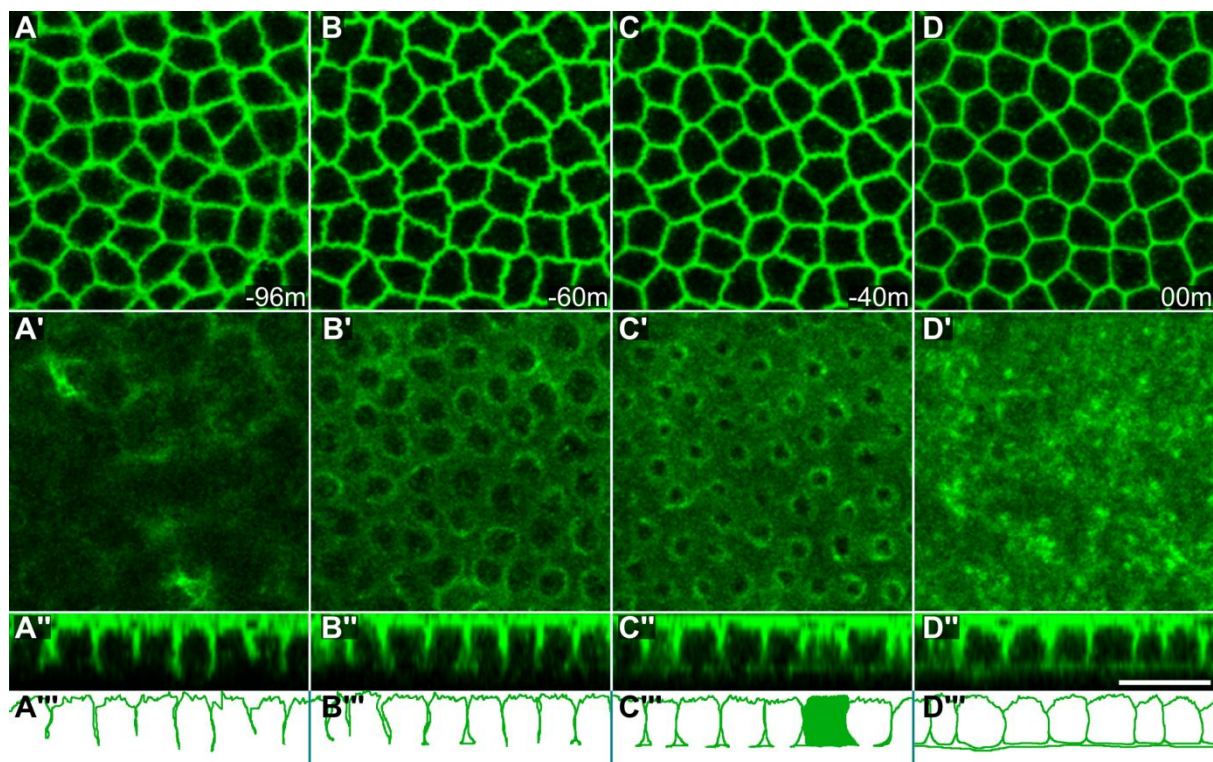


Figure 4.2. Completion of cellularisation. Time series of blastoderm cellularisation during 13th interphase of a GAP43-YFP labelled embryo timed against basal cell closure shown in (D-D''). (A-D) Subapical optical sections showing straightening/tightening of membrane during blastoderm cellularization. (A'-D') Optical sections at basal parts of proto-cells showing membrane constriction and eventual basal cell closure. (A''-D'') orthogonal views showing constriction basal membranes during cellularisation. (A'''-D''') Schematics of orthogonal views, solid colour shows situation where membrane position was ambiguous due to position of cross-section. Scale bar is 25 μ M.

4.2.3 *Innexin-7a* has a novel role in cellularisation in *Tribolium*

My collaborator on this project (Maurijn van der Zee) carried out a small RNAi screen for genes required for cellularisation in *Tribolium*. Out of this screen, one gene caused severe blastoderm defects with high penetrance, and so M.v.d. Zee selected it for further investigation. He found that it is a member of the *Innexin* gene family, and he gave it the title *Innexin-7a* (*Inx-7a*). M.v.d. Zee carried out RT-PCR and qPCR, and found that *Inx-7a* is strongly expressed in ovaries, but barely any expression can be detected in the embryo (van der Zee *et al.*, manuscript in prep.).

To carry out live imaging of the RNAi phenotype, M.v.d. Zee injected pupae with dsRNA against *Inx-7a* then sent the adult beetles to me in Cambridge. I collected eggs from these beetles, injected them with mRNA encoding either GAP43-YFP or LA-GFP, and

carried out live imaging of cellularisation. From these movies, it was apparent that the ingression of membranes is unaffected following knock-down of *Inx-7a* (Fig. 4.3 (A-A'')) and Mov. 4.4). Defects began to arise at the beginning of the uniform blastoderm stage, when scattered proto-cells “dropped out” of the epithelium (Fig. 4.3 (B-B'')). As development proceeded, rather than close off basally, ingressed membrane retracted to the surface of the egg at scattered points across the blastoderm (Fig. 4.3 (C-C'')) and (E-I')). When this occurred, membrane usually retracted first at one side of a protocell before spreading to the other side (Fig. 4.3 (E-I')) and Mov. 4.5). By the end of the interphase, the blastoderm epithelium had large cell-free areas, and only a few proto-cells had undergone basal cell closure (Fig. 4.3 (D-D')). Live imaging using LA-GFP showed that F-actin behaved in the same way as the membrane (not shown).

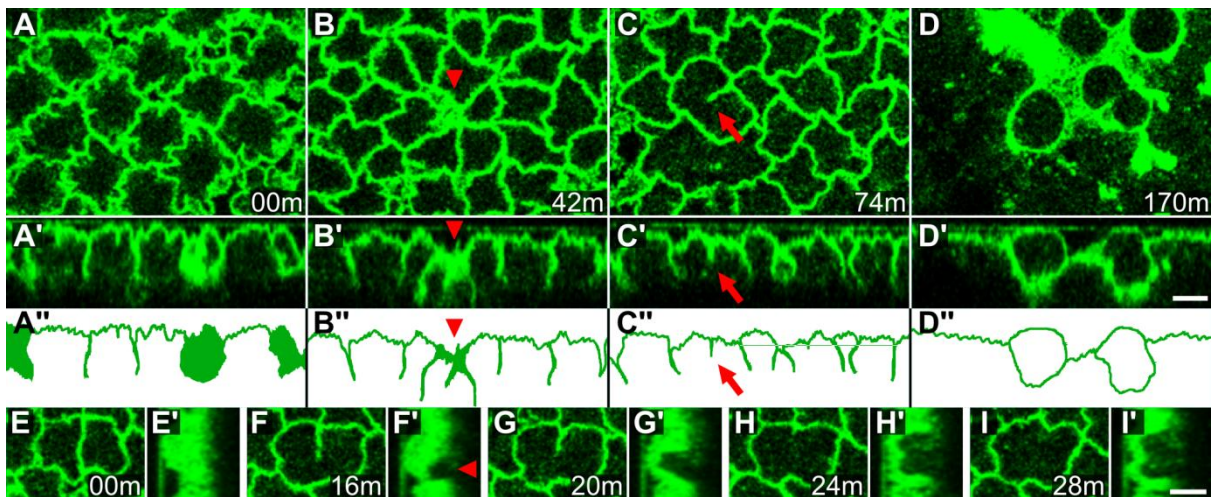


Figure 4.3. *Inx7a* RNAi cellularisation phenotype. (A-D'') Time series of cellularisation defects in a GAP43-YFP labelled embryo following *inx7a* pRNAi, timed against maximum membrane ingression depth shown in (A-A''). (A-D) Subapical optical sections, (A'-D') orthogonal views, (A''-D'') Schematics of orthogonal views, solid colour shows situations where membrane position was ambiguous due to position of cross-section. (A-A'') membrane ingression occurs normally, and blastoderm looks normal at the point of maximum membrane ingression. (B-B'') following the 12th nuclear division, proto-cells delaminate at scattered positions (arrow head). (C-C'') membrane retraction occurs (arrow). (D-D'') most of the egg surface shows no membrane invagination, but some cells have completed basal closure. (E-I') time series of membrane retraction shown as subapical optical sections (E-I) or as orthogonal views (E'-I'). (E, E') membrane is ingressed normally. (F, F') membrane retraction occurs at one side (arrowhead in F'). (G, G' and H, H') membrane retraction spreads to other side. (I, I') following membrane ingression, two proto-cells have been joined

as one proto-cell. Orthogonal views shown in (E'-I') are maximum intensity projections of several microns in the y axis. Scale bar is 10 μ M.

4.2.4 Yolk cleavage in *Tribolium*

Following cellularisation, the nuclei at the cortex of the egg were separated from the underlying yolk, the yolk nuclei (a.k.a. vitellophages) and their accompanying cytoplasm (collectively referred to as the yolk system or yolksac) (Counce, 1961). The yolk system is encapsulated by a plasmalemma, and can therefore be thought of as a large multinucleated cell (Handel et al., 2000). In many insects, the yolk becomes cleaved into smaller compartments, called yolk spheres, and in some cases this even occurs after the germ rudiment has been experimentally removed (Counce, 1961). The purpose of yolk cleavage is not known, and there have been no studies on it using molecular techniques. I was interested to see if *Tribolium* embryos undergo yolk cleavage, and if so when this occurs and if there are any obvious effects on the embryo.

In order to look for the existence of yolk cleavage, I carried out differential interference contrast (DIC) live imaging of embryogenesis on a confocal microscope (Fig. 4.4 and Mov 4.6). At the uniform blastoderm stage, the cortex of the yolk appeared as a mixture of lipid droplets of different sizes and this persisted throughout germ rudiment condensation (Fig. 4.4 (A) and Mov. 4.6). After serosa window closure (see “5. A live imaging study of germband condensation”), large grooves started to form at the surface of the yolk (Fig. 4.4 (B)). Although these grooves were initially transient (Fig. 4.4 (C)), more appeared over time (Fig. 4.4 (D)). After several hours, the grooves stopped retracting to the surface and characteristic yolk spheres formed (Fig. 4.4 (E)). Due to the yolk being engulfed by the embryo, I was unable to determine whether the yolk spheres were transient or if they persisted until after hatching. Secondly, I cannot say whether yolk spheres are continuous in the centre of the egg.

The repeated contraction and relaxation cycles during yolk cleavage are reminiscent of repeated actin-myosin contraction and relaxation cycles, which have been observed during processes such as apical constriction (Martin et al., 2009). To test for the presence of an actin network at the surface of the yolk, I carried out live imaging of embryos in which I had injected LA-GFP mRNA into the yolk after cellularisation to specifically label yolk system actin.

First, I carried out these injections in nGFP transgenic embryos to visualise the nuclei. In these embryos, there was no labelling of F-actin in the embryonic and extraembryonic cells, however, an actin network was visible at the surface of the yolk (Fig. 4.4 (F,F')). To allow easier visualization of the actin network at germband stages, I also injected mRNA for LA-GFP into non-transgenic eggs after cellularisation. In these embryos, the yolk actin network appeared to be evenly distributed over the entire egg (Fig. 4.4 (G)). The fluorescent signal was weaker beneath the germband, but this is most likely due to light scattering from the multiple layers of embryonic and extraembryonic tissue. The LA-GFP is most likely translated by the yolk energids. To check for pulses of myosin contraction during yolk cleavage I tried to develop a live marker of non-muscle myosin II, however, this did not work (see “3. The use of transient expression as a method for live imaging”).

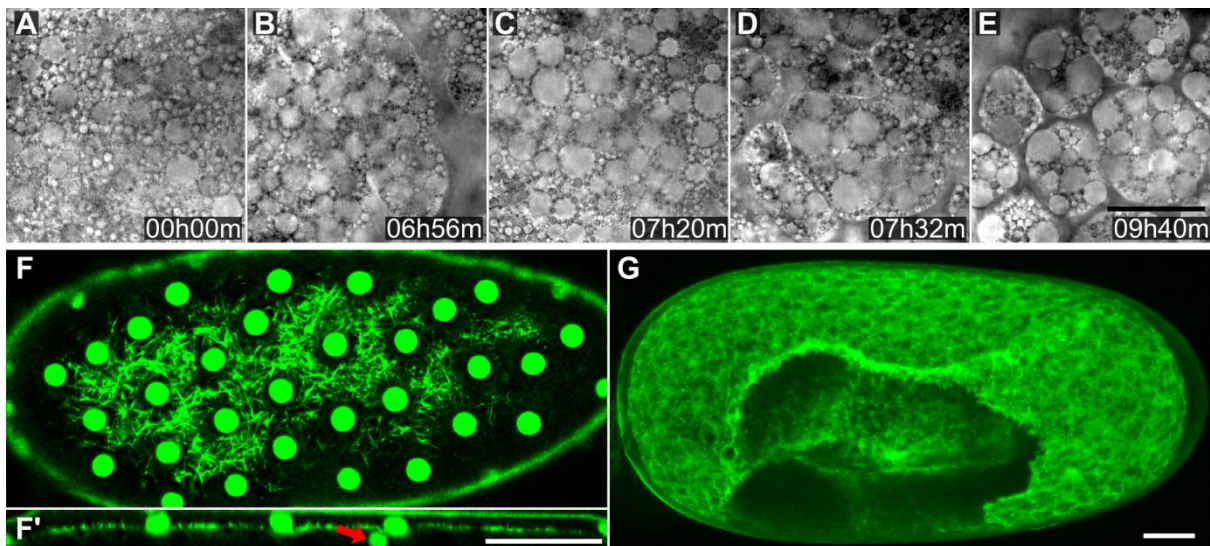


Figure 4.4. Cleavage of the yolk and the presence of an actin network. (A-E) time series of optical sections at the surface of the yolk from a DIC timelapse, timed against the uniform blastoderm stage shown in (A). (A) At the uniform blastoderm stage no grooves are visible. (B) After serosa window closure, grooves are visible as areas devoid of yolk granules. (C) Grooves have disappeared. (D) Grooves form again, and more form. (E) Several hours after first grooves form, stable grooves have now formed. (F) optical section of an nGFP embryo transiently expressing LA-GFP in the yolk only, showing serosal nuclei and F-actin network. (F') orthogonal view of embryo in (F), showing the actin network is beneath the serosa cells. Note yolk nucleus (arrow). (G) average intensity projection of a confocal z-stack of a wild-type embryo at serosa window stage transiently expressing LA-GFP in the yolk only. (F) is a

dorsal view, with anterior to the left. (G) is a ventrolateral view, with anterior to the left, dorsal to the top. All scale bars are 50 μ m.

4.2.5 Effect of yolk cleavage on the germband

After finding that yolk cleavage does occur in *Tribolium*, I was interested to see how the contraction of the yolk into spheres affects the developing germband. For example, it has been observed that the germband “bounces” during elongation (Sarrazin et al., 2012), and I hypothesized that this may be caused by the contraction cycles of the yolk. To observe both the germband and the yolk I performed live imaging of embryos that had been injected with GAP43-YFP mRNA to label membranes.

I found that the “bouncing” is actually the repeated expansion and contraction/relaxation of the germband in the anterior-posterior direction (and to a lesser extent laterally), and that the expansion correlates with each contraction cycle of the yolk (Fig. 4.5 (A,B) and Mov 4.7 and 5.5). Secondly, filopodia-like membrane extensions became visible at the edges of the germband during the expansion phase (Fig. 4.5 (C,D)), and then disappear during the contraction phase (Fig. 4.5 (D,F)).

For a further test of this correlation, I set out to disrupt the function of the vitellophages in some way in the hope of stopping the yolk contractions. During my work on endoderm (see “6. Appendix - Expression pattern of *Tribolium Serpent*”), I had cloned the *Tribolium* ortholog of the GATA factor *serpent*. At the time of yolk cleavage, *Tc-srp* is expressed in an anterior head domain, the amnion and in the yolk nuclei (for the full expression pattern, see “6. Appendix - Expression pattern of *Tribolium Serpent*”). To test whether *Tc-srp* expression is required for yolk cleavage, I performed concurrent embryonic RNAi for *Tc-srp* and live imaging of membranes using GAP43-YFP.

In *Tc-srp* RNAi embryos, condensation of the germband occurred, but the amnion membrane disintegrated during serosa window closure and the germband became surrounded by the spherical membrane remnants of the cells (Fig. 4.5 (G)). In *Drosophila*, *Dm-srp* is required for maintenance of the amnioserosa, therefore, this result was not unexpected (Murakami et al., 2005). After serosa window closure, there was no sign of yolk contractions and yolk spheres did not form (Fig. 4.5 (H) and Mov. 4.7). Secondly, the germband did not undergo the expansion and contraction cycles observed in wildtype embryos (Fig. 4.5 (H) and Mov. 4.7). The germband continued to extend along its anterior-posterior axis, however, it did not move properly within the egg and became buckled (Fig. 4.5 (H)). Together, these data strongly imply that the repeated expansion and contraction of the germband is caused by, or

at least requires the yolk cleavage. While it is likely that the loss of yolk cleavage was caused by the loss of *Tc-srp* function in the yolk nuclei, I cannot rule out the possibility that the degenerating amnion caused the loss of yolk cleavage.

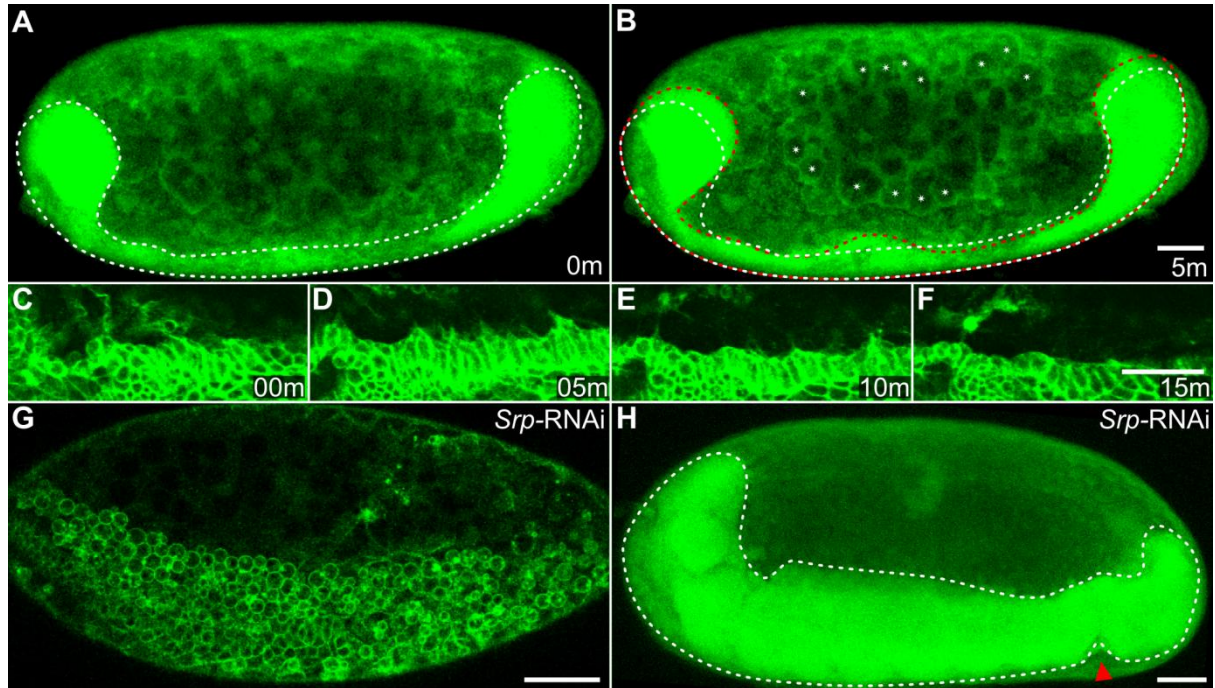


Figure 4.5. Effects of yolk cleavage on the germ band. (A-B) average intensity projections from a timelapse of germband elongation in a GAP43-YFP labelled embryo. (A) at this timepoint during germband elongation very minor yolk cleavage is visible (germband is outlined with white dotted line). (B) during a cycle of yolk cleavage, many furrows become visible in the yolk (asterisks) and the germband expands in the anterior and posterior direction, compare current germband position (red dotted line) with previous germband position (white dotted line). (C-F) average intensity projections of 9 μ M of lateral region of a germband during a round of yolk cleavage, timed to show one round of germband expansion and contraction/relaxation. (C) prior to expansion, lateral part of germband appears smooth. (D) when germband expands laterally, filopodia-like membrane extensions are visible extending from germband towards the yolk. (E-F) as germband contracts/relaxes, membrane extensions disappear. (G-H) Frames from a timelapse of development in a GAP43-YFP labelled embryo following eRNAi for *Tc-Srp*. (G) optical cross section through egg at lateral part of germband showing the degenerated amnion cells. (H) Average intensity projection of a late stage embryo (approximately 21 hours after egg lay) showing a lack of yolk spheres as well as buckle in germband (arrowhead). (A-B) and (G) were made by uniformly enhancing brightness/contrast to show the germband and the membrane-bound yolk spheres. (A-F) are

lateral views, (H-G) are ventrolateral views. All panels have anterior to the left and ventral to the bottom. Scale bars are 50 μ M.

4.3 Discussion

In this chapter I have used some of the live imaging tools presented elsewhere in this thesis (“3. The use of transient expression as a method for live imaging”) to study cellularisation in *Tribolium*. I confirmed previous reports that the uniform blastoderm of *Tribolium* is made up of cuboidal cells, which is more representative of insects than the columnar cells of *Drosophila*. I found the process of membrane invagination in *Tribolium* to be strikingly different from that seen in *Drosophila*. Together with Maurijn van der Zee, I analysed a cellularisation phenotype caused by the knockdown of the *Tribolium* gene *inx7a*. Lastly, I found that the yolk of *Tribolium* becomes cleaved into yolk spheres, a process which is seen in many insects but has not thus far been studied using modern day tools.

4.3.1 Membrane invagination prior to uniform blastoderm formation

The *Drosophila* blastoderm is used as a key example of how the diffusion of mRNA and protein results in gradients that can be used to provide positional information for patterning cell fates (Jaeger, 2011). Despite this paradigm, recent work has shown that the blastoderm is not as homogeneous as was once thought. First of all, many cytoplasmic components, as well as the membrane overlying each nucleus, are compartmentalized (Frescas et al., 2006; Mavrakis et al., 2009). Secondly, diffusion of the Dorsal transcription factor is partially constrained to cytoplasmic islands around each nucleus (DeLotto et al., 2007). Lastly, it has now been shown that the transient mitotic furrows that form between dividing nuclei have a significant impact on diffusion rates (Daniels et al., 2012). Membrane ingression during nuclear cycle 14 complicates the rate of diffusion even further. The mRNA of some genes, such as pair rule genes, has been shown to be apically localized, which means that these gene products behave as if in a cellular environment before cellularisation is complete (Davis and Ish-Horowicz, 1991). The mRNA of gap genes, on the other hand, is not specifically localized and therefore continues to diffuse until cellularisation is complete (Davis and Ish-Horowicz, 1991).

The extent and importance of diffusion of gene products in the *Tribolium* blastoderm is not known, as the dynamics of membrane ingression have not been studied. I have now found that membrane ingression in *Tribolium* begins as soon as nuclei reach the surface of the yolk, and membrane is completely ingressed between nuclei before the final round of uniform blastoderm division. Furthermore, even before membrane ingresses between nuclei, there is a high concentration of membrane vesicles around each nucleus, which may impede diffusion. I hypothesise that diffusion probably still takes place in the early *Tribolium* blastoderm, but at a lower rate than is seen in *Drosophila*. This prediction would be testable by carrying out a study similar to that performed by Daniels et al. (2012).

At the final uniform blastoderm stage (nuclear cycle 13) in *Tribolium*, diffusion is likely to be negligible due to nuclei being completely separated laterally by membrane (although some diffusion may still occur below the proto-cells). This would have interesting implications on cell fate patterning, as it is during this period when many of the changes in gene expression are occurring, for example changes in the *Tc-orthodenticle* expression pattern (Schinko et al., 2008) and dynamic expression of the pair rule gene *Tc-even-skipped* (El-Sherif et al., 2012). In place of diffusion, cell-to-cell communication may play a major role in patterning, as is presumably occurring during germband elongation in *Tribolium*.

I propose that the transient formation of metaphase furrows in *Drosophila* is a derived state, which evolved from a situation similar to that seen in *Tribolium* (membrane ingression starting when nuclei reach the cortex). First of all, metaphase furrows are required in *Drosophila* for the normal segregation of chromosomes during division, showing that some sort of membrane invagination is required for nuclear division at the surface of the egg (Rothwell et al., 1998). Secondly, other insects have been shown to cellularise before forming a uniform blastoderm (Anderson, 1972a; Ho et al., 1997). Lastly, the *Tribolium* blastoderm is more representative of insects in other ways, such as having a blastoderm made up of cuboidal cells. Only the study of the dynamics of membrane ingression in a wide range of insects can confirm this evolutionary scenario. If it proves true, however, it may mean that one of the driving forces for *Drosophila* to lose full membrane ingression from an early blastoderm stage was to allow faster diffusion of maternal and zygotic gene products, which would allow blastoderm cell fates to be established more quickly. If the rate of diffusion is in fact a limiting factor in the time of embryonic development in insects, it would be interesting to look at cellularisation in insects that develop even faster than *Drosophila* and to see if they have faster rates of diffusion across the blastoderm. When performing this study, the size of

the eggs would have to be factored in to the rate of development, as gene products would not need to diffuse as far in smaller eggs.

4.3.2 Evolution of a columnar blastoderm – a case for heterochrony?

As discussed in the introduction, the formation of columnar cells during cellularisation seen in *Drosophila* and other dipterans represents a derived state. The ancestral condition for insects seems to be for cellularisation to give rise to cuboidal cells, and then for the embryonic cells to undergo a cuboidal-to-columnar transition during germ rudiment condensation (Anderson, 1972a; Anderson, 1972b). This latter situation is exactly what occurs in *Tribolium* (for description of cuboidal-to-columnar shift, see “5. A live imaging study of germband condensation”).

In *Drosophila*, the proto-cells become columnar during the fast phase of membrane ingression, when membranes ingress below nuclei (Lecuit, 2004). A similar phase is not observed in *Tribolium*, as membranes stop ingressing when they are below the nuclei. The “fast phase” of membrane ingression seen in *Drosophila* may, therefore, be homologous to apical-basal elongation of embryonic cells seen after cellularisation in *Tribolium* and other insects (Anderson, 1972a; Anderson, 1972b; Roth, 2004). If this is the case, the “fast phase” must have undergone a heterochronic shift from occurring after cellularisation (in most insects) to during cellularisation (in dipterans). Unfortunately, very little is known about cuboidal-to-columnar cell transitions (for a review see St Johnston and Sanson, 2011). This hypothesis could be tested, however, by comparing the rate of membrane ingression during cellularisation in *Tribolium* with the rate of cell elongation during the cuboidal-to-columnar transition. If the rate of cell elongation is significantly faster than the rate of membrane ingression, this would support the heterochrony hypothesis.

Another test would be to find the *Tribolium* orthologs of the genes that are specifically required for the fast phase of cellularisation in *Drosophila*, and to see if they are required for the cuboidal-to-columnar shift in *Tribolium* (but not for cellularisation). There are several examples where the ortholog of a gene involved in cell shape change in *Drosophila* has the same function in another animal, for example *Drosophila Shroom* and vertebrate *Shroom3* are both involved in apical constriction (St Johnston and Sanson, 2011), and preliminary data suggests the same may be true for *Drosophila folded-gastrulation* and the *Tribolium* ortholog of this gene (Dawes-Hoang et al., 2005; S. Roth, personal communication).

4.3.3 Cell closure without contractile actin rings and the role of *inx7a*

Basal cell closure is driven by the contraction of actomyosin rings in *Drosophila*. However, despite the striking similarities in the basal closure of membrane in *Tribolium* and *Drosophila*, I could see no evidence for actin rings in *Tribolium*. One explanation is that the rings were not visible in live embryos because LifeAct does not label the contractile actin rings for some unknown reason. This explanation seems less likely considering that M.v.d. Zee and I used fixed stains to label actin, and we still did not observe these rings (although it is possible we missed the relevant stage). The alternative explanation is that basal cell closure in *Tribolium* occurs in a fundamentally different way to *Drosophila*. If this latter explanation turns out to be true, it would require a completely different model for cell closure.

The model that is proposed in the publication that this work is a part of (van der Zee et al., manuscript in preparation) is that the yolk actin network (described in this chapter) forms prior to basal cell closure, and that the membrane spreads across this network during basal closure. The spreading of the membrane may be driven by the specific insertion of membrane vesicles, similar to what occurs during membrane ingression. As a part of this model, certain proteins would be required to anchor the membrane to the actin network, and one such protein could be *Inx7a*.

The main phenotype observed following knockdown of *inx7a* is the retraction of membranes at the time when they would normally begin basal cell closure. If *inx7a* is required for anchoring membrane to actin for basal cell closure, then the loss of this protein would explain the retraction. In fact, pannexins (a gene family related to innexins) have been shown to be able to bind actin (Bhalla-Gehi et al., 2010). This hypothesis would also explain why *innexin7* is not required for cellularisation in *Drosophila* (Ostrowski et al., 2008); the basal membrane is anchored to a contractile actin ring, which likely requires a type of attachment different from that required in *Tribolium*.

4.3.4 Formation of the yolk spheres – delayed cellularisation?

As described in the introduction, in most non-insect arthropods the yolk is also compartmentalised by membrane during cellularisation. Despite this early incorporation into cells, the yolk usually becomes segregated to the middle of the egg either as a single large cell, or as multiple cells that then merge to form a single large cell, where it remains throughout development until it is engulfed by the midgut.

Insects seem to do things a bit differently, as during cellularisation membrane ingression stops at the surface of the yolk, forming a cellular blastoderm overlying one large multinucleated yolk cell. During later development, however, the yolk may become compartmentalised into yolk spheres. I have found that this yolk cleavage occurs in *Tribolium* and I propose that it is driven by an actomyosin network that is controlled by the yolk nuclei.

Following cellularisation, I discovered the presence of an extensive actin network at the surface of the yolk. Given the dynamics of the repeated contraction and relaxation of yolk cleavage, it is likely that this actin network (together with myosin) is required for the contraction cycles that drive yolk cleavage. This could easily be tested by injecting a cell-impermeable inhibitor of myosin contraction, which would leave the actin in a relaxed state. Whether it is via the actin network or not, the cleavage of the yolk is likely controlled by the yolk nuclei. This hypothesis could be tested by injecting something into the yolk after cellularisation that would cause the death of the yolk nuclei. Some possibilities for what to inject would be the reaper protein that would initiate apoptosis (White et al., 1996), or a cell impermeable small molecule of some sort.

One of the effects of the yolk contraction is the repeated expansion and contraction of the germband. Although germbands continue to elongate when removed from the egg (Sarrazin et al., 2012), there may be some subtle developmental processes that require the expansion and retraction of the germband to occur properly. Another possible role for the formation of the yolk spheres is to make it easier for the elongating germband to grow inside the egg. If the yolk remained as one large cell, the growing germband would need to push its way through the yolk. However, when the yolk is cleaved into smaller compartments, the yolk cells would be able to move more easily around each other as the germband grows. This hypothesis may be supported by the buckling of the elongating germband when yolk cleavage was lost following *Tc-srp* RNAi. However, the buckling may also be a result of the loss of the amnion, or other problems with communication between the yolk and germband. Again, the only way to test this would be to specifically disrupt the yolk cell, either by causing the death of the yolk nuclei or by disrupting the actin network.

5. A LIVE IMAGING STUDY OF GERMBAND CONDENSATION

5.1 Introduction

A key aim of researchers studying development is to understand how molecular processes translate into morphological form. In the field of evolution and development we can take this one step further to examine how the molecular processes change to cause changes in morphological form. In the past decades, molecular and genetic tools of increasing complexity and sophistication have been developed. These tools have allowed researchers to probe the molecular processes underlying development. For the most part, however, the mechanisms that facilitate the translation from molecular process to morphological form have remained a mystery. Over the past 10 years this has begun to change drastically, with an increase in the amount of research into morphogenesis.

This increase in research on morphogenesis has been facilitated in part by the development of tools for live imaging at a cellular level. For example, it is now possible to label cell structures such as nuclei, actin and myosin with fluorescent molecules. A second source of tools for understanding cell behavior comes from physicists. Thanks to interdisciplinary research between biologists, physicists and computational scientists, it is becoming possible to computationally model complex morphogenetic processes at a cellular or tissue level.

5.1.1 *Drosophila* as a model system for the study of morphogenesis

Morphogenetic processes have been examined in several model systems, such as ascidians, fruit flies and nematodes, and this work has recently been the subject of several reviews (Lecuit and Lenne, 2007; Quintin et al., 2008; Rauzi et al., 2010). The fruit fly, *Drosophila melanogaster*, has shown itself to be an excellent system for studying morphogenesis. In fact, out of any animal system, the most well characterized morphogenetic process is dorsal closure in the *D. melanogaster* embryo (Quintin et al., 2008). Other processes that have been studied in *D. melanogaster*, are gastrulation and germband extension, which turn out to be intimately linked (Butler et al., 2009). The imaginal discs of *D. melanogaster* larvae have

also proven to be excellent systems for studying cell shape change (Widmann and Dahmann, 2009), and compartment boundary formation and cell sorting (Lecuit and Lenne, 2007).

These processes studied in *D. melanogaster* also occur in many other insects, and therefore, the findings from this insect are likely to be broadly true for other animals. However, several major developmental events that are present in the majority of insects have been lost or modified in *Drosophila*. One example of this is the type of cellular epithelium that is formed during cellularisation; most insects form a cuboidal epithelium after cellularisation, while *Drosophila* and other dipterans form a columnar epithelium (see “4. Cellularisation in *Tribolium* – a more widely conserved mode than *Drosophila*?”). Another example is the fact that *D. melanogaster* is long germ, while most insects are short/intermediate germ (Peel, 2008).

5.1.2. Morphogenetic consequences of short/intermediate germ development

In long germ embryos, the embryo proper (the germband) occupies the total egg length, and thus there is very little movement of cells when the embryo is forming from a blastoderm. Short/intermediate germ embryos, however, undergo drastic cell movements when forming the germband, which bring about the process of germband condensation and extraembryonic membrane formation. The modern classification of an insect embryo as short or intermediate germ is largely arbitrary, as the original classification system was based on morphological data and also included a separate classification for small and large germ rudiments (for excellent discussions of this see Davis and Patel, 2002; Roth, 2004). The process of embryo formation in both classes is superficially similar, however, and I will therefore not pay any further attention to the distinction here.

The general mode of embryo formation in short/intermediate germ types is as follows (the information for this summary is gathered from Anderson, 1972a; Anderson, 1972b; Davis and Patel, 2002; Nakamura et al., 2010; Roth, 2004). Starting with a blastoderm, which may be uniform or non-uniform (see “4. Cellularisation in *Tribolium* – a more widely conserved mode than *Drosophila*?”), cells condense together at one stereotypical location. In some insects, such as the cricket *Gryllus bimaculatus*, cells initially condense as lateral “pads” of tissue, which then move ventrally and fuse at the ventral midline. Another situation, seen in the beetle *Tribolium castaneum*, is for cells to condense laterally and ventrally at the same time. As condensation occurs, embryonic cells undergo a cuboidal-

columnar transition, which could provide a driving force for condensation (Anderson, 1972b). Unfortunately, very little is known about the underlying molecular processes that cause cuboidal-to-columnar cell transitions (St Johnston and Sanson, 2011).

Condensation of the germband also has to be coordinated with drastic changes in the extraembryonic tissue (which is greatly reduced in long germ insects), whereby the embryo becomes covered ventrally by the amnion and immersed in yolk (in some insects). At the same time, the serosal cells must expand to encapsulate the embryo and all of the yolk. The mechanisms of this movement are poorly understood, but it is clear they must be interconnected, as the process is carried out by a single epithelium, that remains intact until the end of the process.

5.1.3 Condensation and morphogenesis in *Tribolium*

The last major study on germband condensation in an insect was carried out on *Tribolium castaneum* (Handel et al., 2000). This work used scanning electron microscopy to examine the changes in morphology that occur during condensation. The authors were able to propose several hypotheses about mechanisms underlying condensation, however, these hypotheses have not yet been tested. Furthermore, this work was based on fixed tissue, and therefore, the dynamics of the process and the movements of specific cells could not be followed.

Since the early descriptions of condensation (Brown et al., 1994; Handel et al., 2000), a large amount of information has been gathered about the genetic patterning of *Tribolium* embryos via the use of RNA in situ hybridisation and gene knockdown by RNA interference. Most studies only provide broad descriptions of the actual morphological defects caused by knockdown of genes, and attention is instead focussed on the genetic interactions. One key example of this is the analysis of the role that the *Tribolium* ortholog of *caudal* (*Tc-cad*) plays in germband formation (Copf et al., 2004; Schoppmeier et al., 2009).

Tc-cad encodes a homeodomain transcription factor expressed both maternally and zygotically with a crucial role in posterior embryonic patterning (Copf et al., 2004; Schoppmeier et al., 2009; Schulz et al., 1998; Wolff et al., 1998). Tc-Cad protein is first detected throughout the early blastoderm. It then forms a gradient in the late blastoderm spanning the presumptive growth zone, thoracic and gnathal primordia, with highest levels at the posterior pole. Later on, it becomes restricted to the growth zone during germband elongation (Schulz et al., 1998). Knock-down of both the maternal and zygotic components of *Tc-cad* expression by parental RNAi results in severely truncated embryos retaining only

their most anterior pregnathal structures (Copf et al., 2004). However, the underlying cell and tissue dynamics accompanying these germband truncations have never been described.

I believe that the lack of detailed analysis of the effects of gene knockdown on cell behaviour and morphogenesis is partially due to the difficulty of gathering data on the overall morphology of embryos. Secondly, a thorough description of condensation at a cellular level does not exist for *Tribolium* or any other short germ insect. To overcome the first problem, I developed a number of new live imaging markers for *Tribolium* (see “3. The use of transient expression as a method for live imaging”). Using several of these markers, I have carried out an extensive analysis of condensation in *Tribolium* in wildtype embryos. From this analysis I have made a number of hypotheses about how different aspects of condensation occur, and I have proposed a staging scheme for different phases of condensation. Lastly, I carried out a similar analysis in *Tribolium* embryos in which I had disrupted *Tc-cad* function in order to discover the cellular defects that are caused by loss of *Tc-cad*.

5.2 Results

5.2.1 Dynamics of *Tribolium* germband condensation and elongation, and extraembryonic development

Following the uniform blastoderm stage (see “4. Cellularisation in *Tribolium* – a more widely conserved mode than *Drosophila*?”), cells begin to move towards the ventral side of the egg to form the germband. During this process, the prospective amnion and serosa epithelia undergo extensive movements and folding to envelope the germband ventrally and release it into the yolk. I followed these morphogenetic processes in live imaged GAP43-YFP-labeled *Tribolium* embryos from 8 to 21 hours after egg lay (AEL) at 32°C, spanning the uniform blastoderm stage through to germband elongation stages. By tracing both global tissue dynamics as well as single cell behaviours, I classified six distinct stages covering this period of *Tribolium* embryogenesis (Table 5.1; also see relation to other *Tribolium* staging systems in Table 5.2). My interpretations were based on screening more than 20 embryos imaged from different views, and from pair-wise comparisons between 3 wild-type and 3 *Tc-cad* knock-down embryos described in the following section (Fig. 5.1 and Mov. 5.1-5.4). I will first present a broad description of these stages in wildtype and *Tc-cad* RNAi embryos, before focussing on specific processes during condensation.

(Stage 1) The start of this stage was marked by the first global movements of blastoderm cells during the interphase of the 13th cycle, and encompassed completion of cellularisation. All cells in the uniform blastoderm epithelium had the same cuboidal shape (Fig. 5.4 (A-A'')) and Fig. 5.5 (A-A'')). During this stage, I observed minor flows of cells from the two poles towards the middle of the egg, as well as from the dorsal and lateral sides towards the ventral midline (Fig. 5.1 (A,F)). These initial cell movements occurred in the absence of any cell divisions and were accompanied in some embryos by retraction of the posterior pole from the vitelline membrane (Fig. 5.10 (A-B), Fig. 5.5 (A-B'')). Blastoderm cells at the posterior pole then invaginated, forming the primitive pit. It is worth noting here that the extent of posterior pole retraction from the vitelline membrane varied significantly in my time-lapses both in GAP43-YFP labelled embryos (n=10) and in nGFP transgenic embryos imaged (n=10) (e.g. compare Fig. 5.4 (A-B'') with Fig. 5.5 (A-B'')). This variability raises caution about the suitability of this character for accurate staging of *Tribolium* embryos (e.g. see El-Sherif et al., 2012).

(Stage 2) During this next stage, all blastoderm cells moved in concert posteriorly for about one to two cell diameters (Fig. 5.1 (B,G)). Dorsal and lateral cells also continued their movement towards the ventral midline. This stage coincided with the division of the germ rudiment cells to form the differentiated blastoderm, and the earliest morphological differentiation of germband and serosa cells (Fig. 5.1 (G), also see “5.2.3 Formation of the differentiated blastoderm”).

(Stage 3) During this stage, ventrally directed cell movements became predominant; cells in the embryonic rudiment advanced almost in straight trajectories towards the ventral midline (Fig. 5.1 (C)). This medial-lateral condensation of the embryonic rudiment was accompanied by cell intercalation and a reduction in cell surface area as embryonic cells became columnar (Fig. 5.1 (A-H), also see “5.2.5 Cell intercalation and cell contraction”).

This stage also encompassed the posterior and ventral movement of prospective amnion and serosa cells and formation of the posterior amniotic fold (Fig. 5.1 (C,H)). This epithelial rearrangement was accompanied by the progressive submersion of the posterior germband deeper into the yolk coupled with the involution of superficial amnion cells into the inner side of the fold (Fig. 5.1 (C,H), Fig. 5.10 (C) and Mov. 5.1, 5.2 and 5.7; also see section “5.2.7 A possible role for the yolk system in *Tribolium* morphogenesis”). This way, the posterior amniotic fold grew deeper and bent ventrally covering the germband posteriorly. During this stage, involution of amnion cells was accompanied by the posterior and ventral expansion of the serosa epithelium (Fig. 5.1 (H)). The expansion of the serosa was

accompanied, and likely effected by the serosa cells undergoing a cuboidal to squamous transition (Fig. 5.1 (H) and see section “5.2.4 Cell shape changes during condensation”). The end point of this stage is defined as being when the boundary between the serosa and the amnion is located at the posterior egg pole (Fig. 5.1 (H)).

(Stage 4) During this stage, involution of amnion cells continued at the posterior. Secondly, the amniotic fold extended laterally and anteriorly, progressively covering the germband in a posterior to anterior direction (Fig. 5.1 (D,I)). At the same time, the amnion raised slightly around the lateral sides of the condensing head lobes initiating what is generally known as the anterior amniotic fold. The advancing lateral edges of the posterior fold were continuous on either side of the germband with the lateral edges of the anterior fold forming a horseshoe-like amnion cover folded over the lateral sides and posterior half of the germband (Fig. 5.1 (D,I)). After formation of this horseshoe amniotic fold, the amnion folded over the head lobes at the anterior of the germband, resulting in an oval amniotic fold surrounding the open serosa window (Fig. 5.1 (E)). In summary, my live image analysis showed that during stage 4 the posterior amniotic fold first extended into a horseshoe amniotic fold, and then this horseshoe amniotic fold gave rise to the oval amniotic fold surrounding the serosa window (Mov. 5.1 and 5.2).

Throughout stages 3 to 5, the leading edge of the serosa was demarcated by a conspicuous membrane thickening in GAP43-YFP labelled embryos (visible next to tracked serosa cells in Fig. 5.1 (H,I) and Mov. 5.1 and 5.2). This thickening also exhibited a higher concentration of F-actin in time-lapse recordings of LA-GFP labelled embryos (data not shown). The thickening appeared continuous from cell to cell and was reminiscent of intercellular actomyosin cables that have been shown to produce contractile forces in other developmental systems, such as *Drosophila* dorsal closure, zebrafish gastrulation and embryonic wound healing (Behrndt et al., 2012; Kiehart et al., 2000; Rodriguez-Diaz et al., 2008). During stage 3, this serosa cable first increased in length while the serosa epithelium moved around the posterior pole, and then started shortening as it converged towards the rim of the posterior amniotic fold concurrently with amnion involution (Fig. 5.1 (H), also see “5.2.8 Serosa window closure”). During stage 4, the further shortening of the serosa cable coincided with two morphogenetic events. First, it coincided with amnion folding laterally over the head lobes and formation of the horseshoe amniotic fold (Fig. 5.1 (D,I) and Mov. 5.1 and 5.2). Second, it coincided with amnion folding over the head lobes anteriorly and formation of the serosa window (Fig. 5.1 (E) and Mov. 5.1 and 5.2).

Gastrulation of the mesoderm was also taking place throughout stages 3-5 (Fig. 5.7, also see “5.2.6 Gastrulation of the mesoderm”).

While the posterior amniotic fold and mesoderm internalization progressed, the lateral ectodermal cells in the germband stopped their ventral movement before turning anteriorly and coming to a standstill (Fig. 5.1 (D)). Ectodermal cells further to the anterior only ceased their anterior movement later during serosa window closure (Fig. 5.1 (E)). Notably, during these extensive cell movements, the presumptive ventral midline cells moved little in the anterior-posterior axis and not at all in the dorsal-ventral axis (Fig. 5.1 (A-D)). Likewise, the most anterior-ventral region of serosa and amnion cells that moved slightly posteriorly during stages 1 and 2 (Fig. 5.1 (F-G)) stayed fixed in position during stages 3 and 4 (Fig. 5.1 (H-I)). These relatively static cells may reflect either a zero net balance of forces in these epithelial regions, or attachment of these cells to the yolksac or the vitelline membrane.

(Stage 5) Expansion of the serosa epithelium appeared as a smooth and continuous process up to the point when the cable at the leading edge of the serosa lined the circumference of the formed serosa window (Fig. 5.1 (F-I)). After this point, as the window closed, cells at the edge of the serosa window advanced in a zig-zag rather than a direct manner (Fig. 5.1 (J)). For more information about serosa window closure, see “5.2.8 Serosa window closure”). Immediately after window closure and separation of the serosa from the amnion epithelium, the germband occupied 79% of the egg length (79% EL; $\sigma = 4.1$ percentage points; measurements based on 4 embryos). The anterior end of the germband was positioned at 94% EL ($\sigma = 3.2$ percentage points) and the posterior end at 15% EL ($\sigma = 1.8$ percentage points) from the posterior pole (Fig. 5.2 (A)).

(Stage 6) Following amnion and serosa separation, the relative position, size and shape of serosa cells remained unchanged throughout germband elongation (Mov. 5.1 and 5.2). Shortly after the germband was released into the yolk, the head region extended anteriorly, curled dorsally at the anterior pole and stayed in this position throughout axial elongation (Fig. 5.2 (B-C) and Mov. 5.5). As segments were added sequentially from the growth zone, the germband extended posteriorly, curled round the posterior pole and extended along the dorsal side (Fig. 5.2 (B-C) and Mov. 5.5 and 5.7). As described in the previous chapter (“4. Cellularisation in *Tribolium* – a more widely conserved mode than *Drosophila*?”), I observed that the overall length of the germband expanded and contracted repeatedly and this correlated with cleavage of the underlying yolk (Mov. 5.5).

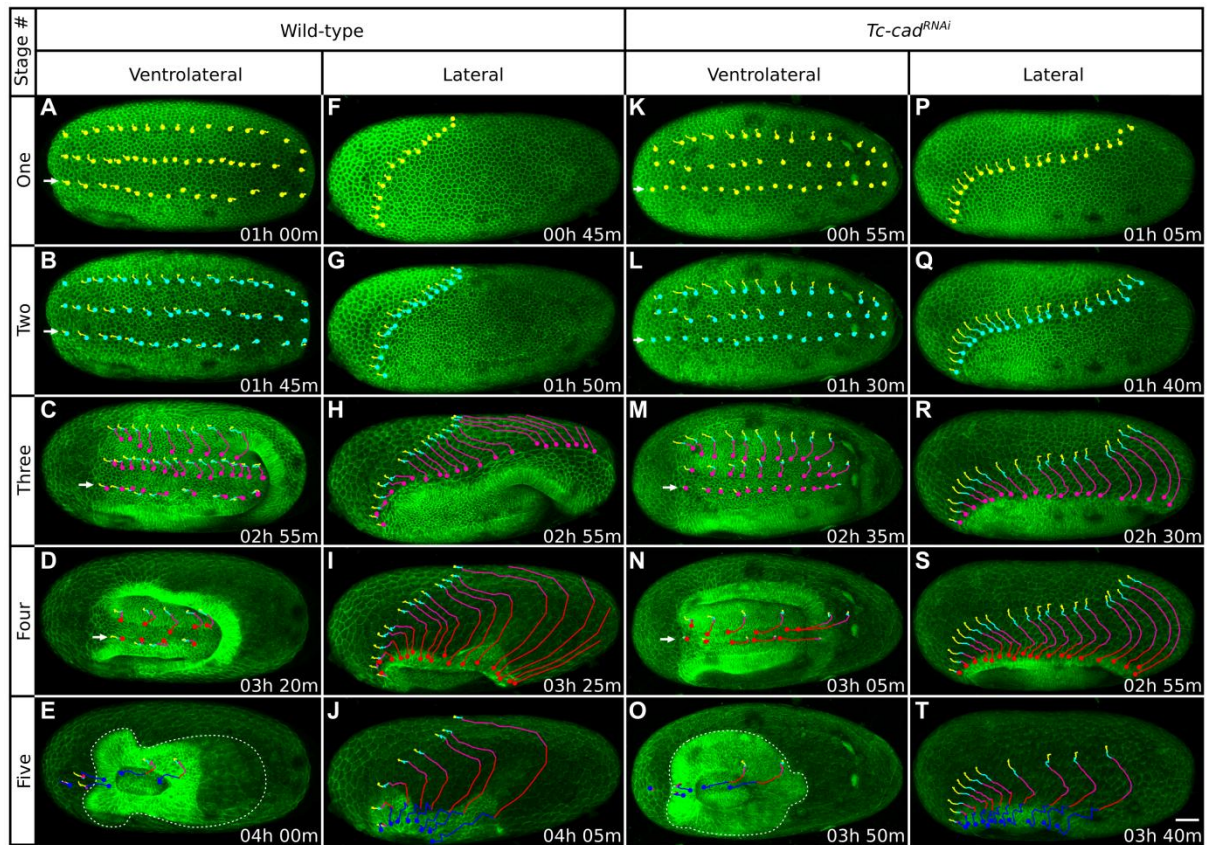


Fig. 5.1. Patterns of cell movement during *Tribolium* embryogenesis in wild-type and *Tc-cad^{RNAi}* embryos. Each column shows a different *GAP43-YFP*-labeled embryo at representative time-points spanning, from top to bottom, stages 1 to 5. (A-E) Ventrolateral views of a wild-type embryo, (F-J) lateral views of a wild-type embryo, (K-O) ventrolateral views of a *Tc-cad^{RNAi}* embryo, and (P-T) lateral views of a *Tc-cad^{RNAi}* embryo. In each embryo, cells were tracked from the beginning of stage 1 (i.e. the onset of coordinated cell movements), and all panels are timed against this starting point. Cell tracks are color-coded according to stages: stage 1 in yellow, 2 in cyan, 3 in magenta, 4 in red and 5 in blue. The corresponding position of cells is indicated with dots, and tracks are displayed up to that time-point. Ventrolateral views show rows of tracked cells across the anterior-posterior axis; in stages 1 to 4, the bottom row (marked with arrows) is very close to the ventral midline; in stage 5, the dotted line outlines the germbands. Lateral views show tracks of leading serosa cells. Please refer to the text for description of cell and tissue movements observed. The fluorescent signal is locally impaired in some embryo regions by autofluorescent and dark blemishes on the vitelline membrane. Average intensity projections, anterior to the left and dorsal to the top. Scale bar is 50 μ m.

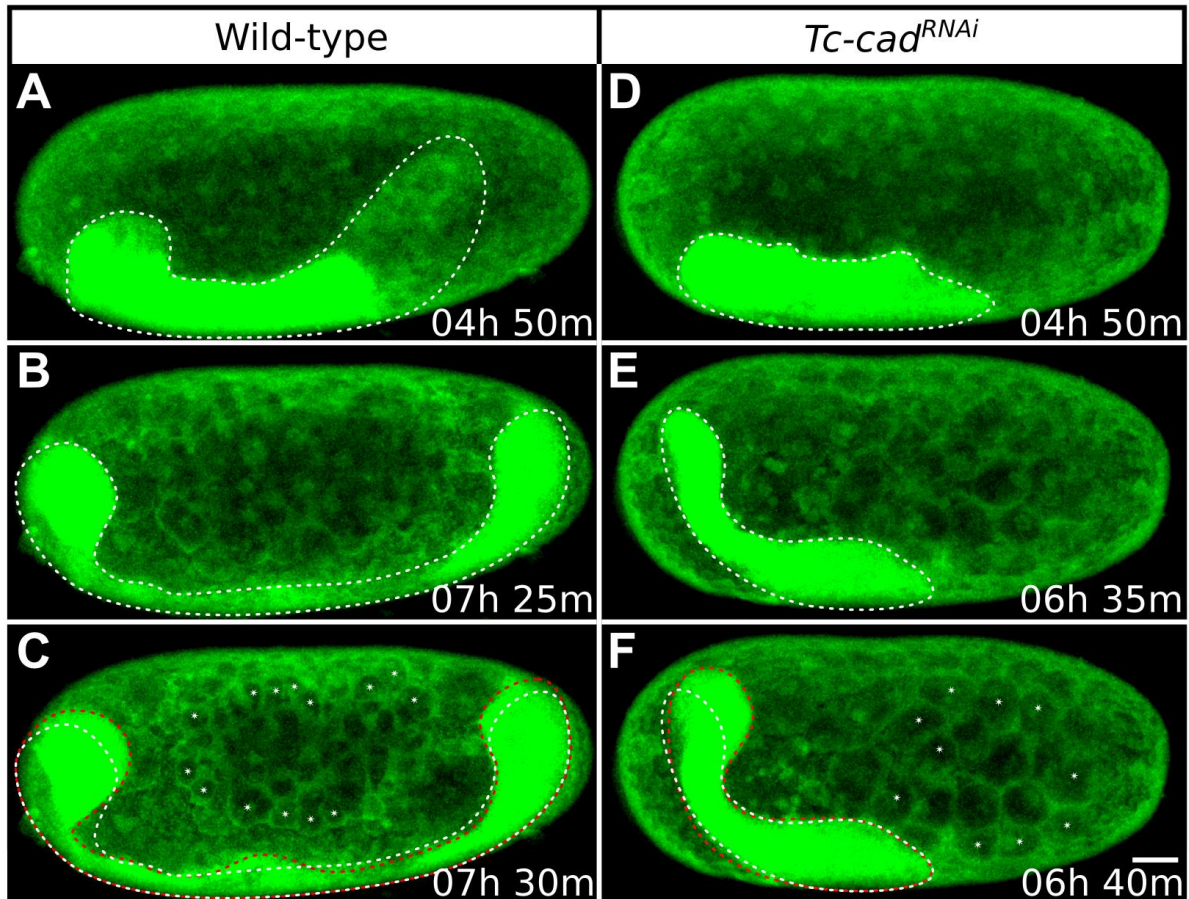


Fig. 5.2. Patterns of *Tribolium germband* elongation in wild-type and *Tc-cad*^{RNAi} embryos. Each column shows a single GAP43-YFP-labeled embryo at progressive time-points during stage 6. (A-C) Lateral views of the wild-type embryo also shown in Fig. 5.1 (F-J), and (D-F) lateral views of the *Tc-cad*^{RNAi} embryo also shown in Fig. 5.1 (P-T). All images are average intensity projections with uniformly enhanced brightness/contrast to show the germband (outlined with dotted line) and the membrane-bound yolk spheres. Panels are timed against the onset of stage 1. (A, D) Size and position of germbands immediately after serosa window closure. The germband is truncated posteriorly after *Tc-cad* RNAi. (B, E) The control germband grows considerably and extends around both poles. The *Tc-cad*^{RNAi} germband fails to grow, but is displaced anteriorly with the head region curved around the anterior pole. (C, F) At the following time-point, both ends of the control embryo and the anterior end of the *Tc-cad*^{RNAi} embryos move towards the dorsal side (previous position indicated with white dotted line and new position with red dotted line). This movement is accompanied by the appearance of extra membrane-bound yolk spheres (asterisks) compared to the previous time-point. Anterior to the left and dorsal to the top. Scale bar is 50 μ m.

Table 5.1. Overview of staging system for *Tribolium* embryogenesis

Time (min) ¹	Staging system ²				
	Stage 1	Stage 2	Stage 3	Stage 4	Stage 5
0	Cell movement				
10					
20					
30					
40	Cell closure				
50	Initiation of 13 th division				
60					
70					
80					
90					
100		Initiation of posterior AF ³			
110					
120					
130					
140					
150					
160					
170			Cable at posterior pole		
180					
190				Horseshoe AF ³	
200					
210				Oval AF ³ forms	
220					
230					
240					
250					
260					
270					
280					
290					
300					
310					Serosa window closure complete
320					
330					
340					

¹ Times are given relative to beginning of phase 1, when global cell movements initiate. Time 0 corresponds approximately to 8.5 hours (± 45 minutes) after egg lay, and to 1 hour (± 20 minutes) after the 12th round of divisions.

² Landmark events are indicated with light grey boxes and elapsed time in between with dark grey boxes. Landmark events defining the transition between stages span two neighbouring columns. Note that some events are more temporally restricted than others indicated by the height of the boxes.

³AF, amniotic fold.

Table 5.2. Relation of this staging system to previously published staging systems of *Tribolium* embryogenesis

<i>Tribolium</i> embryogenesis staging systems	Authors' Nomenclature	Relation to our phase staging system
Handel et al., 2000	7-9.5 hrs AEL ¹	Stage 1
	9-11.5 hrs AEL ¹	Stage 2
	11-12.5 hrs AEL ¹	Stage 3
	12-13.5 hrs AEL ¹	Stage 4
Sarrazin et al., 2012	3.II	Stage 3
	3.III	Stage 4
	4.I to 5.I	Stage 5
El-Sherif et al., 2012	B0	N/A
	B1 to B6	Stage 1
	B7 to B8	Stage 2
	B9	Stage 3
	G1 to G4	Stages 4 to 5

¹ Time after egg lay, study carried out with embryos developing at 30°C.

5.2.2 Altered fate map, tissue and cell dynamics in *Tc-cad* knock-down embryos

My transient labelling method allowed me to describe in detail cell and tissue dynamics in developing wild-type *Tribolium* embryos. I then wanted to make the link between gene function and the observed morphogenetic cell and tissue behaviours. To achieve this, I combined transient expression of fluorescent markers with embryonic RNAi against the *Tribolium caudal* (*Tc-cad*) gene. I co-injected GAP43-YFP mRNA (1 µg/µl) and *Tc-cad* dsRNA (0.8 µg/µl) targeting both *Tc-cad* isoforms A and B, and carried out time-lapse microscopy of injected eggs from blastoderm stage onwards.

In my experiments, embryonic RNAi for *Tc-cad* resulted in abnormally short and wide germbands enveloped by amnion and serosa membranes (Fig. 5.1 (O) and Mov. 5.3 and 5.4), and these germbands completely failed to elongate (Fig. 5.2 (D-F) and Mov. 5.5). This phenotype is weaker than that of maternal RNAi for *Tc-cad*, and likely reflected a partial knock-down of *Tc-cad* function during earlier blastoderm stages and more complete knock-down of *Tc-cad* function during later stages of axial elongation from the posterior growth zone. Importantly, these perturbations caused a moderate change in the fate map of *Tc-cad* knock-down embryos and in the relative proportions of the serosa and embryonic rudiments (see below). Thus, by tracking individual cells in these imaged *Tc-cad* RNAi embryos (Fig. 5.1 and Mov. 5.3 and 5.4), and comparing these to cell movements in normally developing control embryos, I was able to monitor the effects of fate map composition on cell behaviours during *Tribolium* morphogenesis. Below, I describe the differences between *Tc-cad* RNAi and control embryos according to the same six-stage classification described above.

(Stage 1) Embryonic knock-down of *Tc-cad* had no obvious effect on blastoderm formation. RNAi and control embryos were indistinguishable at the uniform blastoderm stage with similar numbers and densities of cuboidal blastoderm cells (compare Fig. 5.1 (A,F) with 5.1 (K,P), Fig. 5.4 (A-A'') with 5.4 (C-C''), and Fig. 5.5 (A-A''') with 5.5 (E-E''')); I counted on average 257 cells ($\sigma = 32$ cells) per 30000 μm^2 in 3 *Tc-cad* knock-down embryos and 268 cells ($\sigma = 32$ cells) in 3 control embryos. The early stage of cell movement, before the onset of cell division, was visible in *Tc-cad* RNAi embryos (Fig. 5.1 (K,P)). The pattern of cell movements in the anterior half was similar to that in control embryos (i.e. cells moved posteriorly and ventrally), but cells in the posterior half moved primarily ventrally and only very little anteriorly (also see stage 2 next).

(Stage 2) During normal development, the major landmark of this stage is the morphological differentiation of embryonic and serosa cells. This differentiation was also evident in *Tc-cad* RNAi embryos (Fig. 5.4 (D-D'') and Fig. 5.5 (F-F''')), but the extent of embryonic cell division, and the pattern of cell shape change, revealed the altered fate map of *Tc-cad* knock-down embryos. In these embryos, the domain of non-dividing and flattening serosa cells was expanded considerably along the dorsal side of the embryo from 55% EL (measured from posterior pole) in wild-type controls ($\sigma = 2.2$ percentage points; measurements based on 4 embryos) to 22% EL after *Tc-cad* RNAi ($\sigma = 1.7$ percentage points; measurements based on 4 embryos) (compare Fig. 5.1 (G) with 5.1 (Q), and see “5.2.4 Cell shape changes during condensation”). From this data, I conclude that after *Tc-cad* knock-down, the serosa primordium occupied most of the dorsal half of the blastoderm, while the

embryonic primordium was restricted to the ventral half of the blastoderm (compare Fig. 5.1 (G) with 5.1 (Q)).

During this stage, tracked cells in *Tc-cad* knock-down embryos continued slight movements along the same trajectories initiated during stage 1 (Fig. 5.1 (L)). Hence, the main difference to control embryos was that cells in the posterior half continued their ventral movement and only few changed direction posteriorly (compare Fig. 5.1 (B) with 5.1 (L)).

(Stage 3) From stage 3 onwards, the differences between control and treated embryos were striking: First, the amnion-serosa boundary moved round the posterior pole of *Tc-cad* RNAi embryos shortly after the serosa started to expand (earlier than in wild-type embryos, Mov. 5.4). During this ventral-posterior movement, the tracks of the leading serosa cells were steeper than in control embryos (compare Fig. 5.1 (H) with 5.1 (R)). Second, the lateral ectodermal cells did not condense directly towards the ventral midline, as in controls, but adopted anterior ventral trajectories (compare Fig. 5.1 (C) with 5.1 (M)). Although the embryonic cells became columnar, no cell intercalation was visible, which resulted in an abnormally short and wide germband (see “5.2.5 Cell intercalation and cell contraction”). Lastly, involution of the amnion was limited, resulting in a much shallower posterior amniotic fold compared to control embryos (compare Fig. 5.1 (C,H) with 5.1 (M,R) and Mov. 3.1 with 3.4 and 3.2 with 3.4).

(Stage 4) During stage 4, the condensing germband in *Tc-cad* RNAi embryos appeared conspicuously straight-sided; it was not constricted behind the head lobes as in control embryos (compare Fig. 5.1 (D) with (N)). This shape difference rendered the dynamics of amnion folding particularly pronounced (Mov. 5.3 and 5.4). First, the shallow posterior amniotic fold extended laterally over the flanks of the germband along its entire length, giving rise to the horseshoe amniotic fold (Fig. 5.1 (N)). After formation of the horseshoe fold, the amnion folded over the head lobes anteriorly forming an oval window over the germband (Fig. 5.1 (O)). The serosa cable, which in control embryos was conspicuous throughout the epibolic movement of the serosa, was only visible in *Tc-cad* RNAi embryos from the time of formation of the horseshoe amniotic fold onwards (compare Fig. 5.1 (H,I) with (R,S)). Once again, I observed a temporal association between serosa cable constriction and amnion fold progression (Mov. 5.3 and 5.4).

Remarkably, during this stage, the lateral ectodermal cells in *Tc-cad* RNAi embryos moved much further anteriorly compared to controls, advancing ahead of the shallow amniotic fold instead of becoming submerged by it and stopping their movement (compare Fig. 5.1 (D) with (N)). As far as I could track these cells, they appeared to stop their anterior

movement only when the oval amniotic fold and serosa window formed (Fig. 5.1 (O)). At the end of this stage, the germband in *Tc-cad* RNAi embryos was much shorter (in the anterior-posterior axis) and wider (in the dorsal-ventral axis) compared to controls (compare Fig. 6.1 (E) with 5.1 (O)). Collectively, my data suggest that the reduced size of the embryonic rudiment, the absence of germband convergent extension by polarized cell intercalation, and the prolonged anterior movement of cells all contribute to germband deformation in *Tc-cad* RNAi embryos.

(Stage 5) The forming serosa window in *Tc-cad* RNAi embryos was more rounded than in control embryos (compare Fig. 5.1 (J) with (T)), but cells at the edge of the window advanced in a zig-zag manner as in controls, suggesting that a similar mechanism of window closure was involved (compare Fig. 5.1 (J) with (T)). After window closure, the serosa membrane in *Tc-cad* knock-down embryos was composed of a larger number of smaller cells compared to controls; I counted on average 97 serosa cells ($\sigma = 9$ cells) per $30000 \mu\text{m}^2$ in 3 *Tc-cad* knock-down embryos versus 76 cells ($\sigma = 3$ cells) in 3 control embryos. This difference is in agreement with the fate map change and the expansion of the serosa primordium in *Tc-cad* knock-down embryos.

At the end of this stage, the *Tc-cad* RNAi germband was truncated, occupying 51% EL ($\sigma = 2.1$ percentage points; measurements based on 4 embryos), unlike 79% EL in controls (compare Fig. 5.1 (E) with (O) and Fig. 5.2 (A) with 5.2 (D)). The anterior end of the germband was positioned at 93% EL ($\sigma = 4.3$ percentage points) and the posterior end reached only 42% EL ($\sigma = 5.3$ percentage points). Thus, after *Tc-cad* knock-down, the anterior end was at about the same position as in wild-type (93% EL vs. 94% EL), but the posterior end was positioned more anteriorly relative to wild-type (42% EL vs. 15% EL).

(Stage 6) I observed no posterior elongation of *Tc-cad* RNAi embryos during stage 6, a stage when the germband normally elongates as new segments are added posteriorly in wild-type embryos (Fig. 5.2 and Mov. 5.5). The head region of the truncated germband extended anteriorly and curled dorsally around the anterior pole as in wild-type, but this was accompanied by a slight anterior shift of the entire germband (Fig. 5.2 (D-E) and Mov. 5.5). I did observe repeated advancement and retraction of the anterior end of the germband in tight temporal association with yolk cleavage, much as in wild-type, but the posterior of the germband exhibited little or no movement (Fig. 5.2 (E-F) and Mov. 5.5).

5.2.3. Formation of the differentiated blastoderm

Handel *et al.* had observed that one round of cell division took place during the period I define as stage 2 (Handel et al., 2000). It seemed to occur largely in the presumptive germ rudiment and it is largely asynchronous (Handel et al., 2000; Handel et al., 2005). From this stage onwards, known as the differentiated blastoderm (Anderson, 1972a; Anderson, 1972b), the distinction between embryonic and extraembryonic cells becomes progressively more pronounced. In order to verify and extend these previous observations, I carried out live imaging of embryos that were transiently expressing H2B-RFP with or without GAP43-YFP. My results confirmed that the 13th divisions occurred exclusively in the presumptive embryonic rudiment, but not in the presumptive serosa (Fig. 5.3 (A-A'')) and Mov. 5.6). My time-lapse recordings of several embryos (prepared and imaged in tandem) showed that cells in the embryonic rudiment divided asynchronously, and that the time taken from first to last cell division varied between 80-110 minutes across embryos.

In *Drosophila*, the first asynchronous post-blastoderm divisions (cycle 14 in *Drosophila* versus cycle 13 in *Tribolium*) are partitioned into distinct clusters of cells dividing together, known as mitotic domains (Foe, 1989). My time-lapse recordings did not reveal any obvious division patterns in *Tribolium* that could resemble mitotic domains. Lastly, in contrast to Handel et al. (2005), I did not observe the earliest divisions at the ventral midline or the anterior rim of the anlage in any embryo.

Based on SEM data of the anlage division, cells protruding from the regular epithelial plane were interpreted as mitotic figures (Handel et al., 2000). I hypothesised that this may be due to interkinetic nuclear migration, which has now been described in many animals (Meyer et al., 2011). To test this hypothesis I looked at how dividing and non-dividing nuclei are positioned with respect to their neighbours in embryos transiently labelled with both H2B-RFP and GAP43-YFP. Before division, nuclei were arranged in the same plane of the blastoderm epithelium (Fig. 5.3 (B)). During division, some nuclei did move apically out of the regular plane of the epithelium (Fig. 5.3 (B') arrow), although others stayed in the plane (Fig. 5.3 (B') arrowhead). I also observed some non-dividing nuclei move out of the regular plane of the epithelium (not shown).

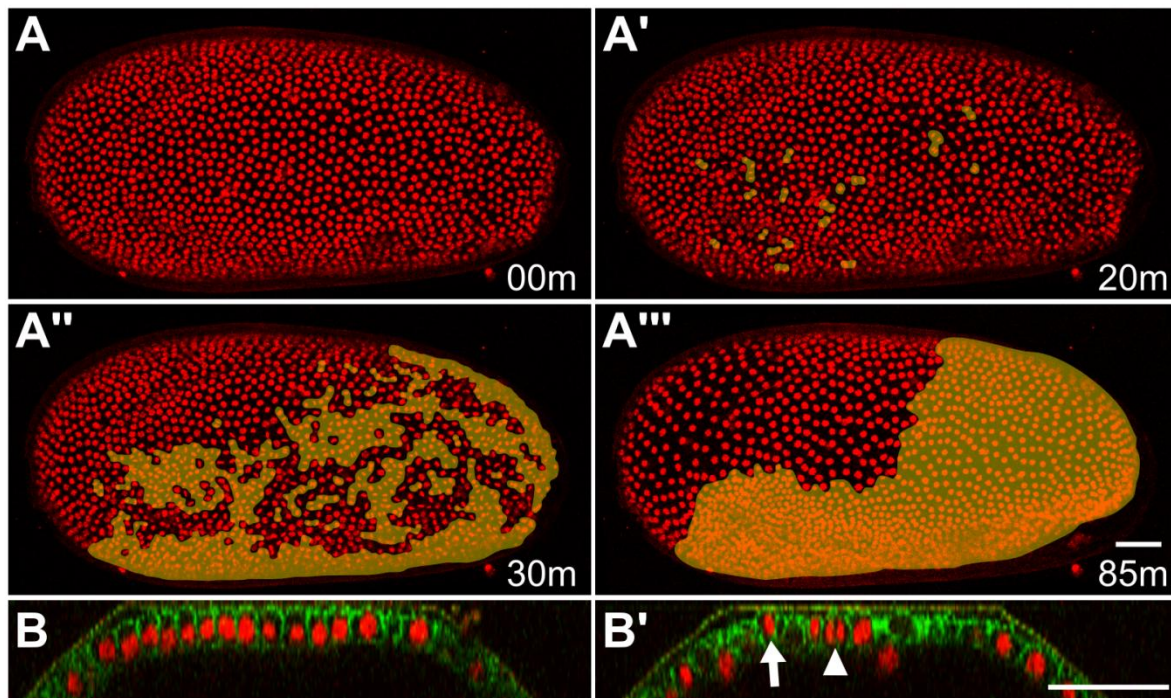


Fig. 5.3. *Tribolium* blastoderm differentiation. (A-A''') Time series of the 13th round of cell divisions during blastoderm differentiation. All panels show average intensity projections of an H2B-RFP-labeled embryo (lateral views, anterior to the left and dorsal to the top) at different stages timed against E. Divided nuclei in the embryonic rudiment are indicated with an orange mask. (A) Nuclei have uniform size and distribution before the onset of 13th divisions. (A'-A'') Asynchronous nuclear divisions are detected throughout the embryonic rudiment, but not in the serosa primordium. (A''') Divided nuclei in the embryonic rudiment become smaller and more tightly packed compared to non-dividing serosa nuclei, which become more widely spaced. (B-B') Cross-sections of blastoderm stage embryo doubly labelled with H2B-RFP and GAP43-YFP (B) before and (B') during 13th round of division. (B) Interphase nuclei are arranged in the regular plane of the epithelium. (B') Dividing nuclei are detected either at the level of the epithelium (arrowhead) or at a more apical level (arrow). A yolk nucleus is visible below the epithelium. Scale bars are 50 μ m.

5.2.4 Cell shape changes during condensation

As mentioned in the previous chapter (“4. Cellularisation in *Tribolium* – a more widely conserved mode than *Drosophila*?”), formation of the differentiated blastoderm is also accompanied by a change in blastoderm cell shapes. At about the same time as the start of the rudiment divisions, embryonic cells became columnar (i.e. elongated in the apical-basal direction), while serosa cells flattened and became squamous (i.e. shortened in the apical-basal direction) (Fig. 5.4 (B-B''')). Following *Tc-cad* RNAi, all cells in the expanded non-

dividing domain flattened and became squamous, showing that they had adopted serosal cell fate (Fig. 5.4 (D-D''')). The domain of dividing and contracting embryonic cells exhibited a corresponding reduction to the ventral side of the embryo (Fig. 5.4 (D-D''')). This distinction persisted throughout condensation in both wildtype and *Tc-cad* RNAi embryos (Fig. 5.5, plus see next section).

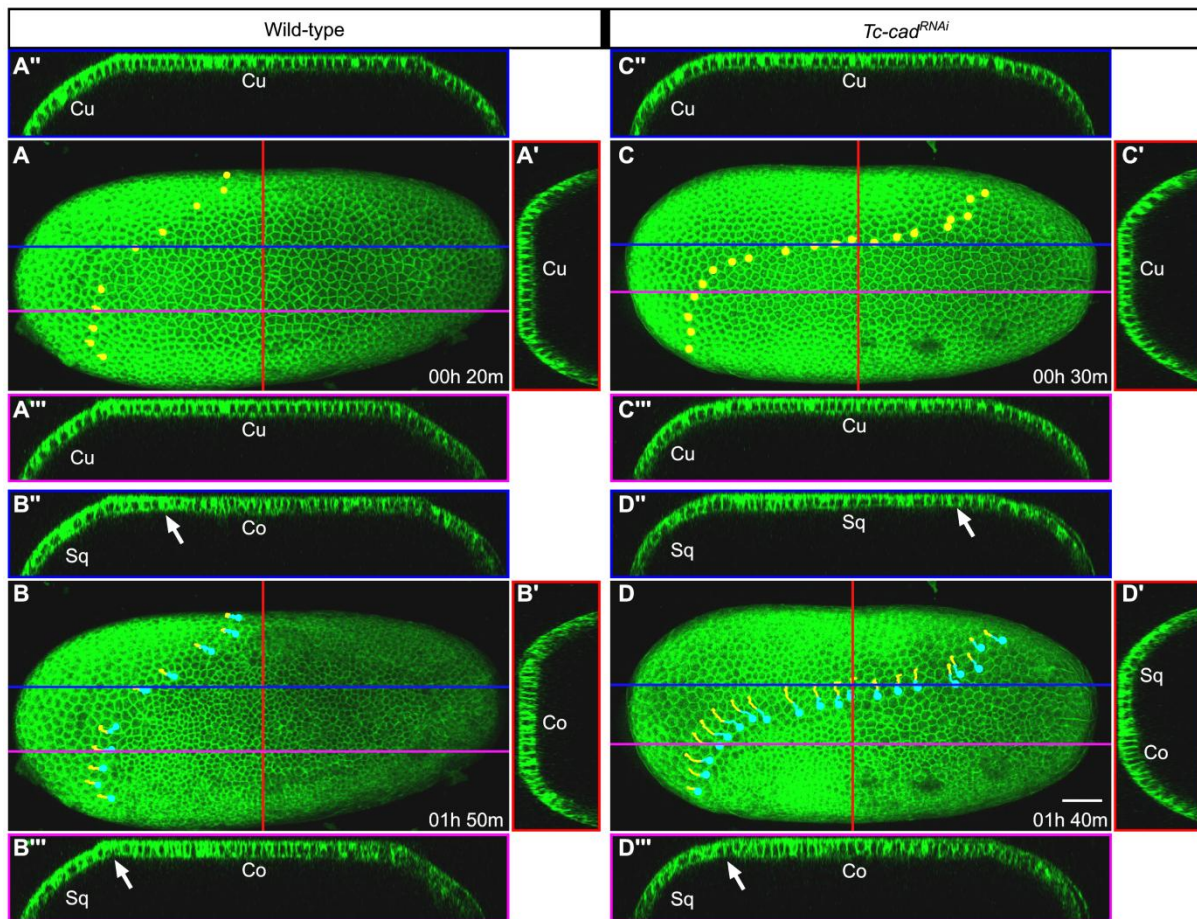


Fig. 5.4. Differential distribution of serosal and embryonic cells in wild-type and *Tc-cad*^{RNAi} differentiated blastoderms. (A-D'') Lateral views and cross-sections of GAP43-YFP-labeled (A-B'') wild-type embryo also shown in Fig. 5.1 (F-J), and (C-D'') *Tc-cad*^{RNAi} embryo also shown in Fig. 5.1 (P-T). (A-D) Average intensity projections, (A'-D') YZ transverse sections, (A''-D'') XZ frontal sections in the dorsal half, (A'''-D''') XZ frontal sections in the ventral half of the blastoderm. The top panels show uniform blastoderm stage embryos at the beginning of stage 1, and bottom panels show differentiated blastoderm stage embryos at the end of stage 2. Yellow and cyan dots mark some of the serosa cells at the border between the serosa and germ rudiment. (A-A'') All cells appear uniform and cuboidal (Cu) in shape. (B-B'') The anterior cap of serosa cells start adopting a squamous

shape (Sq) and the more posterior embryonic cells a columnar shape (Co). The border between flattening serosa and elongating embryonic cells (arrows in B'' and B''') is slightly more posterior in the dorsal half compared to the ventral half. The transverse section in the middle of the embryo in B' shows that all cells along the dorsal-ventral axis exhibit a uniform shape (Co). (C-C''') After Tc-cad knock-down, the uniform blastoderm is composed of cuboidal (Cu) cells as in wild-type controls. (D-D''') The serosa primordium covers most of the dorsal half of the differentiated blastoderm and the embryonic primordium is restricted to the ventral half. The border between flattening serosa and elongating embryonic cells (arrows in D'' and D''') is much more posterior in the dorsal half compared to the ventral half. The transverse section in the middle of the embryo in D' shows a marked difference in shape between serosa cells dorsally (Sq) and embryonic cells ventrally (Co). Anterior is to the left in the average intensity projections and in the XZ sections, apical is to the left in the YZ sections. Scale bar is 50 μ m.

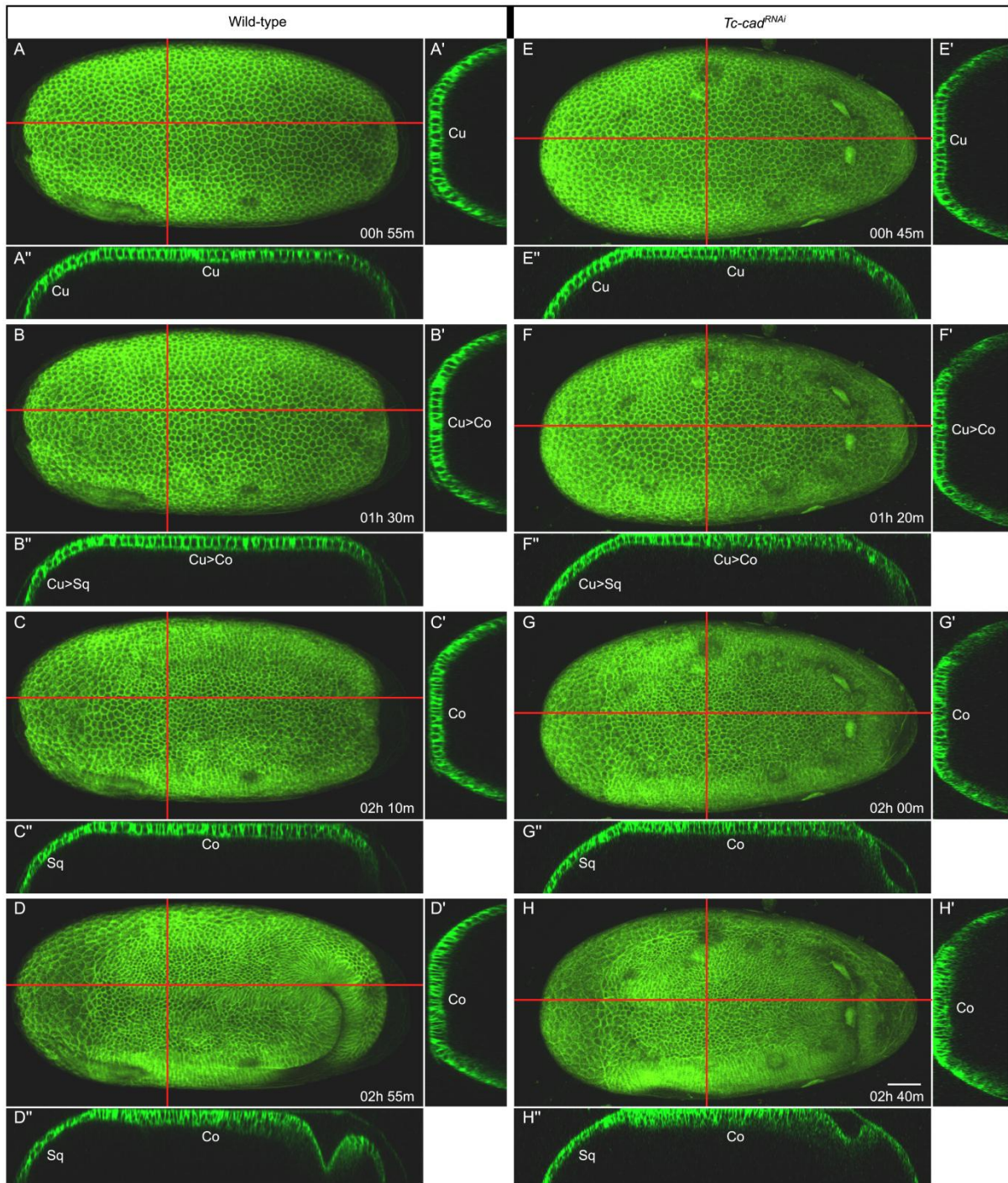


Fig. 5.5. Cell shape changes during *Tribolium* embryogenesis. (A-H'') Ventrolateral views and cross-sections of GAP43-YFP-labeled (A-D'') wild-type embryo also shown in Fig. 5.1 (A-E), and (E-H'') *Tc-cad*^{RNAi} embryo also shown in Fig. 5.1 (K-O). (A-H) Average intensity projections, (A'-H') YZ transverse sections, and (A''-H'') XZ sagittal sections at representative time-points spanning, from top to bottom, the first three stages of *Tribolium* embryogenesis. In each time-point, cells exhibit very similar morphologies in wild-type and *Tc-cad*^{RNAi} embryos. (A-A'' and E-E'') At the end of stage 1, the uniform blastoderm is composed of cuboidal cells (Cu). (B-B'' and F-F'') In the differentiated blastoderm at the

end of stage 2, the serosa cells anteriorly start adopting a squamous shape ($Cu > Sq$) and the rest embryonic cells a columnar shape ($Cu > Co$). (C-D'' and G-H'') During stage 3, the squamous shape of serosa cells (Sq) and the columnar shape of embryonic cells (Co) become progressively more pronounced. In the average intensity projections anterior is to the left, in the YZ sections apical is to the left, and in the XZ sections anterior is to the left and ventral to the top. Scale bar is 50 μm .

5.2.5 Cell intercalation and cell contraction

During stage 3-4, the most prominent movement of germ rudiment cells is from the lateral to the ventral part of the rudiment. To test if this was caused by cell intercalation, I carried out tracking of abutting rows of ectodermal cells. From this analysis I was able to see that the ventral movement was effected at least in part by the oriented intercalation of cells between their dorsal and ventral neighbours (Fig. 5.6 (A-B)). In *Tc-cad* RNAi embryos, however, I found no evidence for cell intercalation in *Tc-cad* RNAi embryos (Fig. 5.6 (C-D)). As a result, the germband failed to undergo convergence in the dorsal-ventral axis and extension in the anterior-posterior axis (compare Fig. 5.1 (E) with (O)).

I also found that there was a decrease in the apical area of cells both in wildtype and in *Tc-cad* RNAi embryos to about 75% and 73% of their original size, respectively (measured from total apical area of labelled cells shown in Fig. 5.1). Given that cells are elongating in the apical-basal axis (previous section), this decrease in apical area likely reflects contraction of the outline of the cell at all apical-basal positions.

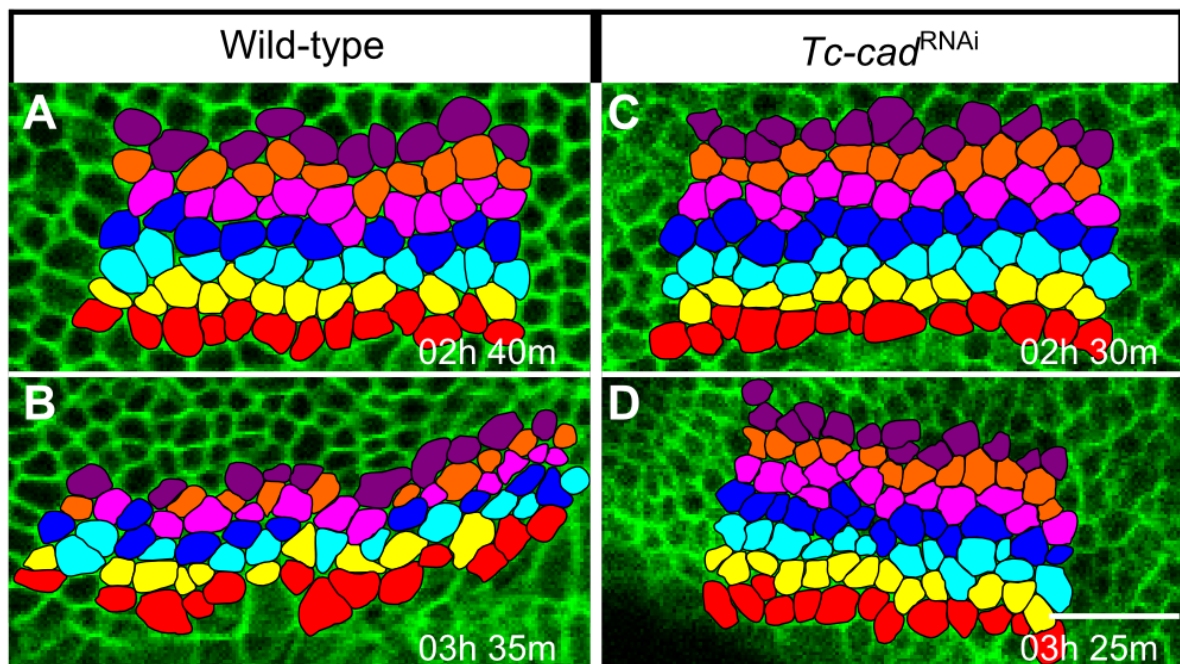


Fig. 5.6. Cell behaviours during *Tribolium* germband condensation in wild-type and *Tc-cad*^{RNAi} embryos. (A-B) Cell intercalation in wild-type embryo and (C-D) absence thereof in *Tc-cad*^{RNAi} embryo. Panels show ventrolateral views of GAP43-YFP-labeled embryos at two time-points during stages 3 (top) and 4 (bottom). All panels are arranged with anterior to the left and show average intensity projections of 6 μm substacks covering the anterior left side of the condensing germbands. Abutting rows of ectodermal cells, highlighted with different colours, were tracked after their 13th division. (A-B) Cells in each row become separated by ventral or dorsal neighbouring cells in the wild-type. This cell intercalation narrows the highlighted cluster of cells in the dorsal-ventral axis and lengthens it in the anterior-posterior axis. (C-D) Rows of cells remain contiguous as no cell intercalation takes place after *Tc-cad* RNAi. Scale bars are 50 μm .

5.2.6 Gastrulation of the mesoderm

During stages 3 to 5, the mesoderm of the condensing germband underwent gastrulation. My studies with live imaging of wildtype embryos labelled with GAP43-YFP confirmed previous descriptions carried out with sectioned and stained fixed embryos (Fig. 5.7; compare with Handel et al., 2005). Mesoderm internalization progressed from posterior to anterior and the internalized mesoderm appeared single-layered anteriorly and multi-layered posteriorly. I observed the characteristic bottle shape of apically constricting mesodermal cells and ventral furrow formation in anterior, but not in posterior germband regions (compare Fig. 5.7 (C''') with (D'')).

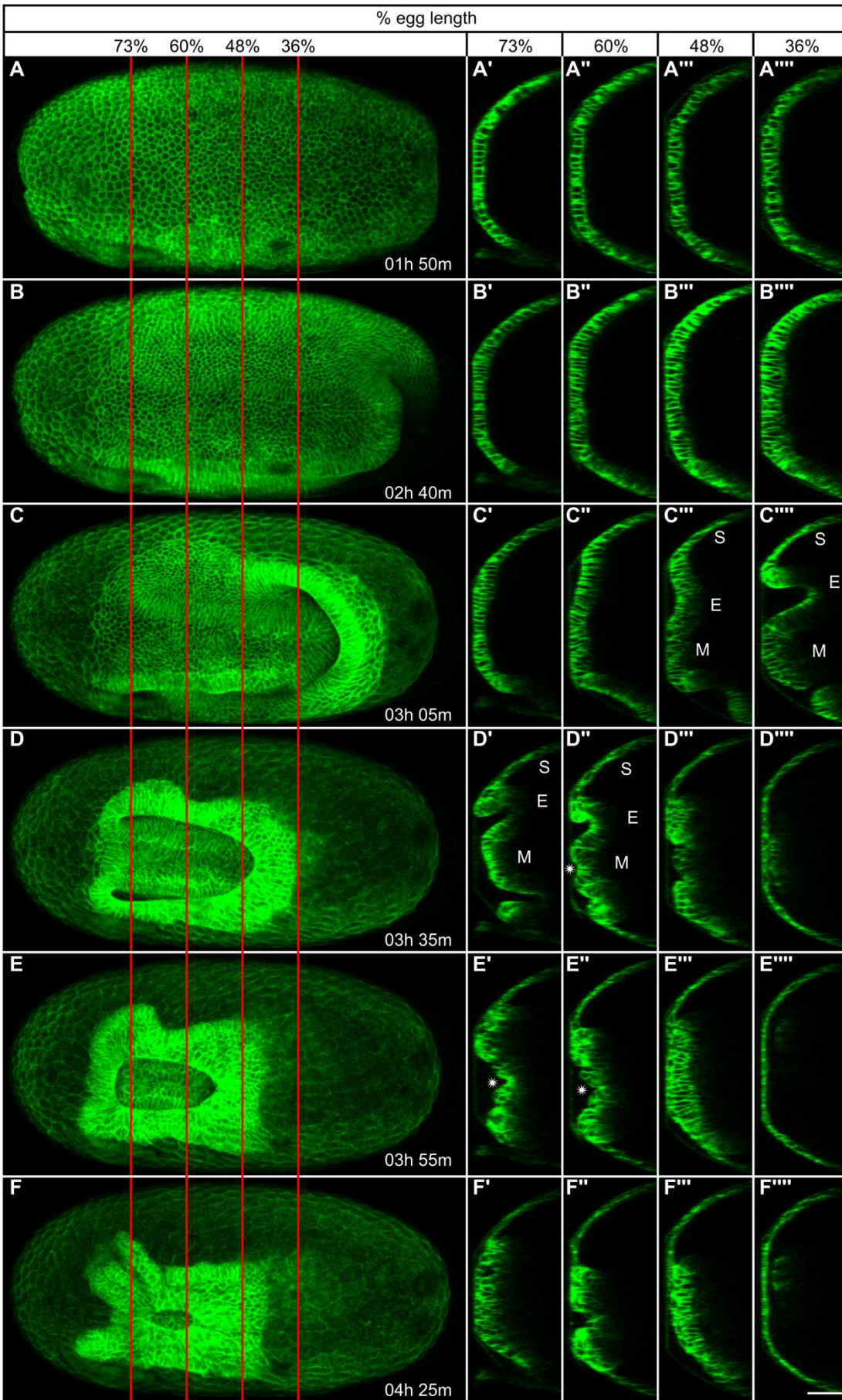


Fig. 5.7. Germband condensation and gastrulation in *Tribolium* wild-type embryo. (A-F''''') Ventrolateral views and transverse YZ sections of a GAP43-YFP-labeled wild-type embryo also shown in Fig. 5.1 (A-E). (A-F) Average intensity projections, (A'-F') transverse sections at 73% EL, (A''-F'') transverse sections at 60% EL, (A'''-F''') transverse sections at 48% EL, and (A''''-F''''') transverse sections at 36% EL at representative time-points spanning, from top to bottom, stages 2 to 5 of *Tribolium* embryogenesis. Note that the characteristic bottle shape of apically constricting mesodermal cells and ventral furrow formation are visible in anterior but not in posterior germband regions (compare C'''' with D''). M, internalizing mesoderm; E, ectoderm; S, serosa; *, ventral furrow. Scale bar is 50 μ m.

Mesoderm internalization in *Tc-cad* knock-down embryos advanced from posterior to anterior, but this stage difference was not as pronounced as in control embryos due to decreased germband length (Fig. 5.8). Unlike in control embryos, the apically constricting mesodermal cells and the ventral furrow were visible along the entire length of the truncated germband (Fig. 5.8 (D'-D''')). It should be stressed here that in my time-lapse recordings the fluorescence signal emitted from mesodermal cells deteriorated upon cell internalization and completely disappeared upon germband submersion by the amnion and serosa epithelia. This limitation did not allow me to achieve the spatial resolution previously obtained (Handel et al., 2005), nor was I able to describe cell and tissue dynamics during later stages of gastrulation.

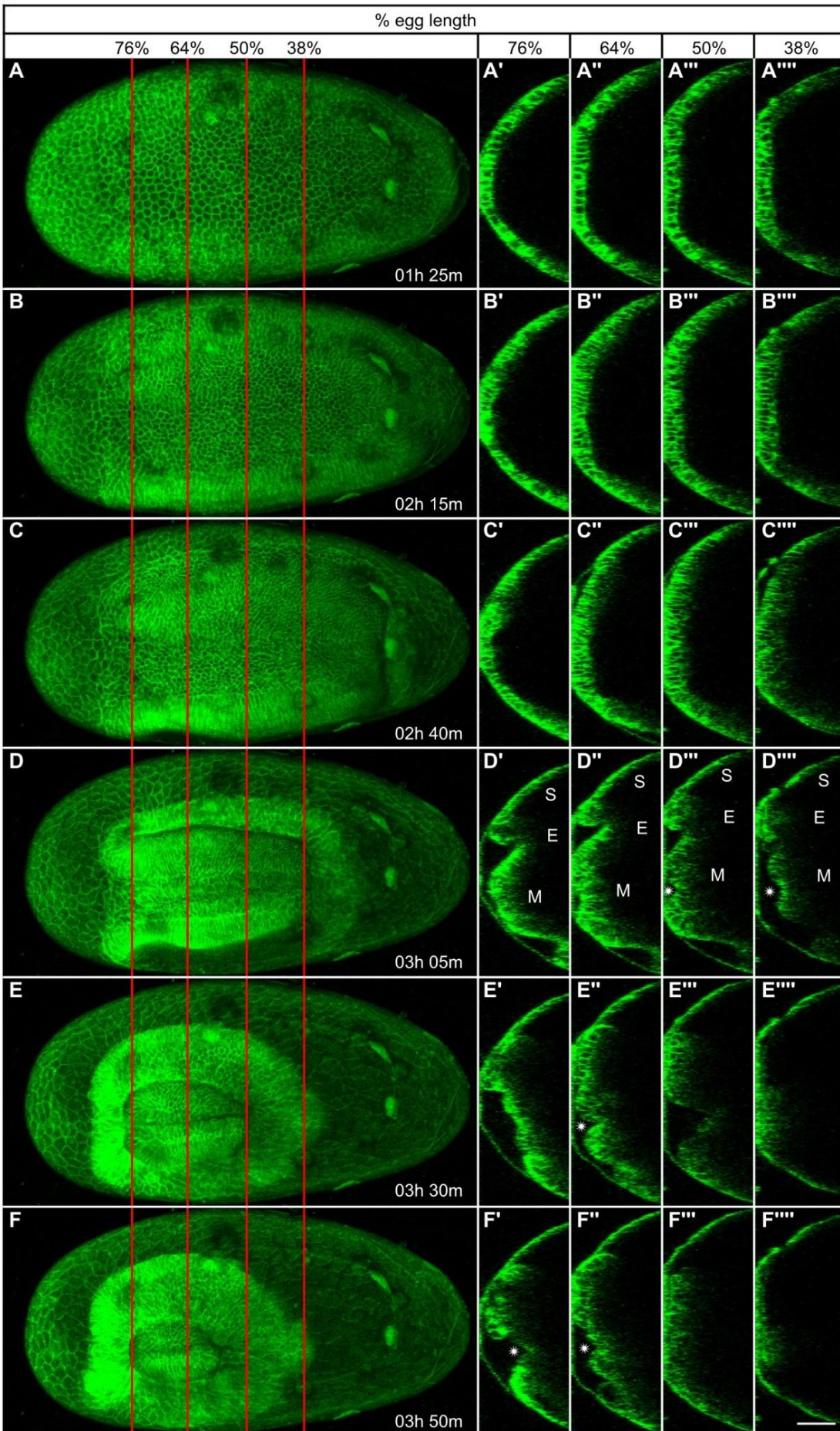


Fig. 5.8. Germband condensation and gastrulation in *Tribolium* *Tc-cad*^{RNAi} embryo. (A-F''''') Ventrolateral views and transverse YZ sections of a GAP43-YFP-labeled *Tc-cad*^{RNAi} embryo also shown in Fig. 5.1(K-O). (A-F) Average intensity projections, (A'-F') transverse sections at 76% EL, (A''-F'') transverse sections at 64% EL, (A'''-F''') transverse sections at 50% EL, and (A''''-F''''') transverse sections at 38% EL at representative time-points spanning, from top to bottom, stages 2 to 5 of *Tribolium* embryogenesis. Note that the apically constricting mesodermal cells and the ventral furrow are visible along the entire length of the truncated germband (see D'-D'''''). M, internalizing mesoderm; E, ectoderm; S, serosa; *, ventral furrow. Scale bar is 50 μ m.

I also observed a small number of cells delaminating at the anterior most medial part of the embryonic rudiment, adjacent to the amnion/serosa boundary (Fig. 5.9). These cells are most likely the anterior-medial mesenchymal cells described recently by other authors (Kittelman et al., 2013). I believe that these cells could be the *Tribolium* head mesoderm precursors as they have been shown to express the mesodermal transcription factor *twist* (Handel et al., 2005; personal observation), but they internalize separately to the trunk mesoderm similar to the majority of head mesoderm cells in *Drosophila* (de Velasco et al., 2006).

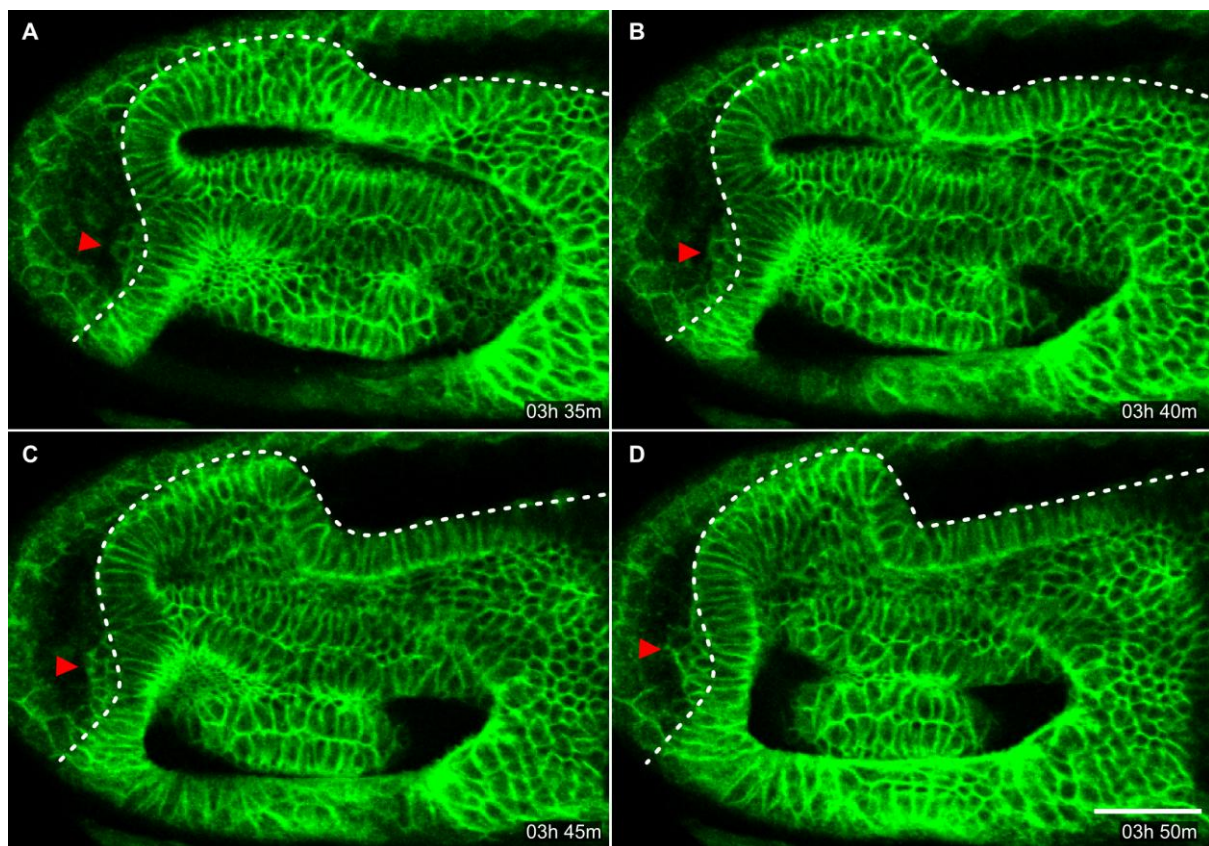


Fig. 5.9 Gastrulation in *Tribolium* wild-type embryo. (A-D) Optical sections through condensing germ band of a GAP43-YFP-labeled wild-type embryo also shown in Fig. 5.1 (A-E). Cells can be seen delaminating at anterior medial region of germ band, marked with red arrowhead. Germ band is outlined by dotted line. Each frame is an average projection of 9 μm . Panels are timed against onset of stage 1. Scale bar is 50 μm .

5.2.7 A possible role for the yolk system in *Tribolium* morphogenesis

The yolk of insect eggs, together with its accompanying reticular cytoplasm, yolk nuclei and membrane (collectively referred to as the yolk system or yolksac) plays various roles during insect development (Counce, 1961; Counce, 1973). The yolk system is a source of nutrients for the developing embryo, but it is also involved in embryo morphogenesis, including formation of the embryonic rudiment, blastokinesis and dorsal closure (Counce, 1961; Reed et al., 2004; Rickoll, 1976). In *Tribolium*, I have already described the effects of yolk cleavage on the embryo during germband elongation (see “4. Cellularisation in *Tribolium* – a more widely conserved mode than *Drosophila*?”). Handel et al. (2000) described a number of possible interactions between the yolk system and the overlying epithelia during condensation in *Tribolium*. I examined the earliest and most prominent of these interactions, the involvement of the yolk system in the formation of the posterior amniotic fold. I combined differential interference contrast microscopy with fluorescence confocal microscopy to simultaneously monitor the yolk movement, while imaging tissue dynamics in H2B-RFP labelled embryos (Fig. 5.10 (A-F’) and Mov. 5.7).

During stages 1 and 2, the yolk appeared to contract globally in concert with the surrounding blastoderm epithelium. A more pronounced yolk depression was observed locally at the posterior pole during primitive pit invagination (Fig. 5.10 (A-B’)). During stages 3 and 4, I replicated previous observations (Brown et al., 1994; Handel et al., 2000) that a posterior dorsal wedge of yolk moved around the posterior pole, bent ventrally and advanced anteriorly, exhibiting strikingly similar dynamics to the formation and advance of the posterior amniotic fold (Fig. 5.10 (C,C’) and Mov. 5.7). The yolk fold came to a standstill at the end of stage 4, around the time of serosa window formation (Fig. 5.10 (D,D’)). The yolk fold stayed in the same position during the period of serosa closure (stage 5) and started retracting posteriorly only later during stage 6 upon axial elongation (Fig. 5.10 (E,E’) and Mov. 5.7). The yolk fold retracted in tight temporal association with the extending posterior end of the growing germband. This coupled movement did not stop when the yolk fold levelled out with the rest yolksac at the posterior pole (Fig. 5.10 (E,E’)). Instead, it continued

dorsally as the posterior germband curled around the posterior pole and kept extending along the dorsal side displacing the abutting yolk further anteriorly (Fig. 5.10 (F,F') and Mov. 5.7).

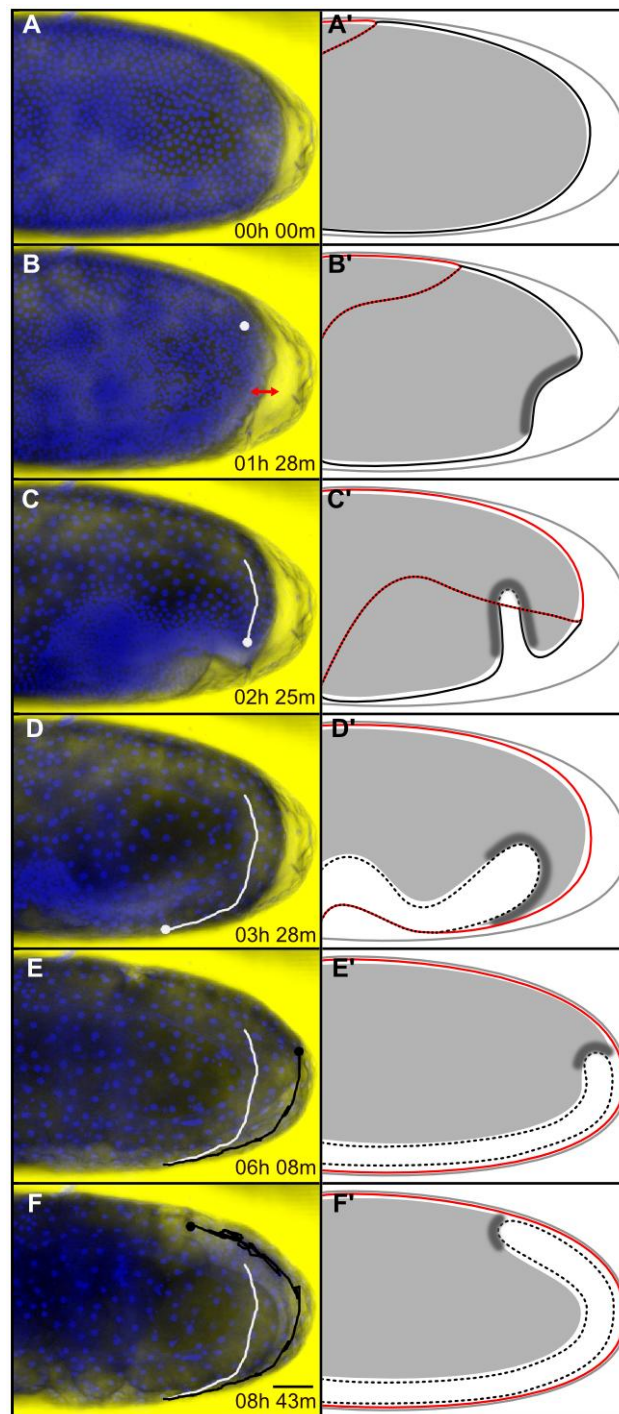


Fig. 5.10. Posterior yolk sac dynamics relative to *Tribolium* germband condensation and elongation. (A-F) Time series of posterior yolk sac deformation in an H2B-RFP-labeled embryo, and (A'-F') corresponding schematic representations. Panels A-F show average intensity projections of the posterior half of the same embryo timed against the first time-point shown in A. At each time-point, the DIC image of the embryo was overlaid with the

corresponding H2B-RFP signal shown in blue. In panels B-F, the dot indicates the position of the leading edge of the posterior yolk-fold. The white track marks the early ventral extension of the yolk-fold and the black track marks its dorsal retraction up to the corresponding time-point. In panels A'-F', the vitelline membrane is shown with a grey line, the serosa outline with a red line, the amnion/serosa boundary with a dotted red/black line, the condensing and internalized elongating embryonic rudiment with solid and dotted black lines, respectively, the yolksac with filled grey, and the presumptive posterior yolksac-germband attachment by darker shading. (A-A') Uniform blastoderm stage. (B-B') Differentiated blastoderm stage showing blastoderm and yolk depression at the posterior pole (double red arrow). (C-C') The posterior dorsal wedge of yolk extends ventrally during posterior amniotic fold formation. Note the concurrent amnion involution during yolk-fold extension. (D-D') The yolk-fold completes its ventral extension when posterior amnion involution stops and serosa window forms. (E-E') Yolk-fold retraction is tightly coupled to posterior germband extension. The yolk levels out posteriorly when the translucent germband reaches the posterior pole. (F-F') Yolksac displacement continues dorsally as the translucent germband extends around the posterior pole. Lateral views, anterior to the left and dorsal to the top. Scale bar is 50 μ m.

These observations point to a physical connection between the posterior pole of the yolksac and the posterior end of the germband during condensation and extension stages that could play a key role during *Tribolium* epithelial rearrangement (see Discussion). This interpretation is further supported by the phenotypes observed in *Tc-cad* knock-down embryos. In particular, the shallowness of the posterior amniotic fold, the lack of posterior germband submersion into the yolk and the reduced bouncing of the posterior of the germband may be related to abnormal patterning of posterior germband structures and improper attachment to the yolksac.

As another test of this hypothesis, I looked at the dynamics of the yolk fold following knock-down of *Tc-srp*, which results in yolk defects and degeneration of the amnion (see “4. Cellularisation in *Tribolium* – a more widely conserved mode than *Drosophila*?”). In these embryos, the posterior amnion fold forms and condensation proceeds normally up to stage 4 (Fig. 5.11 compare (A) with (B), and Mov. 5.8), at which point the amnion begins to degenerate and the posterior of the germband moves to the surface of the egg prematurely (Fig. 5.11 compare (A'-A'') with (B'-B'')). It also appears as if the yolksac membrane retracts to the anterior (Mov. 5.8), however, I have not been able to verify this. The premature

movement of the germband to the surface of the egg strongly supports the hypothesis that there is attachment between the yolk and the posterior of the germband. However, it does not answer the question of whether this attachment is necessary for germband condensation and/or elongation.

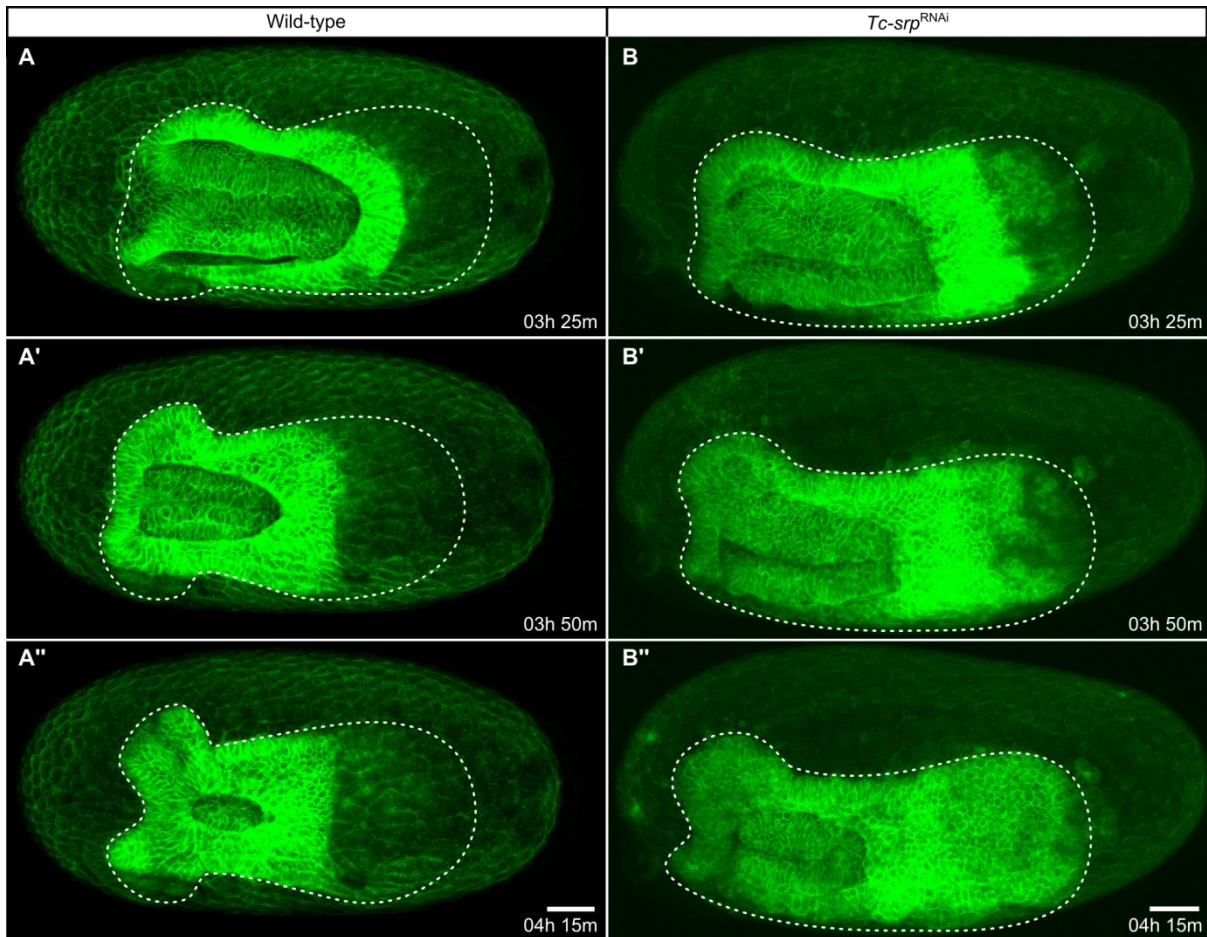


Fig. 5.11. Dynamics of the yolkfold in wild-type and $Tc-srp^{RNAi}$ embryos. Each column shows a single GAP43-YFP-labeled embryo at progressive time-points during stages 4-5. (A-A'') Ventrolateral views of the wild-type embryo also shown in Fig. 5.1 (A-E), and (B-B'') ventrolateral views of the $Tc-srp^{RNAi}$ embryo also shown in Fig. 4.5 (G). Although serosa cells are less visible in the $Tc-srp^{RNAi}$ embryo, they appeared normal when looked at in individual sections. (A and B) At the end of stage 4, the yolk fold is visible in both embryos by the way it occludes the posterior of the germband (although it is less prominent in the $Tc-srp^{RNAi}$ embryo). (A'-A'' and B'-B'') As the serosa window closes during stage 5, the amnion degenerates in the $Tc-srp^{RNAi}$ embryo and the posterior of the germ band moves to the surface of the egg. Serosa window closure also appears to be retarded in the $Tc-srp^{RNAi}$ embryo. Germ band outlines were visualised using method shown in Fig. 3.2, and are outlined with a

white dotted line. Panels are timed against onset of stage 1. Anterior to the left and dorsal to the top. Scale bars are 50 μ m.

5.2.8 Serosa window closure

During condensation, the boundary between the amnion and the serosa must first lengthen as it moves around the posterior pole (stages 1-3), and then shorten as the serosa window closes (stages 4-5). I was interested in finding out more about the effects of this process on the cells that make up the boundary between the two tissues. While I was unable to accurately track amnion cells due to tissue folding, I was able to follow serosa cells at different parts of the boundary by tracking the cells in timelapses of GAP43-YFP labelled embryos taken of different views of the egg.

Given that serosa cells are becoming wide and flat as lengthening occurs, my null hypothesis was that the lengthening of the boundary is effected entirely by cell shape change. Alternatively, the population of cells at the border may not be stable, and there may be some cell intercalation occurring (in addition to cell shape change). To test between these hypotheses, I identified the serosa cells at the boundary when it was at the posterior pole of the embryo (end of stage 3; Fig. 5.12 (A') and (B')). I then tracked these cells backwards in time to the uniform blastoderm stage (Fig. 5.12 (A) and (B)). From this analysis I found that cell intercalation took place in addition to cell shape change, although the patterns of cell intercalation were surprising.

First of all, cells that make up the posterior half of the boundary at the end of stage 3 had undergone neighbour exchange such that additional cells were added to the boundary during the lengthening process (Fig. 5.12 (A-B'), yellow labelled cells). Cells more anterior to this, however, underwent neighbour exchange in the opposite pattern, such that the number of cells at the boundary decreased during the lengthening process (Fig. 5.12 (B-B'), cyan labelled cells). Cells at the anterior of the boundary do not undergo intercalation (Fig. 5.12 (B-B'), magenta labelled cells).

During the shortening stage, cells around the entire serosa boundary underwent intercalation, such that the number of cells at the boundary decreased during serosa window closure (Fig. 5.12 (C-C')). After serosa window closure, there were several cells that could not be unambiguously tracked back to the serosa primordium (Fig. 5.12 (C'), pink labelled cells). This was true for all 3 timelapses in which I carried out extensive tracking, and may imply that some of the cells that divided during the rudiment division actually ended up at the

surface as serosa cells. However, my evidence for this hypothesis is weak, and further analysis with timelapses recorded at higher resolution need to be carried out.

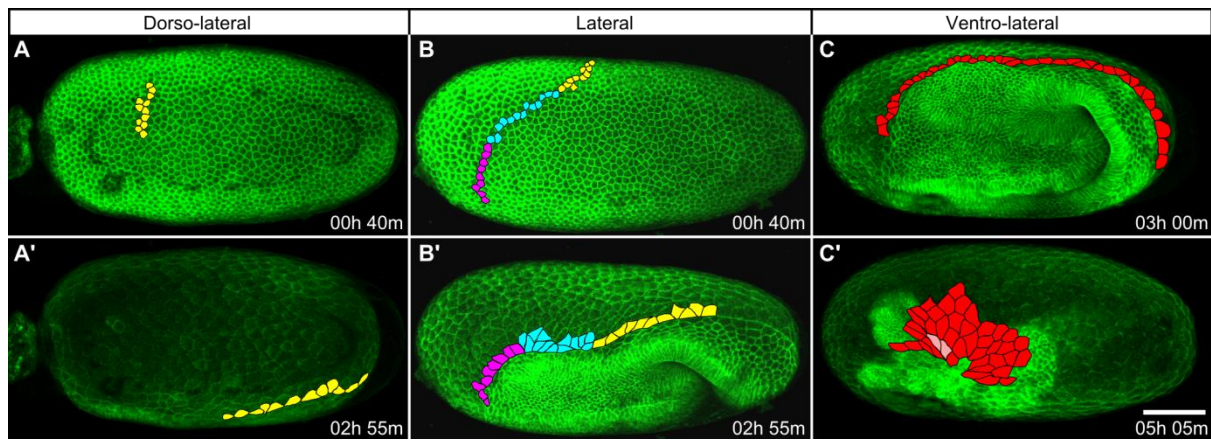


Fig. 5.12 Serosa cell behaviours during serosa window closure in wildtype *Tribolium* embryos. (A-C') Each column shows a single GAP43-YFP-labelled embryo at two times during serosa window closure. Serosa cells were identified at the end of stage 3 (A', B' and C) and either tracked backwards to the stage 1 (A and B) or forwards to serosa window closure at the end of stage 5 (C'). (A-B') During stages 1-3, cells could be differentiated into three subpopulations; one population in which some cells undergo intercalation to add more cells to the boundary (yellow labelled cells), one population that undergoes intercalation to remove cells from the boundary (cyan labelled cells) and one population that does not undergo any intercalation (magenta labelled cells). (C-C') During stages 4-5, all populations underwent intercalation to remove cells from the boundary (red labelled cells), and some cells became visible in the serosa epithelium that had not been at the boundary before (pink labelled cells). Panels are timed against onset of stage 1. Anterior to the left and dorsal to the top. Scale bars are 50 μ m.

5.3 Discussion

5.3.1 Formation of the differentiated blastoderm

In *Tribolium* and other insects, the formation of the differentiated blastoderm is caused by a combination of cell condensation and an increase in mitotic activity of the germ rudiment (Anderson, 1972b; Handel et al., 2000). From my live imaging of nuclei, I found compelling evidence that all rudiment cells divide once, and that serosa cells do not divide at all. One way to confirm this would be to carry out live imaging of embryos labelled with H2B-RFP

from multiple views at the same time, for example multi-view SPIM microscopy (Tomer et al., 2012). This approach would allow the unambiguous tracking of all nuclei within a single embryo. From this data, it would also be possible to confirm the variation in the length of time taken from the first to last division that I observed.

If all rudiment cells do in fact divide once, it is possible that this division may simply be another round of blastoderm division, albeit one that is excluded from serosa cells. In *Drosophila* embryos, the cycles of nuclear division occur rapidly until cycle 14 when a long interphase occurs and cellularisation takes place (See “4. Cellularisation in *Tribolium* – a more widely conserved mode than *Drosophila*?”). The change in rate of division is due to degradation of the string and twine proteins (the *Drosophila* homologs of Cdc25), which results in inactivation of Cdk1 (Farrell and O’Farrell, 2013). Following DNA replication, cells are unable to undergo mitosis until reactivation of Cdk1 via zygotic expression of string (Farrell and O’Farrell, 2013).

In *Tribolium* embryos, nuclear division is rapid until nuclear cycle 13, when a long interphase takes place and cellularisation is completed. It is possible that the change in division dynamics is also caused by degradation of the *Tribolium* homolog, or homologs, of Cdc25. If so, the subsequent division of the rudiment cells would require zygotic expression of the Cdc25 homolog(s). Non-synchronised expression of the Cdc25 homolog(s) would then explain the asynchronous divisions observed during rudiment division. A study of the *Tribolium* homolog(s) of Cdc25, as well as other factors involved in this pathway such as the *Tribolium* homolog of *Dm-tribbles* (Farrell and O’Farrell, 2013), is required to test these hypotheses.

Irrespective of the molecules involved, the lack of division in the serosa could be explained in two ways. Mitosis may be specifically driven in the rudiment by the expression of patterning genes such as *Tc-cad* in the posterior and *Tc-orthodenticle* in the anterior (Schinko et al., 2008; Schulz et al., 1998). This seems unlikely, however, as *Tc-cad* becomes expressed in the anterior serosa following knockdown of *Tc-zen2*, but the relevant nuclei do not appear to divide, and are still sparsely distributed at the differentiated blastoderm stage (Schoppmeier et al., 2009). Alternatively, mitosis may be specifically repressed in the serosa by a gene such as *Tc-zen1*, which is expressed in the serosa rudiment and is required for serosa formation (van der Zee et al., 2005). These models could easily be tested by overexpression of the candidate genes via transient expression. For example, the domain of either *Tc-cad*, *Tc-otd* or *Tc-zen1* could be expanded by injecting mRNA for these genes at the blastoderm stage. The effects on the embryos could then be easily analysed either by live

imaging using the H2B-RFP marker, or in fixed specimens via *in situ* hybridisation of the gene in question and an antibody for cell division.

5.3.2 The contribution of cell shape change to condensation

During stage one there is a global movement of cells towards the middle of the embryo. This movement is likely effected by a subtle change in cell shape and/or cell intercalation. I was not able to observe such processes in my data, however, this is most likely due to the resolution at which I performed my time lapse recordings. In order to make more precise measurements of cell shape changes, it would be necessary to make timelapse recordings at higher magnification focussed on small sections of the blastoderm.

From the rudiment division onwards (stage 2), embryonic cells undergo a major change in shape from cuboidal to columnar and the embryonic epithelium eventually becomes pseudostratified (Handel et al., 2005). In other insects, this change in cell shape has been proposed to be a key driving force of condensation (Anderson, 1972b). The logic is that the transition of the embryonic ectoderm from a cuboidal epithelium to a columnar epithelium must result in a reduction in apical and basal surface area in order to conserve the same cell volume. The decrease in cell surface area observed during stages 3-4 provides preliminary support for this hypothesis. Unfortunately, I was unable to accurately measure whether cells maintained the same volume throughout condensation in *Tribolium*. The decrease in fluorescence signal at the base of columnar cells, and the extensive movements of cells made it impossible to accurately measure cell volume in the same cells at different points in condensation (something that could be overcome via multi-view SPIM live imaging).

Long germ insects have evolved different ways of forming columnar epithelia without major condensation. In dipterans, such as *Drosophila*, a columnar epithelium forms during cellularisation, something which is possible because of a thick layer of periplasm at the surface of the egg (Anderson, 1973; also see “4. Cellularisation in *Tribolium* – a more widely conserved mode than *Drosophila*?”). A more complicated situation is seen in another long germ insect, the honeybee *Apis mellifera*. Following cellularisation, *Apis* exhibits a uniform cuboidal blastoderm similar to that of *Tribolium* (DuPraw, 1967). Embryonic cells then undergo a period of cell division (perhaps homologous to the *Tribolium* rudiment division), during which time a layer of periplasm accumulates beneath the embryonic ectoderm, but not beneath the presumptive serosa (DuPraw, 1967). The embryonic cells then “unite” with the

underlying periplasm as they undergo a cuboidal-columnar transition (DuPraw, 1967). This union with the underlying periplasm facilitates an increase in cell volume, and therefore the embryonic epithelium is able to undergo a cuboidal-columnar transition without a decrease in overall surface area (DuPraw, 1967).

This work raises a number of questions, such as how the periplasm is taken up by cells, and whether other insects also develop in this way. First of all, however, this work should be verified using modern molecular techniques. For example, the periplasm located beneath the epithelium could be labelled by injecting a membrane-impermeable fluorescent dye beneath the blastoderm after cellularisation. If the dye gets taken up by the embryonic epithelium during the cuboidal-columnar transition it would support the original findings.

5.3.3 The role of convergent extension in condensation and axis elongation

In my experiments, I was able to observe polarized cell movements that narrow the *Tribolium* germband in the dorsal-ventral axis (convergence) and lengthen it in the anterior-posterior axis (extension). Convergent extension was also reported by Sarrazin et al. (2012) during early germband elongation (immediately after condensation) and it is likely that this is continuous with what I observed. Taken together, these results suggest that the method of anterior-posterior axis extension that has been observed not only in other arthropods (Irvine and Wieschaus, 1994; Kanayama et al., 2011), but also in other Metazoa (Keller, 2002; Steinmetz et al., 2007), is conserved in *Tribolium*.

My new finding that *Tc-cad* activity is required for cell intercalation (but not for cell contraction) during *Tribolium* germband convergent extension has many similarities to the *Drosophila* paradigm. In *Drosophila*, it is well documented that normal anterior-posterior patterning is also required for polarized cell intercalation during germband extension (Butler et al., 2009; Irvine and Wieschaus, 1994). In particular, stripe expression of the pair-rule segmentation genes like *even-skipped*, leading to the striped arrangement of alternate cell fates, is necessary for normal germband extension (Irvine and Wieschaus, 1994; Zallen and Wieschaus, 2004). There is evidence that embryonic patterning controls embryo morphogenesis through the polarized distribution and function of effector molecules (such as contractile actomyosin networks and adhesion proteins) driving cell rearrangement during tissue deformation (Bertet et al., 2004; Blankenship et al., 2006; Zallen and Wieschaus, 2004). Previous work in *Tribolium* has shown that *Tc-cad* acts as a gap gene regulating stripe expression of the *even-skipped* (*Tc-eve*) pair-rule gene; disruption of *Tc-cad* expression leads

to missing or aberrant *Tc-eve* stripes (Copf et al., 2004; Schoppmeier et al., 2009). Furthermore, *Tc-eve* knock-down results in severely truncated and deformed *Tribolium* germbands similar to *Tc-cad* knock-down (Choe et al., 2006). Following this line of argument, it seems plausible that the effect of *Tc-cad* on *Tribolium* germband convergent extension could be channelled through the control of *Tc-eve* and/or of other *Tribolium* pair-rule genes, and that the loss of elongation observed following disruption of *Tribolium* pair-rule orthologs is at least partially explained by a loss of convergent extension.

Despite the superficial similarities, germband extension in *Drosophila* is not considered to be homologous to germband elongation in short and intermediate germband insects (Davis and Patel, 2002). This is because germband elongation in the latter group was previously thought to be caused entirely by cell division (Davis and Patel, 2002). Given the findings of myself and others (Sarrazin et al., 2012), it seems that germband elongation in *Tribolium* is initially driven by convergent extension. I hypothesise that this phase of convergent extension is homologous to germband extension in *Drosophila*. During condensation in *Tribolium*, cell intercalation is presumably balanced by the reduction in apical and basal surface area of cells (during the formation of a columnar epithelium) such that the forming germband does not elongate extensively. In *Drosophila* on the other hand, cells are already columnar and cell intercalation results in extensive germband elongation. Cell stretching also plays a role during convergent extension in *Drosophila* (Butler et al., 2009), and it will be interesting to see if similar cell behaviours can be observed in *Tribolium* following more in-depth imaging and analysis.

5.3.4 The role of the yolk in condensation

The most dramatic and complex tissue rearrangements during stages 3 and 4 occur during formation and advance of the posterior amniotic fold under the ventral face of the condensing germband. A key observation to explain posterior amniotic fold dynamics came from the coupled movement (and standstill) of the yolk fold and the posterior end of the embryo, first during germband condensation and amniotic fold progression (stages 4 and 5), and later on during germband elongation (stage 6). This observation suggested the presence of a tight physical connection between the primitive pit region of the blastoderm and the posterior pole of the yolksac. This hypothesis is further supported by the defects observed following *Tc-srp* RNAi, and the data already presented in Handel et al. (2000).

The suggestion that the basal surfaces of the posterior amnion and germband are tightly linked to the yolk sac has a number of important implications for my model of early embryo morphogenesis. First, embryonic rudiment condensation is coupled with posterior amniotic fold progression. As the embryonic rudiment condenses ventrally during stage 3, the anchor on the yolk sac would force the posterior end of the forming germband to bend into the yolk and the abutting posterior amnion to fold onto the germband. Second, as condensation proceeds, the anchor pulls the posterior germband and amnion deeper into the yolk. This pulling force drives amnion involution from the blastoderm surface into the inner side of the fold to cover its growing surface, and the movement of the amnion/serosa boundary (serosa cable) towards the rim of the posterior amniotic fold. Any active force exerted by the yolk could be caused by the extensive actin network that I found at the surface of the yolk (see “4. Cellularisation in *Tribolium* – a more widely conserved mode than *Drosophila*?”). Third, the posterior yolk sac fold bends ventrally and extends anteriorly dragged by the involuting amnion that is tightly attached to its inner surface. Extension of the yolk sac fold ceases during stage 4 together with posterior amnion involution.

The evidence I have provided in support of this hypothesis is still weak, and experiments similar to those described previously for disrupting yolk and vitellophage function are required (4. Cellularisation in *Tribolium* – a more widely conserved mode than *Drosophila*?). For example, it would be possible to test whether the yolk-actin network plays a role in condensation by injecting a membrane impermeable inhibitor of actin or myosin activity into the yolk immediately after cellularisation.

5.3.5 The amnion/serosa boundary during condensation

I also observed the presence of a conspicuous membrane thickening at the amnion/serosa boundary throughout stages 3 to 5. This thickening resembles a contractile actomyosin cable, such as those previously shown to drive coordinated cell movements during embryonic development and wound healing (Behrndt et al., 2012; Kiehart et al., 2000). My observations suggest that contraction of this cable might play an active role in different processes during stages 4 and 5, after it has passed around the posterior pole. During stage 4, contraction of the cable correlates with amniotic fold progression. I propose that the contractile force exerted by the cable from the rim of the posterior amniotic fold drives folding of the anterior amnion during this stage. In the beginning, the cable pulls the amnion over the lateral edges of the head lobes and, later on, over the anterior edge of the head lobes. During stage 5, contraction

of the cable correlates, and likely drives, closure of the serosa window. A similar model for contraction of the serosa window rim using a purse string mechanism has also been previously suggested by Handel et al. (2000). Based on the zig-zag movement of leading serosa cells, which initiate during anterior amnion folding and continue throughout serosa window closure, it appears that contraction of the cable occurs in pulses. However, as my timelapses were carried out at a relatively slow temporal resolution (5 minutes between time points) it is not clear how these pulses correlate with sub-cellular myosin contractions. Timelapse recordings at higher temporal resolution are required, as well as live imaging of the dynamics of myosin during window closure.

I also found that intercalation of serosa cells takes place at the boundary between the amnion and serosa. When the boundary is decreasing in length (the lateral part of the boundary in stages 1-3, and the entire boundary in stages 4-5), cells move away from the boundary via intercalation. The opposite pattern of intercalation takes place in the posterior half of the boundary during stages 1-3 when this part of the boundary increases in length. During epiboly in zebrafish, the expansion of the enveloping cell layer (the EVL) occurs in a remarkably similar manner to *Tribolium* serosa expansion. The main driving force for expansion of the EVL is proposed to be caused by an actomyosin ring at the leading edge of the tissue (Behrndt et al., 2012). Cell rearrangements are also thought to be important, however, as EVL cells undergo intercalation such that the number of cells at the margin decreases as the opening constricts (Köppen et al., 2006), similar to the serosa in *Tribolium*.

The serosa in *Tribolium* and the EVL in zebrafish are also similar in morphology (both are made up of squamous cells), function (both become the outer protective layer surrounding the embryo) and final fate (both are extraembryonic). Given these similarities, the two tissues represent an interesting example of convergent evolution.

5.3.6 Genetic evidence supporting my proposed model

My imaging study has provided correlative evidence, but not direct proof, for a number of processes and forces postulated to drive *Tribolium* epithelial rearrangement. However, support for my model is already available from previous gene expression studies and knock-down phenotypes in fixed *Tribolium* embryos that can now be revisited in the light of my new findings.

The *Tribolium zerknüllt-1* gene (*Tc-zen1*) is expressed in the presumptive serosa at the anterior pole of blastoderm stage embryos (van der Zee et al., 2005). *Tc-zen1* knock-down

changes the blastoderm fate map in the opposite direction to my *Tc-cad* knock-down experiments; all blastoderm cells acquire the embryonic rudiment fate at the expense of the anteriorly located serosa cells (van der Zee et al., 2005). Most importantly, the following observations were made in these *Tc-zen1* knocked-down embryos: 1) The germband condensed ventrally and elongated normally. 2) The posterior amniotic fold formed and covered the germband posteriorly, but never expanded anteriorly. 3) The anterior amnion failed to cover the head lobes anteriorly and the entire head region appeared enlarged. 4) The embryo was not covered by any extraembryonic membrane ventrally with the exception of the abdominal region. All these observations are in accordance with my proposed model that germband condensation is an autonomous process that drives initiation of the posterior amniotic fold formation, and that expansion of the posterior amniotic fold, formation of the horseshoe and oval amniotic fold and closure of the amniotic cavity all require serosa function.

5.3.7 Future work on condensation

In my model for *Tribolium* embryogenesis, condensation of the embryonic rudiment plays a central role throughout tissue remodelling from the two-dimensional blastoderm to the three-dimensional enveloped germband. Embryonic rudiment condensation is accompanied by cell divisions, cell shape changes, cell rearrangement, tissue folding and mesoderm internalization along the ventral midline of the germband. To dissect *in vivo*, and to model the contribution of all these complex cell behaviours to embryonic condensation, more sophisticated imaging techniques will be required, allowing deeper light penetration, multi-view imaging and faster acquisition rates for higher temporal resolution (Gao et al., 2012; Khairy and Keller, 2011; Tomer et al., 2012; Weber and Huisken, 2012). Several important aspects of my model that need to be tested include the tight physical association between the primitive pit region of the blastoderm and the posterior pole of the yolk sac, and the contractile force exerted by the intercellular cable at the leading edge of the serosa. It is also likely that apical constriction of cells plays an active role in mesoderm invagination at the ventral furrow, and perhaps in folding of the amnion. In *Drosophila*, the gene *folded-gastrulation* has a major role in controlling apical constriction of cells (Dawes-Hoang et al., 2005). The *Tribolium* ortholog of this gene has recently been discovered (S. Roth, personal communication), and it will be interesting to see how it functions during germband condensation.

It is also important to combine the aforementioned research on morphogenesis into the currently available data on transcription factor networks. A large amount of data exists on the expression patterns of key patterning genes, as well as the consequences of disrupting these genes. Unfortunately, the published data is usually presented in a way that makes it impossible to accurately align expression patterns with each other, and with live imaging data such as that presented in this chapter. While such alignments are going to be a difficult task for some time to come, the process would be made easier if authors would follow several guidelines. First of all, higher temporal resolution is needed when presenting expression patterns for genes that have dynamic expression patterns or at stages when tissues are undergoing rapid rearrangements. Secondly, the use of fluorescent *in situ* hybridisation approaches and confocal microscopy will allow better spatial resolution of the expression patterns of genes. Lastly, if the expression pattern of a gene is being studied during the process of condensation, the expression pattern could be described with relation to morphological landmarks such as percentage egg length and with relation to the staging system presented in this chapter.

6. APPENDIX - EXPRESSION PATTERN OF *TRIBOLIUM SERPENT*

During the final stage of my PhD, I set out to combine the live imaging tools described in “3. The use of transient expression as a method for live imaging” with current genetic techniques for studying the expression and function of genes. The biological question I had in mind was “where does the endoderm come from in *Tribolium*?” As discussed in the next section, the primitive pit tissue may in fact be the hindgut and posterior midgut primordium, and I was interested to see if I could use some of my live imaging tools, such as the membrane marker and the histone marker, to extend our knowledge of primitive pit formation. I was also intending to carry out lineage analysis on the primitive pit tissue using the photoconvertible actin marker. Finally, I planned to combine my live imaging approaches with knockdown of genes that are expressed in the primitive pit tissue and in the endoderm. To begin with, I wanted to use fluorescent RNA *in situ* hybridisation techniques to characterise the expression patterns of genes that may be involved with primitive pit formation, hindgut formation and endoderm specification. While I did not have time to achieve most of these goals, I was able to gather high resolution fluorescent *in situ* data for several genes, including the *Tribolium* orthologs of *tailless*, *wingless*, *forkhead*, *twist*, *caudal* and *brachyenteron*. The expression patterns of all of these genes are published and I do not have anything significant to add. However, I also characterised the expression pattern of the *Tribolium* ortholog of *serpent*, and as this has not been published before, I am presenting it in this appendix.

6.1 Introduction

According to classical descriptions, the endoderm of short and intermediate germ insects only forms during late development (Roth, 2004). There is some evidence from fate-mapping experiments, however, that primordia for the posterior endoderm/midgut is already present at the blastoderm stage (Handel et al., 2000). Based on this data, it has been suggested that the primitive pit tissue in *Tribolium* may be the posterior midgut primordium (Handel et al., 2000).

In order to look at endoderm specification in arthropod embryos, some authors have used the expression pattern of orthologs of the *Drosophila* gene *forkhead*, which is expressed in the midgut primordium in *Drosophila* embryos (Akiyama-oda and Oda, 2003; Schroder et

al., 2000; Weigel et al., 1989). However, *forkhead* is also expressed in both the foregut and the hindgut, which are both derived from ectoderm. Given that the foregut and hindgut primordia are specified adjacent to the anterior and posterior midgut primordia (respectively), it is not possible to differentiate one tissue from another using the expression pattern of *forkhead*.

Another key gene in *Drosophila* endoderm specification that is not expressed in the foregut or hindgut is the GATA factor *serpent* (Abel et al., 1993; Rehorn et al., 1996). Other genes from the GATA family of transcription factors are also involved in germ layer specification in deuterostomes and lophotrochozoans (Gillis et al., 2008; Rehorn et al., 1996). The earliest expression of *Dm-srp* is seen at the blastoderm stage, when it is expressed in all presumptive endoderm cells; two populations at the termini of the embryo and a population at the anterior ventral region of the embryo (Abel et al., 1993; Rehorn et al., 1996). The cells at the anterior and posterior termini are internalised by formation of the stomodeum and the proctodeum, respectively (Rehorn et al., 1996). The cells at the anterior-ventral region also express the mesodermal transcription factor *twist*, invaginate with the ventral furrow and are thought to give rise to haemocytes as well as part of the anterior midgut (de Velasco et al., 2006). *Dm-srp* is also expressed in the amnioserosa and the vitellophages (Abel et al., 1993; Rehorn et al., 1996). Following germband elongation, *Dm-srp* stops being expressed in the midgut cells and the amnioserosa, but persists in the presumptive haemocytes (Abel et al., 1993; Rehorn et al., 1996). Expression also appears in the fat body primordium at about this stage (Abel et al., 1993; Rehorn et al., 1996).

I was interested to see if the *Tribolium* homolog of *Srp* also marks the endoderm in *Tribolium*, and if so, when the expression appears. *Tc-srp* has already been identified in a phylogenetic study of the GATA factors in ecdysozoans and Lophotrochozoans (Gillis et al., 2008). The authors of the study suggest the gene name GATA456ba for *Dm-srp* homologs, however, for this work I will use the name *Tc-srp*. I cloned this gene, and carried out RNA *in situ* hybridisation on *Tribolium* embryos from 1-48 hours after egg lay (aged at 32°C). By using the FastRed staining reaction I was able to image embryos using fluorescence confocal microscopy.

6.2 Results and Discussion

Unlike in *Drosophila*, *Tc-srp* transcripts were maternally provided in *Tribolium* embryos and were ubiquitously distributed (Fig. 6.1 (A-C)). At about the final uniform blastoderm stage

(nuclear cycle 13, stage 1 according to scheme in “5. A live imaging study of germband condensation”), expression was lost from the blastoderm cells, but was maintained in the vitellophages (Fig. 6.1 (D)). This change in expression pattern may reflect a switch from maternal expression to zygotic expression and rapid degradation of maternal RNA.

Following the division of the germ rudiment (stage 2), expression persisted in the vitellophages and a patch of expression appeared at the anterior medial region of the germ rudiment in superficial cells (Fig. 6.1 (F)). Based on live imaging studies with H2B-RFP-labelled embryos at this stage (“5. A live imaging study of germband condensation” and data not shown), there was no evidence of migration of the vitellophages to this region, and therefore, this is likely a *de novo* patch of expression.

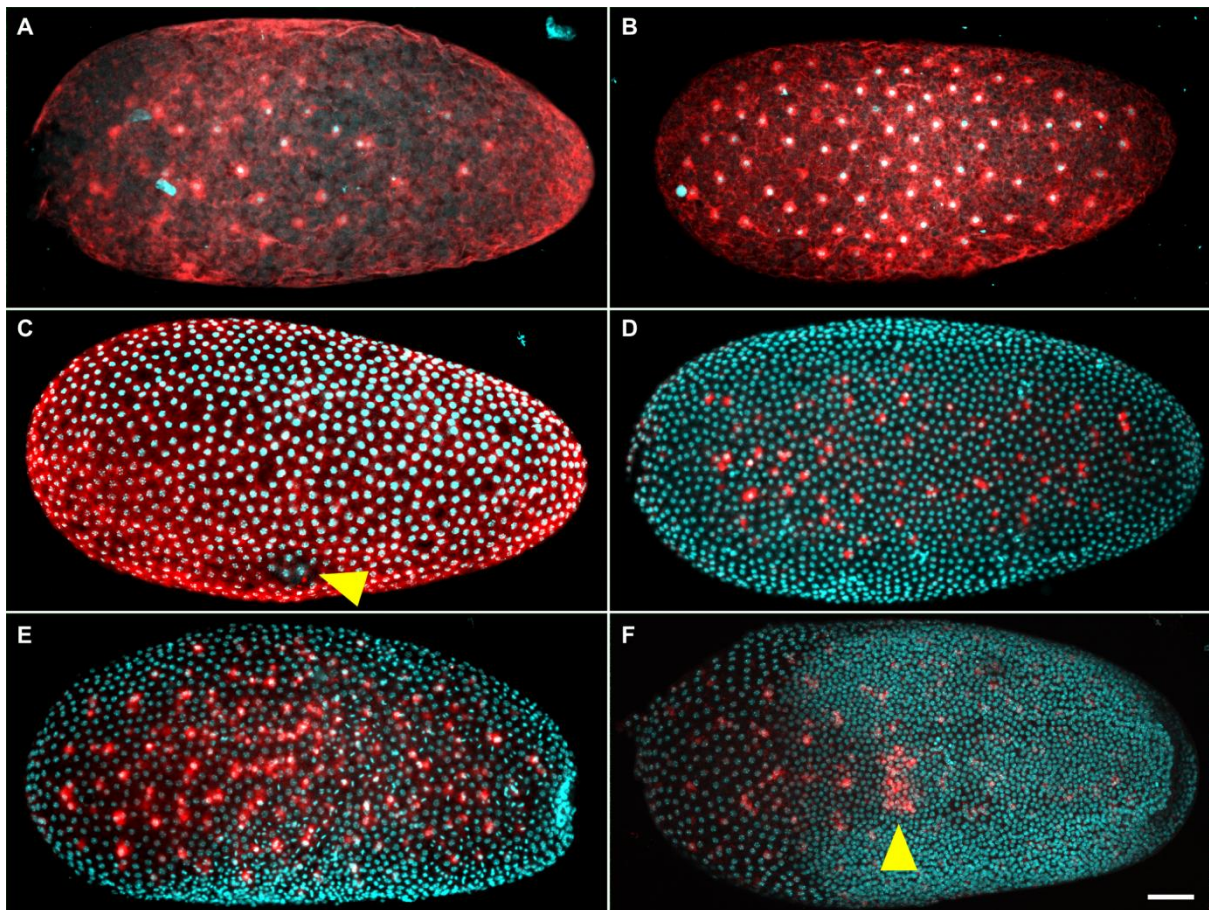


Fig. 6.1. Distribution of *Tc-srp* mRNA in blastoderm and differentiated blastoderm stage embryos. Nuclei are shown in cyan, *Tc-srp* mRNA is shown in red. (A-B) In preblastoderm embryos, *Tc-srp* mRNA is distributed over the surface of the egg, and is also in energids within the yolk. (C) *Tc-srp* mRNA remains uniformly distributed after nuclei reach the surface of the egg. Arrowhead marks a damaged patch of blastoderm. (D) At the final uniform blastoderm stage (Stage 1), *Tc-srp* mRNA is lost from the surface of the egg, but

persists in vitellophages. (E) During the germ rudiment division (Stage 2), expression persists in vitellophages. (F) As condensation proceeds (Stage 3), a patch of expression appears at an anterior-ventral position (arrowhead). All images are projections of confocal stacks. In all panels anterior is to the left, (E) is a lateral view with ventral to the bottom, (F) is a ventral view. Scale bar is 50 μ m.

The anterior-medial expression was maintained throughout condensation, and these cells invaginated at the anterior region of the ventral furrow during stages 3-5 (Fig. 6.2 (A-A'')). During stage 4, weak expression also became visible in amnion cells at the amnion/serosa boundary (not shown), and this expression strengthened during stage 5 (Fig. 6.2 (A-A'')). These cells are reminiscent of the “necklace cells” that have been observed during serosa window closure in *Schistocerca* (Dearden et al., 2000).

I was surprised by the apparent lack of expression at the posterior of the germband. To confirm that this was not an artefact due to light scattering caused by the overlying tissue I imaged several embryos from the dorsal side (Fig. 6.2 (B-B'')). This analysis confirmed that there was no expression at the posterior, and also showed that expression was maintained in the vitellophages (Fig. 6.2 (B-B'')).

When the serosa window closed (end of Stage 5), expression was still visible in the amnion (Fig. 6.2 (C₁-C₁'')) and in the anterior medial region of the germband (Fig. 6.2 (C₂-C₂'')) although these cells were now completely internalised (Fig. 6.2 (C₃-C₃'')). If expression in amnion cells is stable, the fact that mRNA is visible in amnion cells away from the position of window closure suggests that the amnion cells undergo a similar process of intercalation during window closure as is observed in the serosa (compare expression pattern in Fig. 4.2 with cell tracking in Fig. 5.12). It is also likely that *Tc-srp* becomes expressed more widely in the amnion, as knockdown of the gene results in degeneration of the amnion (See “4. Cellularisation in *Tribolium* – a more widely conserved mode than *Drosophila*?” also see later expression of *Tc-srp*)

I hypothesise that the anterior medial population of *Tc-srp* expressing cells is homologous to the anterior ventral population of cells in *Drosophila* that gives rise to haemocytes and a portion of the endoderm based on three things. First of all, these cells co-express the *Tribolium* ortholog of the *twist* transcription factor (Handel et al., 2005). Secondly, these cells invaginate with the ventral furrow rather than with the stomodeum, which is yet to form. Lastly, extensive tissue rearrangements occur at the anterior of the embryo such that the lateral head lobes fold together and merge to form the final head

(Kittelman et al., 2013). The stomodeum forms during this tissue folding, and the cells that end up at the base of the stomodeum seem to originate from almost the anterior most point of the germ rudiment (immediately posterior to the presumptive amnion).

To test this hypothesis, I looked for a marker that I could use to differentiate the haemocyte primordium from the anterior midgut primordium. In *Drosophila*, both *glial cells missing* and *glial cells missing 2* are co-expressed with *Dm-srp* in the anterior ventral population of cells. By reciprocal BLAST analysis, I found that *Tribolium* only has a single *glial cells missing* (*Tc-GCM*) ortholog. I cloned this gene and carried out RNA *in situ* hybridisation. From this analysis, I found that there is no expression of *Tc-GCM* in the *Tc-srp* expressing cells, but that *Tc-GCM* is expressed in punctate spots in the ectoderm at late germband stages as it is in *Drosophila* (data not shown). Given the complete lack of the anterior expression domain, these data do not confirm or refute my hypothesis about the identity of the anterior ventral *Tc-srp* expressing cells.

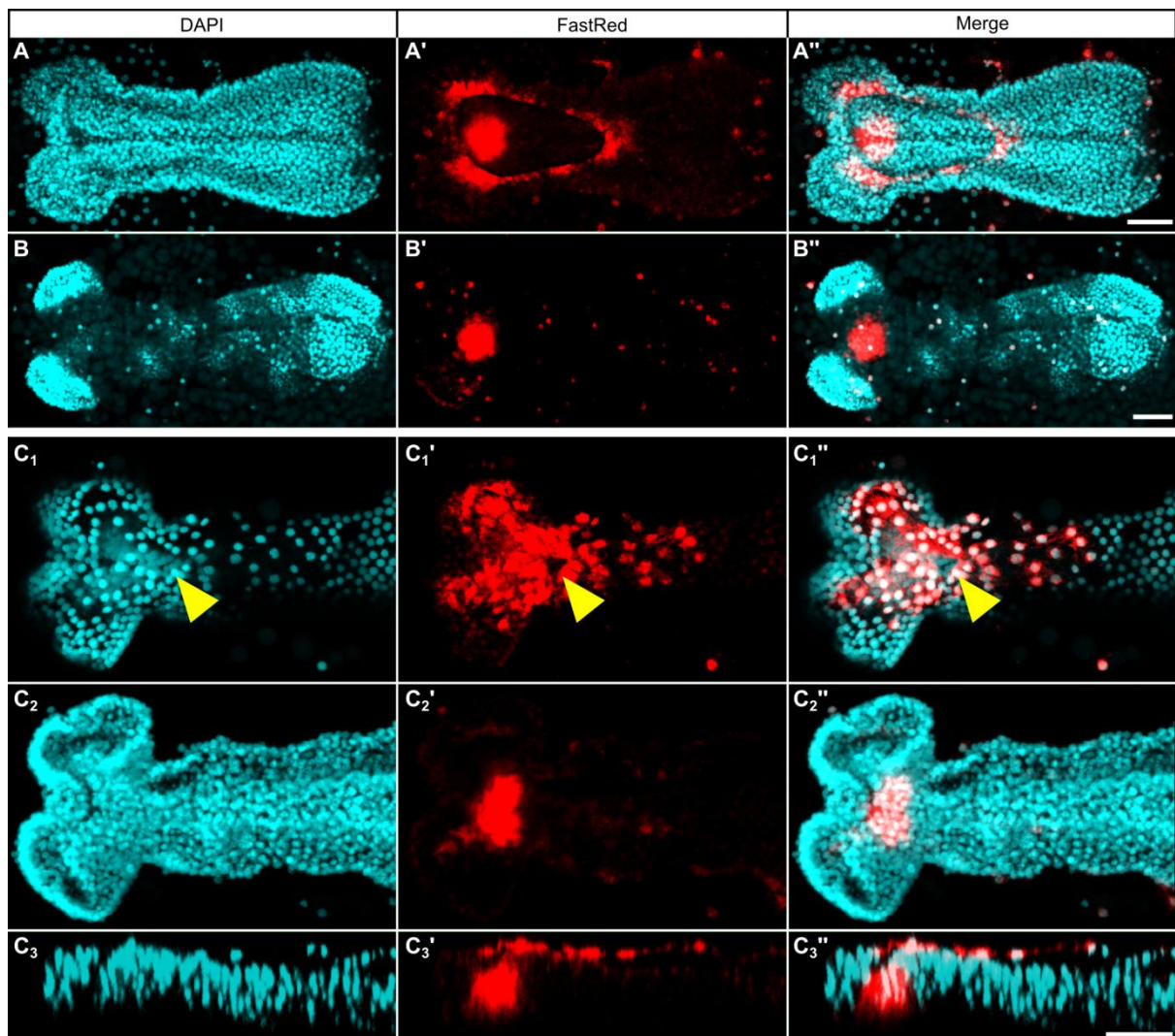


Fig. 6.2. Distribution of *Tc-srp* mRNA in germbands during serosa window closure. Nuclei are shown in cyan (A-C₃), *Tc-srp* mRNA is shown in red (A'-C₃'). (A-A'') During stage 5, the medial population of *Tc-srp* expressing cells invaginate with the ventral furrow, and expression becomes visible in the amnion cells surrounding the serosa window. Expression is also visible in the vitellophages (scattered *Tc-srp* expressing cells around germband). (B-B'') Dorsal view of a germband dissected off the egg showing lack of *Tc-srp* at the posterior. (C₁-C₃'') Different views of the same embryo at the time of serosa window closure. (C₁-C₁'') Projections of amnion layer showing expression in amnion and position of window closure (arrowhead). (C₂-C₂'') Projections of embryonic tissue showing expression in anterior-medial population of cells. (C₃-C₃'') XZ section at midline of germband showing Z positions of *Tc-srp* expressing cells. All panels show projections of confocal stacks, except for (C₃-C₃''). Anterior is to the left in all panels, (A-A'') and (C₁-C₂'') are ventral views, (B-B'') is a dorsal view. All germbands have been dissected from the yolk and flat mounted. Scale bar is 50 μm.

At the end of germband elongation/segmentation *Tc-srp* expression became visible in a population of cells at the posterior terminus of the germband (Fig. 6.3 (A-A'')), and this expression persisted during germband retraction (Fig. 6.3 (B-B'')). Given the position of this population of cells at the base of the proctodeum, it is highly likely that they are the posterior midgut cells.

This finding strongly suggests that the posterior endoderm is only specified at the end of segmentation. This is surprising as the expression patterns of *Tc-brachyenteron* and *Tc-forkhead* suggest that the hindgut primordium is present from a much earlier time (Berns et al., 2008; Kispert et al., 1994). It would be very interesting to look at the dynamics of *Tc-srp* expression in relation to *Tc-twi* expression, as the posterior domain of *Tc-srp* seems to appear immediately after the posterior domain of *Tc-twi* disappears.

At the anterior of the embryo, expression was present in a diffuse population of cells (Fig. 6.3 (A') arrowhead) and in a population of tightly clustered cells (Fig. 6.3 (A') arrow). Both populations were located beneath the ectoderm cell layer. Based on expression pattern alone, I have not been able to determine whether these two populations are descended from the original anterior population of *Tc-srp* expressing cells, or if one population is from *de novo* expression of *Tc-srp*. During germband retraction, three populations of cells became visible at the anterior; two appeared to be either side of the stomodeum and one appeared to be located beneath the stomodeum (Fig. 6.3 (B-B'')). A similar pattern is seen at the anterior

of *Drosophila* embryos; the populations either side of the stomodeum are thought to be haemocytes, while the population at the base of the stomodeum is the anterior midgut primordium (Rehorn et al., 1996). Unfortunately, I was not able to image the stomodeum at germband retraction stages due to light scattering caused by the overlying appendages, and therefore, I cannot say for sure whether the anterior medial patch of cells is at the base of the stomodeum. Advanced cell labelling experiments are required to uncover the origin of these different populations of cells.

Expression also became visible at the dorso-lateral regions of the germband at the end of segmentation (Fig. 6.3 (A-A'')), and this expression strengthened during germband retraction (Fig. 6.3 (B-B'')). Given the location and timing of this expression, I hypothesise that these lateral cells are the fat body primordium. *Tc-srp* was also expressed in scattered cells throughout the germband, and these may be migrating haemocytes. From whole mount preparations, I was able to observe expression in the vitellophages (not shown). Lastly, I cannot say for sure whether the expression in the amnion was maintained, as the amnion is removed from the embryo during my fixation and devitellinisation procedure. The fragments of amnion that remain at the lateral regions of the germband did show weak expression (Fig. 6.3), but this needs to be looked at more carefully in embryos with intact amnion membranes.

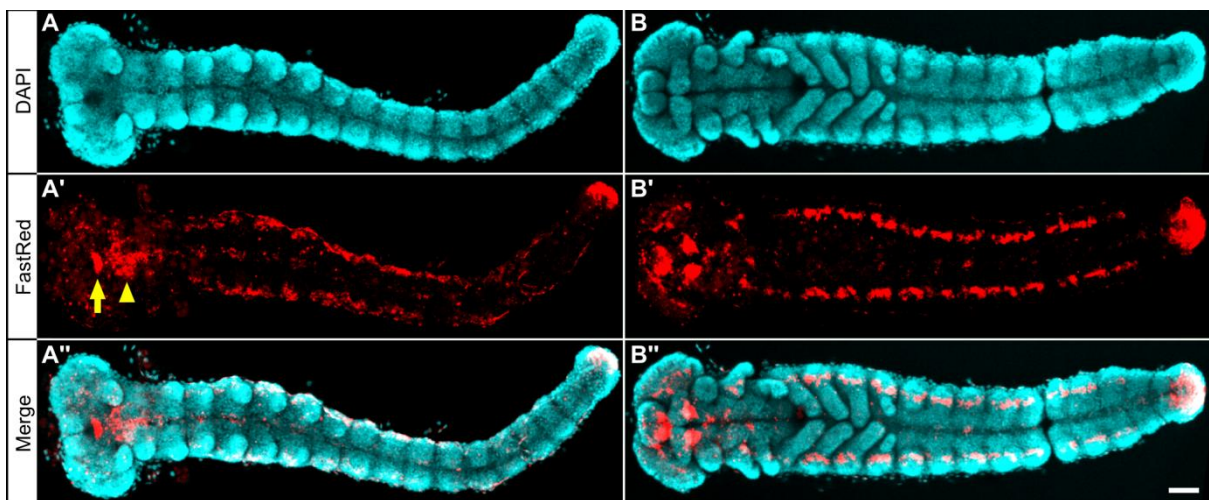


Fig. 6.3. Distribution of *Tc-srp* mRNA in germbands after segmentation is complete. Nuclei are shown in cyan (A-B), *Tc-srp* mRNA is shown in red (A'-B'). (A-A'') after segmentation expression is visible at the posterior, in lateral stripes, and in scattered cells throughout the germband. At the anterior, expression is visible in a scattered population of cells (arrowhead) and in a dense population of cells (arrow). (B-B'') During germband retraction, expression persists at the posterior, in the lateral stripes, and in scattered cells throughout

the germband. At the anterior, expression is visible in two dense populations of cells either side of the midline, and one dense population of cells at the midline. All panels show projections of confocal stacks. Anterior is to the left in all panels and all panels are ventral views. All germbands have been dissected from the yolk and flat mounted. Scale bar is 50 μ m.

Expression pattern analysis of more genes, knockdown analysis and cell labelling experiments are now required to confirm my hypotheses about the anterior and posterior midgut primordia, the haemocyte primordium and the fat body primordium. If my hypotheses turn out to be correct, the only obvious difference in the spatial expression pattern of *Dm-srp* and *Tc-srp* is that *Tc-srp* RNA is maternally contributed. Even the expression in the amnion of *Tribolium* may be homologous to the expression in the amnioserosa of *Drosophila*. There are several differences in the timing of the expression domains, and this likely relates to the fact that *Drosophila* goes through embryogenesis three times faster than *Tribolium* (24 hours versus 72 hours, respectively). Given the similar spatial expression pattern but different timing, it will now be very interesting to see how *Tc-srp* is regulated. For example, the expression of *Dm-srp* at the anterior and posterior termini is regulated by the terminal system via the genes *Dm-tailless* and *Dm-huckebein*. In *Tribolium*, the terminal system has no role in patterning the anterior of the embryo, and neither *Tc-tailless* nor *Tc-huckebein* are expressed at the same time and place as *Tc-srp*. It will also be interesting to see whether the orthologs of *serpent* in other arthropods mark the same tissues as *Dm-srp* and *Tc-srp* do.

7. CONCLUDING REMARKS

7.1 Combining the study of gene regulatory networks with cell biology

The majority of research on the evolution of development in arthropods has focussed on looking at the expression patterns of specific genes, and seeing how these expression patterns are affected when one or more genes are knocked down via RNAi. Using this approach, we have learned bits and pieces about how specific gene regulatory networks known from *Drosophila* function in different arthropods, and the general conclusion is that some things are conserved and some are divergent. One major problem with this approach is that the evolutionary distance between the species being compared is usually hundreds of millions of years. Over this length of time, the expression patterns of genes and regulatory relationships between them can change drastically.

A second major problem is that the morphogenesis of the embryos being compared is often drastically different. We do not have a thorough understanding of embryo formation at a cellular level in any arthropod other than *Drosophila*. This information is essential in order to discover how transcription factors control cell behaviour to produce the overall form of the embryo. Once we have that information for multiple animals, we can begin to make detailed comparisons in order to uncover what has changed, and how.

During my PhD, I have made several steps towards solving this second problem. I have developed new live imaging tools for studying *Tribolium* embryogenesis at a cellular level, and I have implemented these tools using a non-transgenic approach that should be widely applicable to other arthropod embryos (“3. The use of transient expression as a method for live imaging”). I have shown how these tools can be used to study processes such as cellularisation (“4. Cellularisation in *Tribolium* – a more widely conserved mode than *Drosophila*?”), and the morphogenesis of embryo condensation (“5. A live imaging study of germband condensation”). It is my hope that the fluorescent labelling approach, the labelling tools, and my analyses of *Tribolium* embryogenesis will prove to be useful for the evolution and development community for future studies in *Tribolium* and other non-model systems.

7.2 Future directions

In my future work, I hope to develop new approaches for more fine scale manipulation of gene function in order to move beyond the limitations of the RNAi approach. I will combine these new approaches with the live imaging tools described in this thesis as well as with the detailed analysis of gene expression patterns to try to uncover how gene regulatory networks control morphogenesis in *Tribolium*. I also plan to carry out similar studies in species that are relatively closely related, but that still exhibit divergent modes of embryogenesis, such as short, intermediate and long germ Coleopteran species. From this work, I hope to uncover how the evolution of gene regulatory networks drives changes in morphogenesis and embryonic form.

8. MOVIE LEGENDS

Movie 4.1. Membrane ingression during cellularisation. Time lapse of membrane ingression between nuclei in an *nGFP* transgenic embryo also labelled with *GAP43-YFP*. Movie shows optical sections either at the level of the nuclei. Timelapse starts approximately 20 minutes after nuclei reach the surface, and is timed against that point.

Movie 4.2. Membrane behaviour during protocell division. Time lapse of orthogonal view of membrane ingression during final uniform blastoderm division in a *GAP43-YFP* labelled embryo, timed from just before division begins.

Movie 4.3. Completion of cellularisation. (A-C) Time lapse of blastoderm cellularisation during 13th interphase of a *GAP43-YFP* labelled embryo timed against basal cell closure. (A) Subapical optical section showing straightening/tightening of membrane during blastoderm cellularization. (B) Optical section at basal parts of proto-cells showing membrane constriction and eventual basal cell closure. (C) Orthogonal view showing constriction basal membranes during cellularisation.

Movie 4.4. *Inx7a* RNAi cellularisation phenotype. Time lapse of cellularisation defects in a *GAP43-YFP* labelled embryo following *inx7a* pRNAi, timed against maximum membrane ingression depth. Movie shows a subapical optical section.

Movie 4.5. Membrane retraction caused by *Inx7a* RNAi. Time lapse of membrane retraction in a *GAP43-YFP* labelled embryo following *inx7a* pRNAi. Movie shows subapical optical section (left panel) or as orthogonal view (right panel). Orthogonal views are maximum intensity projections of several microns in the y axis.

Movie 4.6. Cleavage of the yolk. Timelapse of optical section at the surface of the yolk from DIC imaging, timed against the uniform blastoderm stage. Anterior to the left and dorsal to the top.

Movie 4.7. Effects of yolk cleavage on the germband. Time lapse recordings of *GAP43-YFP*-labelled wildtype embryo (top panel) or *Tc-srp*^{RNAi} embryo (bottom panel) during germband elongation. Movies start at the point of serosa window closure. Movies

show average projections that were altered by uniformly enhancing brightness/contrast to show the germband and the membrane-bound yolk spheres. Anterior to the left and dorsal to the top.

Movie 5.1. Timelapse wild-type condensation (ventrolateral view). Fluorescence time-lapse recording of a *Tribolium* wild-type embryo labelled with GAP43-YFP (also shown in Fig. 5.1 (A-E)). In each time-point, the movie shows an average intensity projection. The position of tracked cells is indicated with yellow dots; cell tracks are not included to allow visualization of the embryo. Ventrolateral view, anterior is towards the left.

Movie 5.2. Timelapse wild-type condensation (lateral view). Fluorescence time-lapse recording of a *Tribolium* wild-type embryo labelled with GAP43-YFP (also shown in Fig. 5.1(F-J)). In each time-point, the movie shows an average intensity projection. The position of tracked serosa cells is indicated with yellow dots; cell tracks are not included to allow visualization of the embryo. Lateral view, anterior is towards the left and dorsal towards the top.

Movie 5.3. Timelapse of condensation after *Tc-cad*^{RNAi} (ventrolateral view). Fluorescence time-lapse recording of a *Tribolium* *Tc-cad*^{RNAi} embryo labelled with GAP43-YFP (also shown in Fig. 5.1(K-O)). In each time-point, the movie shows an average intensity projection. The position of tracked cells is indicated with yellow dots; cell tracks are not included to allow visualization of the embryo. Ventrolateral view, anterior is towards the left.

Movie 5.4. Timelapse of condensation after *Tc-cad*^{RNAi} (lateral view). Fluorescence time-lapse recording of a *Tribolium* *Tc-cad*^{RNAi} embryo labelled with GAP43-YFP (also shown in Fig. 5.1(P-T)). At each time-point, the movie shows an average intensity projection. The position of tracked serosa cells is indicated with yellow dots; cell tracks are not included to allow visualization of the embryo. Lateral view, anterior is towards the left and dorsal to the top.

Movie 5.5. Time lapse of germband extension in wild-type and *Tc-cad*^{RNAi} embryos. Combination of two fluorescence time-lapse recordings of *Tribolium* wild-type (top) and *Tc-cad*^{RNAi} (bottom) embryos labelled with GAP43-YFP also shown in Fig. 5.2. At each time-

point, the movie shows average intensity projections with enhanced brightness/contrast to show the germbands and the membrane-bound yolk spheres. Lateral views, anterior is towards the left and dorsal towards the top.

Movie 5.6. Confocal imaging of the 13th round of cell divisions during *Tribolium* blastoderm differentiation. Fluorescence timelapse recording of a *Tribolium* embryo labelled with H2B-RFP also shown in Fig. 5.3 (A-A’’’). In each time-point, the movie shows an average intensity projection. Lateral view, anterior is towards the left and dorsal towards the top.

Movie 5.7. DIC/confocal imaging of *Tribolium* germband condensation and elongation relative to yolksac dynamics. Combination of differential interference contrast microscopy with fluorescence confocal microscopy for time-lapse recording of a *Tribolium* embryo labelled with H2B-RFP (also shown in Fig. 5.10). In each time-point, the movie shows the DIC image of the embryo (left panel), as well as the DIC image overlaid with the corresponding H2B-RFP fluorescence signal in blue (right panel). The dot indicates the position of the leading edge of the posterior yolk-fold. The white track marks the early ventral extension of the yolk-fold and the grey track marks its dorsal retraction up to the corresponding time-point. Lateral view, anterior is towards the left and dorsal to the top.

Movie 5.8. Dynamics of the yolkfold in wild-type and *Tc-srp*^{RNAi} embryos. Time lapse recordings of GAP43-YFP-labeled wildtype embryo (top panel) or *Tc-srp*^{RNAi} embryo (bottom panel) during stages 4-5. Movies are timed against onset of stage 1. Anterior to the left and dorsal to the top.

9. BIBLIOGRAPHY

- Abel, T., Michelson, A. M. and Maniatis, T.** (1993). A *Drosophila* GATA family member that binds to *Adh* regulatory sequences is expressed in the developing fat body. *Development (Cambridge, England)* **119**, 623–33.
- Akiyama-oda, Y. and Oda, H.** (2003). Early patterning of the spider embryo: a cluster of mesenchymal cells at the cumulus produces Dpp signals received by germ disc epithelial cells. *Development* **130**, 1735–1747.
- Alwes, F. and Scholtz, G.** (2004). Cleavage and gastrulation of the euphausiacean *Meganycitphanes norvegica* (Crustacea, Malacostraca). *Zoomorphology* **123**, 125–137.
- Anderson, D. T.** (1972a). The Development of Hemimetabolous Insects. In *Developmental systems. Insects, Vol 1* (ed. Counce, S. J. and Waddington, C. H.), pp. 95–163. New York: Academic Press.
- Anderson, D. T.** (1972b). The Development of Holometabolous Insects. In *Developmental systems. Insects, Vol 1* (ed. Counce, S. J. and Waddington, C. H.), pp. 165–242. New York: Academic Press.
- Anderson, D. T.** (1973). *Embryology and Phylogeny in Annelids and Arthropod*. Pergamon Press.
- Angelini, D. R. and Kaufman, T. C.** (2005). Functional analyses in the milkweed bug *Oncopeltus fasciatus* (Hemiptera) support a role for Wnt signaling in body segmentation but not appendage development. **283**, 409–423.
- Behrndt, M., Salbreux, G., Campinho, P., Hauschild, R., Oswald, F., Roensch, J., Grill, S. W. and Heisenberg, C.-P.** (2012). Forces driving epithelial spreading in zebrafish gastrulation. *Science (New York, N.Y.)* **338**, 257–60.
- Benton, M. A., Akam, M. and Pavlopoulos, A.** (2013). Cell and tissue dynamics during *Tribolium* embryogenesis revealed by versatile fluorescence labeling approaches. *Development* **140**, 3210–3220.
- Berns, N., Kusch, T., Schröder, R. and Reuter, R.** (2008). Expression, function and regulation of Brachyenteron in the short germband insect *Tribolium castaneum*. *Development genes and evolution* **218**, 169–79.
- Bertet, C., Sulak, L. and Lecuit, T.** (2004). Myosin-dependent junction remodelling controls planar cell intercalation and axis elongation. *Nature* **429**, 667–671.

- Bhalla-Gehi, R., Penuela, S., Churko, J. M., Shao, Q. and Laird, D. W.** (2010). Pannexin1 and pannexin3 delivery, cell surface dynamics, and cytoskeletal interactions. *The Journal of biological chemistry* **285**, 9147–60.
- Blankenship, J. T., Backovic, S. T., Sanny, J. S. P., Weitz, O. and Zallen, J. A.** (2006). Multicellular Rosette Formation Links Planar Cell Polarity to Tissue Morphogenesis. *Developmental Cell* **11**, 459–470.
- Brena, C. and Akam, M.** (2012). The embryonic development of the centipede *Strigamia maritima*. *Developmental biology* **363**, 290–307.
- Brown, S. J., Patel, N. H. and Denell, R. E.** (1994). Embryonic expression of the single *Tribolium engrailed* homolog. *Developmental Genetics* **15**, 7–18.
- Browne, W. E., Price, A. L., Gerberding, M. and Patel, N. H.** (2005). Stages of embryonic development in the amphipod crustacean, *Parhyale hawaiiensis*. *Genesis (New York, N.Y. : 2000)* **42**, 124–49.
- Bucher, G.** (2009). The Beetle Book. *Online release 1-2*,.
- Butler, L. C., Blanchard, G. B., Kabla, A. J., Lawrence, N. J., Welchman, D. P., Mahadevan, L., Adams, R. J. and Sanson, B.** (2009). Cell shape changes indicate a role for extrinsic tensile forces in *Drosophila* germ-band extension. *Nature cell biology* **11**, 859–64.
- Carroll, S.** (2005). *Endless Forms Most Beautiful: The New Science of Evo Devo and the Making of the Animal Kingdom*. W. W. Norton & Company.
- Chasan, R. and Anderson, K.** (1989). The role of easter, an apparent serine protease, in organizing the dorsal-ventral pattern of the *Drosophila* embryo. *Cell* **56**, 391–400.
- Chesebro, J. E., Pueyo, J. I. and Couso, J. P.** (2012). Interplay between a Wnt-dependent organiser and the Notch segmentation clock regulates posterior development in *Periplaneta americana*. *Biology Open*.
- Choe, C. P., Miller, S. C. and Brown, S. J.** (2006). A pair-rule gene circuit defines segments sequentially in the short-germ insect *Tribolium castaneum*. *Proceedings of the National Academy of Sciences of the United States of America* **103**, 6560–4.
- Copf, T., Schröder, R. and Averof, M.** (2004). Ancestral role of caudal genes in axis elongation and segmentation. *Proceedings of the National Academy of Sciences of the United States of America* **101**, 17711–5.
- Counce, S. J.** (1961). THE ANALYSIS OF INSECT EMBRYOGENESIS. *Annual Review Entomology* 295–312.
- Counce, S. J.** (1973). The Causal Analysis of Insect Embryogenesis. In *Developmental systems. Insects, Vol 2* (ed. Counce, S. J. and Waddington, C. H.), pp. 1–156. New York: Academic Press.

- Daniels, B. R., Rikhy, R., Renz, M., Dobrowsky, T. M. and Lippincott-schwartz, J.** (2012). Multiscale diffusion in the mitotic *Drosophila melanogaster* syncytial blastoderm.
- Darwin, C.** (1859). *The Origin of Species*. London: John Murray.
- Darwin, C. and Wallace, A. R.** (1958). On the tendency of species to form varieties; and on the perpetuation of varieties and species by natural means of selection. *Journal of the Proceedings of the Linnean Society of London. Zoology* 3.
- Davis, I. and Ish-Horowicz, D.** (1991). Apical localization of pair-rule transcripts requires 3' sequences and limits protein diffusion in the *Drosophila* blastoderm embryo. *Cell* **67**, 927–40.
- Davis, G. K. and Patel, N. H.** (2002). SHORT, LONG, AND BEYOND: Molecular and Embryological Approaches to. *Annual Review Entomology* 669–99.
- Dawes-Hoang, R. E., Parmar, K. M., Christiansen, A. E., Phelps, C. B., Brand, A. H. and Wieschaus, E. F.** (2005). Folded Gastrulation, Cell Shape Change and the Control of Myosin Localization. *Development (Cambridge, England)* **132**, 4165–78.
- De Velasco, B., Mandal, L., Mkrtchyan, M. and Hartenstein, V.** (2006). Subdivision and developmental fate of the head mesoderm in *Drosophila melanogaster*. *Development genes and evolution* **216**, 39–51.
- Dearden, P., Grbic, M., Falciani, F. and Akam, M.** (2000). Maternal expression and early zygotic regulation of the *Hox3/zen* gene in the grasshopper *Schistocerca gregaria*. *Evolution & development* **2**, 261–70.
- DeLotto, R., DeLotto, Y., Steward, R. and Lippincott-Schwartz, J.** (2007). Nucleocytoplasmic shuttling mediates the dynamic maintenance of nuclear Dorsal levels during *Drosophila* embryogenesis. *Development (Cambridge, England)* **134**, 4233–41.
- Duncan, E. J., Benton, M. A. and Dearden, P. K.** (2013). Canonical terminal patterning is an evolutionary novelty. *Developmental biology* **377**, 245–61.
- DuPraw, E. J.** (1967). The Honeybee Embryo. In *Methods in Developmental Biology* (ed. Wilt, F. H. and Wessells, N. K.), pp. 183–218. New York: Thomas Y. Crowell Company.
- Ellis-davies, G. C. R.** (2007). Caged compounds: photorelease technology for control of cellular chemistry and physiology. *Nature Methods* **4**, 619–628.
- El-Sherif, E., Averof, M. and Brown, S. J.** (2012). A segmentation clock operating in blastoderm and germband stages of *Tribolium* development. *Development (Cambridge, England)* **4346**, 4341–4346.
- Extavour, C. G.** (2005). The fate of isolated blastomeres with respect to germ cell formation in the amphipod crustacean *Parhyale hawaiiensis*. *Developmental biology* **277**, 387–402.

- Farrell, J. a and O'Farrell, P. H.** (2013). Mechanism and regulation of Cdc25/Twine protein destruction in embryonic cell-cycle remodeling. *Current biology: CB* **23**, 118–26.
- Foe, V. E.** (1989). Mitotic domains reveal early commitment of cells in *Drosophila* embryos. *Development (Cambridge, England)* **107**, 1–22.
- Frescas, D., Mavrikis, M., Lorenz, H., Delotto, R. and Lippincott-Schwartz, J.** (2006). The secretory membrane system in the *Drosophila* syncytial blastoderm embryo exists as functionally compartmentalized units around individual nuclei. *The Journal of cell biology* **173**, 219–30.
- Gao, L., Shao, L., Higgins, C. D., Poulton, J. S., Peifer, M., Davidson, M. W., Wu, X., Goldstein, B. and Betzig, E.** (2012). Noninvasive Imaging beyond the Diffraction Limit of 3D Dynamics in Thickly Fluorescent Specimens. *Cell* **151**, 1370–1385.
- Gillis, W. Q., Bowerman, B. a and Schneider, S. Q.** (2008). The evolution of protostome GATA factors: molecular phylogenetics, synteny, and intron/exon structure reveal orthologous relationships. *BMC evolutionary biology* **8**, 112.
- Grimaldi, D. and Engel, M.** (2005). *Evolution of the Insects*. Cambridge University Press.
- Handel, K., Grünfelder, C. G., Roth, S. and Sander, K.** (2000). *Tribolium* embryogenesis: a SEM study of cell shapes and movements from blastoderm to serosal closure. *Development Genes and*.
- Handel, K., Basal, A., Fan, X. and Roth, S.** (2005). *Tribolium castaneum* twist: gastrulation and mesoderm formation in a short-germ beetle. *Dev. Genes Evol.* **215**, 13–31.
- Harris, T. J. C., Sawyer, J. K. and Peifer, M.** (2009). *How the cytoskeleton helps build the embryonic body plan: models of morphogenesis from Drosophila*. 1st ed. Elsevier Inc.
- Hatta, K., Tsujii, H. and Omura, T.** (2006). Cell tracking using a photoconvertible fluorescent protein. *Nature protocols* **1**, 960–7.
- Hejnal, A.** (2010). A twist in time--the evolution of spiral cleavage in the light of animal phylogeny. *Integrative and comparative biology* **50**, 695–706.
- Hejnal, A., Schnabel, R. and Scholtz, G.** (2006). A 4D-microscopic analysis of the germ band in the isopod crustacean *Porcellio scaber* (Malacostraca, Peracarida)-developmental and phylogenetic implications. *Development genes and evolution* **216**, 755–67.
- Hilbrant, M., Damen, W. G. M. and McGregor, A. P.** (2012). Evolutionary crossroads in developmental biology: the spider Parasteatoda tepidariorum. *Development (Cambridge, England)* **139**, 2655–62.
- Ho, K., Dunin-Borkowski, O. M. and Akam, M.** (1997). Cellularization in locust embryos occurs before blastoderm formation. *Development* **124**, 2761–8.

- Irvine, K. D. and Wieschaus, E.** (1994). Cell intercalation during *Drosophila* germband extension and its regulation by pair-rule segmentation genes. *Development (Cambridge, England)* **120**, 827–41.
- Izeddin, I., Specht, C. G., Lelek, M., Darzacq, X., Triller, A., Zimmer, C. and Dahan, M.** (2011). Super-resolution dynamic imaging of dendritic spines using a low-affinity photoconvertible actin probe. *PloS one* **6**, e15611.
- Jaeger, J.** (2011). The gap gene network. *Cellular and molecular life sciences : CMLS* **68**, 243–74.
- Kainz, F., Ewen-Campen, B., Akam, M. and Extavour, C. G.** (2011). Notch/Delta signalling is not required for segment generation in the basally branching insect *Gryllus bimaculatus*. *Development (Cambridge, England)* **138**, 5015–26.
- Kalinka, A. T., Varga, K. M., Gerrard, D. T., Preibisch, S., Corcoran, D. L., Jarrells, J., Ohler, U., Bergman, C. M. and Tomancak, P.** (2010). Gene expression divergence recapitulates the developmental hourglass model. *Nature* **468**, 811–814.
- Kanayama, M., Akiyama-Oda, Y. and Oda, H.** (2010). Early embryonic development in the spider *Achaearanea tepidariorum*: Microinjection verifies that cellularization is complete before the blastoderm stage. *Arthropod structure & development* **39**, 436–45.
- Kanayama, M., Akiyama-Oda, Y., Nishimura, O., Tarui, H., Agata, K. and Oda, H.** (2011). Travelling and splitting of a wave of hedgehog expression involved in spider-head segmentation. *Nature communications* **2**, 500.
- Keller, R.** (2002). Shaping the Vertebrate Body Plan by Polarized Embryonic Cell Movements. *Science* **298**, 1950–1954.
- Khairy, K. and Keller, P. J.** (2011). Reconstructing embryonic development. *Genesis (New York, N.Y. : 2000)* **49**, 488–513.
- Kiehart, D. P., Galbraith, C. G., Edwards, K. a, Rickoll, W. L. and Montague, R. a** (2000). Multiple forces contribute to cell sheet morphogenesis for dorsal closure in *Drosophila*. *The Journal of cell biology* **149**, 471–90.
- Kispert, a, Herrmann, B. G., Leptin, M. and Reuter, R.** (1994). Homologs of the mouse *Brachyury* gene are involved in the specification of posterior terminal structures in *Drosophila*, *Tribolium*, and *Locusta*. *Genes & Development* **8**, 2137–2150.
- Kittelmann, S., Ulrich, J., Posnien, N. and Bucher, G.** (2013). Changes in anterior head patterning underlie the evolution of long germ embryogenesis. *Developmental biology* **374**, 174–184.
- Kontarakis, Z., Pavlopoulos, A., Kiupakis, A., Konstantinides, N., Douris, V. and Averof, M.** (2011). A versatile strategy for gene trapping and trap conversion in emerging model organisms. *Development (Cambridge, England)* **138**, 2625–30.

- Köppen, M., Fernández, B. G., Carvalho, L., Jacinto, A. and Heisenberg, C.-P.** (2006). Coordinated cell-shape changes control epithelial movement in zebrafish and *Drosophila*. *Development (Cambridge, England)* **133**, 2671–81.
- Kotadia, S., Crest, J., Tram, U., Riggs, B. and Sullivan, W.** (2010). Blastoderm Formation and Cellularisation in *Drosophila melanogaster*. *Life Sciences* 1–8.
- Lecuit, T.** (2004). Junctions and vesicular trafficking during *Drosophila* cellularization. *Journal of cell science* **117**, 3427–33.
- Lecuit, T. and Lenne, P.-F.** (2007). Cell surface mechanics and the control of cell shape, tissue patterns and morphogenesis. *Nature reviews. Molecular cell biology* **8**, 633–44.
- Lynch, J. a., El-Sherif, E. and Brown, S. J.** (2012). Comparisons of the embryonic development of *Drosophila*, *Nasonia*, and *Tribolium*. *Wiley Interdisciplinary Reviews: Developmental Biology* **1**, 16–39.
- Martin, A. C., Kaschube, M. and Wieschaus, E. F.** (2009). Pulsed contractions of an actin-myosin network drive apical constriction. *Nature* **457**, 495–9.
- Mavrakis, M., Rikhy, R. and Lippincott-Schwartz, J.** (2009). Plasma membrane polarity and compartmentalization are established before cellularization in the fly embryo. *Developmental cell* **16**, 93–104.
- Mavrakis, M., Pourquié, O. and Lecuit, T.** (2010). Lighting up developmental mechanisms: how fluorescence imaging heralded a new era. *Development (Cambridge, England)* **137**, 373–87.
- Mazumdar, A. and Mazumdar, M.** (2002). How one becomes many: blastoderm cellularization in *Drosophila melanogaster*. *BioEssays : news and reviews in molecular, cellular and developmental biology* **24**, 1012–22.
- Meijering, E., Dzyubachyk, O. and Smal, I.** (2012). *Methods for cell and particle tracking*. 1st ed. Elsevier Inc.
- Meyer, T. H., van Endert, P. M., Uebel, S., Ehring, B. and Tampé, R.** (1994). Functional expression and purification of the ABC transporter complex associated with antigen processing (TAP) in insect cells. *FEBS letters* **351**, 443–7.
- Meyer, E. J., Ikmi, A. and Gibson, M. C.** (2011). Interkinetic nuclear migration is a broadly conserved feature of cell division in pseudostratified epithelia. *Current biology : CB* **21**, 485–91.
- Mittmann, B. and Wolff, C.** (2012). Embryonic development and staging of the cobweb spider *Parasteatoda tepidariorum* C. L. Koch, 1841 (syn.: *Achaearana tepidariorum*; *Araneomorphae*; *Theridiidae*). *Development genes and evolution* **222**, 189–216.
- Murakami, R., Okumura, T. and Uchiyama, H.** (2005). GATA factors as key regulatory molecules in the development of *Drosophila* endoderm. *Development, growth & differentiation* **47**, 581–9.

- Nakamura, T., Yoshizaki, M., Ogawa, S., Okamoto, H., Shinmyo, Y., Bando, T., Ohuchi, H., Noji, S. and Mito, T.** (2010). Imaging of Transgenic Cricket Embryos Reveals Cell Movements Consistent with a Syncytial Patterning Mechanism. *Current biology : CB* **20**, 1641–1647.
- Nunes Da Fonseca, R., von Levetzow, C., Kalscheuer, P., Basal, A., van Der Zee, M. and Roth, S.** (2008). Self-regulatory circuits in dorsoventral axis formation of the short-germ beetle *Tribolium castaneum*. *Developmental cell* **14**, 605–15.
- Oakley, T. H., Wolfe, J. M., Lindgren, A. R. and Zaharoff, A. K.** (2013). Phylotranscriptomics to bring the understudied into the fold: monophyletic ostracoda, fossil placement, and pancrustacean phylogeny. *Molecular biology and evolution* **30**, 215–33.
- Ostrowski, K., Bauer, R. and Hoch, M.** (2008). The *Drosophila* Innexin7 Gap Junction Protein Is Required for Development of the Embryonic Nervous System. *Cell Communication and Adhesion* **15**, 155–167.
- Pavlopoulos, A. and Averof, M.** (2005). Establishing genetic transformation for comparative developmental studies in the crustacean *Parhyale hawaiiensis*. *Proceedings of the National Academy of Sciences of the United States of America* **102**, 7888–93.
- Peel, A. D.** (2008). The evolution of developmental gene networks: lessons from comparative studies on holometabolous insects. *Philosophical transactions of the Royal Society of London. Series B, Biological sciences* **363**, 1539–47.
- Peel, A. D., Chipman, A. D. and Akam, M.** (2005). Arthropod segmentation: beyond the *Drosophila* paradigm. *Nature reviews. Genetics* **6**, 905–16.
- Pfeiffer, B. D., Ngo, T.-T. B., Hibbard, K. L., Murphy, C., Jenett, A., Truman, J. W. and Rubin, G. M.** (2010). Refinement of tools for targeted gene expression in *Drosophila*. *Genetics* **186**, 735–55.
- Quintin, S., Gally, C. and Labouesse, M.** (2008). Epithelial morphogenesis in embryos: asymmetries, motors and brakes. *Trends in genetics : TIG* **24**, 221–30.
- Rafiqi, A. M., Lemke, S., Ferguson, S., Stauber, M. and Schmidt-Ott, U.** (2008). Evolutionary origin of the amnioserosa in cyclorrhaphan flies correlates with spatial and temporal expression changes of zen. *Proceedings of the National Academy of Sciences of the United States of America* **105**, 234–9.
- Rauzi, M. and Lenne, P.-F.** (2011). *Cortical forces in cell shape changes and tissue morphogenesis.*
- Rauzi, M., Lenne, P.-F. and Lecuit, T.** (2010). Planar polarized actomyosin contractile flows control epithelial junction remodelling. *Nature* **468**, 1110–1114.
- Reed, B. H., Wilk, R., Schöck, F. and Lipshitz, H. D.** (2004). Integrin-dependent apposition of *Drosophila* extraembryonic membranes promotes morphogenesis and prevents anoikis. *Current biology : CB* **14**, 372–80.

- Regier, J. C., Shultz, J. W., Zwick, A., Hussey, A., Ball, B., Wetzer, R., Martin, J. W. and Cunningham, C. W.** (2010). Arthropod relationships revealed by phylogenomic analysis of nuclear protein-coding sequences. *Nature* **463**, 1079–83.
- Rehorn, K. P., Thelen, H., Michelson, a M. and Reuter, R.** (1996). A molecular aspect of hematopoiesis and endoderm development common to vertebrates and *Drosophila*. *Development (Cambridge, England)* **122**, 4023–31.
- Rembold, M., Loosli, F., Adams, R. J. and Wittbrodt, J.** (2006). Individual cell migration serves as the driving force for optic vesicle evagination. *Science (New York, N.Y.)* **313**, 1130–4.
- Rickoll, W. L.** (1976). Cytoplasmic continuity between embryonic cells and the primitive yolk sac during early gastrulation in *Drosophila melanogaster*. *Developmental biology* **49**, 304–10.
- Riedl, J., Crevenna, A. H., Kessenbrock, K., Yu, J. H., Neukirchen, D., Bradke, F., Jenne, D., Holak, T. A., Werb, Z., Sixt, M., et al.** (2008). Lifeact : a versatile marker to visualize F-actin. *Nature Methods* **5**, 605–607.
- Roberts, D. B.** (1986). *DrosophilaL a practical approach*. Oxford University Press, USA.
- Rodriguez-Diaz, A., Toyama, Y., Abravanel, D. L., Wiemann, J. M., Wells, A. R., Tulu, U. S., Edwards, G. S. and Kiehart, D. P.** (2008). Actomyosin purse strings: renewable resources that make morphogenesis robust and resilient. *HFSP journal* **2**, 220–37.
- Roth, S.** (2004). Gastrulation in Other Insects. In *Gastrulation. From Cells to Embryo* (ed. Stern, C. D.), pp. 105–121. New York: Cold Spring Harbor Laboratory Press.
- Rothwell, W. F., Fogarty, P., Field, C. M. and Sullivan, W.** (1998). Nuclear-fallout, a *Drosophila* protein that cycles from the cytoplasm to the centrosomes, regulates cortical microfilament organization. *Development (Cambridge, England)* **125**, 1295–303.
- Royou, A., Sullivan, W. and Karess, R.** (2002). Cortical recruitment of nonmuscle myosin II in early syncytial *Drosophila* embryos: its role in nuclear axial expansion and its regulation by Cdc2 activity. *The Journal of cell biology* **158**, 127–37.
- Royou, A., Field, C., Sisson, J. C., Sullivan, W. and Karess, R.** (2004). Reassessing the Role and Dynamics of Nonmuscle Myosin II during Furrow Formation in Early *Drosophila* Embryos □. **15**, 838–850.
- Sarrazin, A. F., Peel, A. D. and Averof, M.** (2012). A segmentation clock with two-segment periodicity in insects. *Science (New York, N.Y.)* **336**, 338–41.
- Schindelin, J., Arganda-Carreras, I., Frise, E., Kaynig, V., Longair, M., Pietzsch, T., Preibisch, S., Rueden, C., Saalfeld, S., Schmid, B., et al.** (2012). Fiji: an open-source platform for biological-image analysis. *Nature methods* **9**, 676–82.
- Schinko, J. B., Kreuzer, N., Offen, N., Posnien, N., Wimmer, E. a and Bucher, G.** (2008). Divergent functions of orthodenticle, empty spiracles and buttonhead in early head

- patterning of the beetle *Tribolium castaneum* (Coleoptera). *Developmental biology* **317**, 600–13.
- Schinko, J., Posnien, N., Kittelmann, S., Koniszewski, N. and Bucher, G.** (2009). Single and double whole-mount in situ hybridization in red flour beetle (*Tribolium*) embryos. *Cold Spring Harbor protocols* **2009**, pdb.prot5258.
- Schoppmeier, M., Fischer, S., Schmitt-Engel, C., Löhr, U. and Klingler, M.** (2009). An ancient anterior patterning system promotes caudal repression and head formation in ecdysozoa. *Current biology : CB* **19**, 1811–5.
- Schroder, R., Eckert, C., Wolff, C. and Tautz, D.** (2000). Conserved and divergent aspects of terminal patterning in the beetle *Tribolium castaneum*. *Proceedings of the National Academy of Sciences of the United States of America* **97**, 6591–6.
- Schulz, C., Schröder, R., Hausdorf, B., Wolff, C. and Tautz, D.** (1998). A caudal homologue in the short germ band beetle *Tribolium* shows similarities to both, the *Drosophila* and the vertebrate caudal expression patterns. *Development genes and evolution* **208**, 283–289.
- Sokoloff, A. and Shrode, R.** (1962). Survival of *Tribolium castaneum* Herbst after rocket flight into the ionosphere. *Aerosp Med.*
- St Johnston, D. and Sanson, B.** (2011). Epithelial polarity and morphogenesis. *Current opinion in cell biology* **23**, 540–6.
- Steinmetz, P. R. H., Zelada-González, F., Burgtorf, C., Wittbrodt, J. and Arendt, D.** (2007). Polychaete trunk neuroectoderm converges and extends by mediolateral cell intercalation. *Proceedings of the National Academy of Sciences of the United States of America* **104**, 2727–32.
- Telford, M. J., Bourlat, S. J., Economou, A., Papillon, D. and Rota-Stabelli, O.** (2008). The evolution of the Ecdysozoa. *Philosophical Transactions of the Royal Society B: Biological Sciences* **363**, 1529–1537.
- Tomer, R., Khairy, K., Amat, F. and Keller, P. J.** (2012). Quantitative high-speed imaging of entire developing embryos with simultaneous multiview light-sheet microscopy. *Nat Meth* **9**, 755–763.
- Trautwein, M. D., Wiegmann, B. M., Beutel, R., Kjer, K. M. and Yeates, D. K.** (2012). Advances in insect phylogeny at the dawn of the postgenomic era. *Annual review of entomology* **57**, 449–68.
- Untergasser, A., Cutcutache, I., Koressaar, T., Ye, J., Faircloth, B. C., Remm, M. and Rozen, S. G.** (2012). Primer3--new capabilities and interfaces. *Nucleic acids research* **40**, e115.
- Van der Zee, M., Berns, N. and Roth, S.** (2005). Distinct Functions of the *Tribolium* *zerknüllt* Genes in Serosa Specification and Dorsal Closure. *Current Biology* **15**, 624–636.

- Waddington, C. H. and Counce, S. J.** (1972a). *Developmental Systems: Insects, Volume 1*. Academic Press.
- Waddington, C. H. and Counce, S. J.** (1972b). *Developmental Systems: Insects, Volume 2*. Academic Press.
- Weber, M. and Huisken, J.** (2012). Omnidirectional microscopy. *Nat Meth* **9**, 656–657.
- Weigel, D., Bellen, H. J., Jiirgens, G. and Jüickle, H.** (1989). Primordium specific requirement of the homeotic gene fork head in the developing gut of the *Drosophila* embryo. 201–210.
- White, K., Tahaoglu, E. and Steller, H.** (1996). Cell Killing by the *Drosophila* Gene reaper. **271**, 805–807.
- Widmann, T. J. and Dahmann, C.** (2009). Wingless signaling and the control of cell shape in *Drosophila* wing imaginal discs. *Developmental biology* **334**, 161–73.
- Wilson, M. J. and Dearden, P. K.** (2011). Diversity in insect axis formation: two orthodenticle genes and hunchback act in anterior patterning and influence dorsoventral organization in the honeybee (*Apis mellifera*). *Development (Cambridge, England)* **138**, 3497–507.
- Wolff, C., Schröder, R., Schulz, C., Tautz, D. and Klingler, M.** (1998). Regulation of the *Tribolium* homologues of caudal and hunchback in *Drosophila*: evidence for maternal gradient systems in a short germ embryo. *Development (Cambridge, England)* **125**, 3645–54.
- Yasuda, K., Yu, P., Kirschning, C. J., Schlatter, B., Schmitz, F., Heit, A., Bauer, S., Hochrein, H. and Wagner, H.** (2005). Endosomal Translocation of Vertebrate DNA Activates Dendritic Cells via TLR9-Dependent and -Independent Pathways. *The Journal of Immunology* **174** , 6129–6136.
- Zallen, J. A. and Wieschaus, E.** (2004). Patterned Gene Expression Directs Bipolar Planar Polarity in *Drosophila*. *Developmental Cell* **6**, 343–355.